



UNIVERSITY OF
KWAZULU-NATAL

INYUVESI
YAKWAZULU-NATALI

**Production of nanocellulose from renewable resources and
conductivity measurements of polypyrrole hybrid nanocomposites**

by

Nadia Nirmal

Dissertation submitted in fulfilment of the academic requirements for the degree of

Master of Science

School of Chemistry and Physics, University of KwaZulu-Natal, Durban

As the candidate's supervisor, I have approved this dissertation for submission.

Prof. W. E. van Zyl

Name



Signature

20 June 2018

Date

I can do all things through Christ who strengthens me

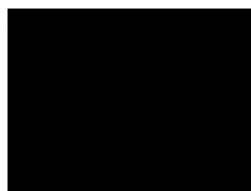
Philippians 4:13

DECLARATION I: PLAGIARISM

I, Nadia Nirmal, declare that the experimental work described in this dissertation was carried out at the School of Chemistry and Physics, University of KwaZulu-Natal, Westville campus, between January 2017 and June 2018, under the supervision of Prof. W. E. van Zyl, and that:

1. The research reported in this thesis, except where otherwise indicated, and is my original research.
2. This thesis has not been submitted for any degree or examination at any other university.
3. This thesis does not contain other persons' data, pictures, graphs or other information, unless specifically acknowledged as being sourced from other persons.
4. This thesis does not contain other persons' writing, unless specifically acknowledged as being sourced from other researchers. Where other written sources have been quoted, then:
 - i Their words have been re-written, but the general information attributed to them has been referenced
 - ii Where their exact words have been used, then their writing has been placed in italics and inside quotation marks and referenced.
5. This thesis does not contain text, graphics or tables copied and pasted from the Internet, unless specifically acknowledged, and the source being detailed in the thesis and in the References sections.

Signed:

A solid black rectangular box redacting the signature of the author.

Name: Nadia Nirmal

Date: 20 June 2018

ABSTRACT

The extraction of nanocellulose (NC) from i) bacterial cellulose (grown using "Symbiotic 'Colony' of Bacteria and Yeast" or SCOBY), ii) Whatman filter paper, and iii) hardwood pulp was successfully investigated in this study. Acid hydrolysis was applied to these three materials and nano-fibrous whiskers were formed. When the nano-fibres were subjected to dialysis, the nano-fibres exhibited a crystalline structure known as nanocrystalline cellulose (NCC). Harmless disposal of the residual hydrolysis acid by-product is still an obstacle that hinders large-scale production of NCC and NCC-based nanocomposites. In this work, the hydrolysis products of NC without further separation was studied to produce nanofibrous cellulose (NFC). The NFC structural integrity was compared to conventional NCC. The structural composition was verified using Fourier-transform infrared spectroscopy (FT-IR) and Raman spectroscopy. The nanofibers were examined with Scanning Electron Microscopy coupled with Energy Dispersive X-ray spectroscopy (SEM-EDS) and Transmission Electron Microscopy (TEM).

The dimensions of the nanocellulose were within the nanometre range that has acceptable aspect ratios for ideal stress transfer of the fibre-matrix interaction. For the various nanocellulose samples, i.e. from Bacterial cellulose, Whatman Filter paper and hardwood pulp, it was found that the concentration of the dialysis-free nano-fibrous cellulose has a higher concentration and longer dimensions than that of dialysed nanocrystalline cellulose. The nanocellulose was then utilized as a stabilizer for the synthesis of polypyrrole using a pyrrole monomer and ferric chloride hexahydrate initiator that produced a well dispersed network of polypyrrole@nanocellulose (PPy@NC) hybrid nanocomposite. Various concentrations were produced to find the optimum ratio of polypyrrole to nanocellulose to give excellent stability and dispersity. The ratio of 1:1 polypyrrole to nanocellulose exhibited good suspension of the nanohybrid, forming a well dispersed network. The nanohybrid formation was confirmed using TEM, SEM, FT-IR, Raman spectroscopy and Ultraviolet-visible spectroscopy (UV-Vis). Interestingly, the PPy@NC nanohybrid could be easily isolated from the polymerization products due to the decreased surface charge. The PPy@NC nanohybrid was subsequently suspended in polyvinyl alcohol (PVA), which facilitated the construction of a continuous PPy@NC conductive network in the polymer

matrix for both NCC and NFC. The development of a novel resistivity apparatus and tests were conducted for the first time on all samples using an expedient method and the results were similar with that of the commonly used but restrictive four-point probe method. The PPy@NFC/PVA nanocomposite showed significant improvement in electrical conductivity and mechanical properties when compared with neat PPy/PVA composites and exhibited slightly improved performance when compared to the dialysed nanocellulose composite, PPy@NCC/PVA, at the same ratio. This was due to the dialysis-free synthesis process allowing the residual hydrolysis acid to act as a doping agent for the synthesized PPy, endowing PPy@NFC nanohybrid with improved electrical conductivity. Dialysis is a time-consuming step during acid hydrolysis, and this study investigated the both the effect of products formed and their electrical properties with and without the dialysis step. It was found that the nanohybrid synthesized from bacterial nanocellulose in a dialysis-free step, showed a resistivity of 2.341 Ω/m that has an improved resistivity result compared to the nanohybrid prepared from bacterial cellulose that was dialysed which was 2.928 Ω/m ; a lower resistance value allows for greater conductance. The nanohybrid made from nanocellulose sourced from Whatman filter paper, that was not subjected to dialysis gave a better resistivity of 2.287 Ω/m as compared to the nanohybrid from the nanocellulose subjected to dialysis, which was 4.954 Ω/m . The dialysis-free hardwood pulp nanohybrid produced a nanohybrid with a resistance of 6.515 Ω/m and the dialysed gave a resistance of 8.402 Ω/m which had the greatest opposition of the flow of current through the material. When the samples were viewed under a microscope before and after being subjected to an applied voltage, the samples retained their integrity and could be re-used several times. This work conclusively demonstrated that by capitalizing on the physiognomies of nanocellulose not subjected to dialysis, its unique traits can be further exploited for useful applications. By avoiding the costly and laborious dialysis step, one could easily utilize the residual acid as a doping agent that contributed to the desired conductance required. The straightforward and sustainability of this dialysis-free and in-situ doping synthesis of the PPy@NFC nanohybrid should facilitate in a significant way the scalable fabrication and application of nanocellulose based conductive nanocomposites with high performance.

ABBREVIATIONS

AGU	Anhydroglucopyranose units
BC	Bacteria Cellulose
BNCC	Bacterial Nanocrystalline Cellulose
ddH ₂ O	Double distilled water
FT-IR	Fourier-transform infrared spectroscopy
HS	Hestrin-Schramm
NC	Nanocellulose
NCC	Nano-Crystalline Cellulose
NFC	Nano-Fibrous Cellulose
PPy@NC	Polypyrrole-Nanocellulose
PPy@NCC	Polypyrrole- Nanocrystalline Cellulose
PPy@NFC	Polypyrrole- Nano-Fibrous Cellulose
PVA	Polyvinyl alcohol
SCOBY	Symbiotic Culture of Bacteria and Yeast
SEM-EDS	Scanning Electron Microscopy coupled with Energy Dispersive X-ray Spectroscopy
TEM	Transmission Electron Microscopy
UV-Vis	Ultraviolet- Visible Spectroscopy

PREFACE

The experimental work described in this dissertation was carried out in the School of Chemistry and Physics, University of KwaZulu-Natal (Westville Campus), Durban, from January 2017 to June 2018, under the supervision of

Professor W. E. Van Zyl

This study is an original work of the author and has been submitted in partial fulfillment of the academic requirements for obtaining a M.Sc. Degree in Chemistry.

ACKNOWLEDGEMENTS

The financial assistance of the National Research Foundation (NRF) towards this research is hereby acknowledged. Opinions expressed, and conclusions arrived at, are those of the author and are not necessarily to be attributed to the NRF.

I would like to thank my supervisor, Prof. W. E. Van Zyl for his support and guidance throughout this project. His knowledge and positivity has indeed inspired me.

Thanks to Prof. F. Petruccione, Marco Mariola, Michael Niven Pillay and Segun Ajibola for their assistance and guidance throughout my learning. As well as Subashen Naidu, Vishal Bharuth and Vashen Moodley for the instrumentation training and aid.

Appreciation to my loving partner, Dr. A. P. Bedessy, the first man I loved, and the first man to love me, thank you for the inspiration and unique ideas throughout my research.

A special thanks to my mother, Pam and brother, Nadir Nirmal for their tolerance, unlimited motivation and infinite prayers. And thanks to my best friend Waseem Mahomed, for the upliftment and enthusiasm to never give up.

And most importantly, I would like to thank my Lord, Jesus Christ, for extending his grace and love upon me and granting me this privilege, (Proverbs 4).

TABLE OF CONTENTS

Chapter 1

1. Introduction.....	1
1.1. Problem identification.....	9
1.2. Purpose of the study.....	9
1.3. Aims of the study.....	9
1.4. The objectives.....	10
1.5. Important research questions.....	10
1.6. Overview.....	10
1.7. References.....	11

Chapter 2

2.1. Background.....	17
2.1.2. Bacterial grown cellulose.....	17
2.1.3. Whatman filter paper.....	18
2.1.4. Hardwood pulp.....	19
2.2. Experimental procedure for preparation of nanocellulose.....	20
2.2.1. Preparation of nanocellulose from bacterial cellulose.....	20
2.2.1.1. Preparation of SCOBY.....	20
2.2.1.2. Preparation of Bacterial Cellulose (BC) using SCOBY.....	20
2.2.1.3. Preparation of bacterial nanocellulose.....	21
2.2.1.4. Preparation of nanocellulose from Bacterial cellulose: dialysis- free method.....	22
2.2.2. Preparation of nanocellulose from Whatman filter paper.....	22
2.2.2.1. Preparation of nanocellulose from Whatman filter paper- dialysis method.....	22

2.2.2.2. Preparation of nanocellulose from Whatman filter paper-dialysis-free method.....	23
2.2.3. Preparation of nanocellulose from hardwood pulp.....	23
2.2.3.1. Preparation of nanocellulose from hardwood pulp- dialysis-method.....	23
2.2.3.2. Preparation of nanocellulose from Whatman filter paper-dialysis- free method.....	24
2.2.4. Characterisation parameters	24
2.3. Results and discussion.....	25
2.3.1. Average concentration of dialyzed and dialysis-free nanocellulose from bacterial grown cellulose, Whatman filter paper and hardwood pulp.....	27
2.3.2. SEM-EDS imaging of dialyzed and dialysis-free nanocellulose from bacterial grown cellulose, Whatman filter paper and hardwood pulp.....	28
2.3.3. FT-IR spectra for dialyzed and dialysis-free nanocellulose grown from bacterial cellulose, Whatman filter paper and hardwood pulp.....	31
2.3.4. Raman spectra for dialyzed and dialysis-free nanocellulose from bacterial grown cellulose, Whatman filter paper and hardwood pulp.....	33
2.3.5. TEM imaging with calculated aspect ratio for dialyzed and dialysis-free nanocellulose from bacterial grown cellulose, Whatman filter paper, and hardwood pulp.....	35
2.4. References.....	40

Chapter 3

3.1. Background to Polypyrrole@Nanocellulose Polymer Samples.....	43
3.2. Experimental Procedure for Varying Ratios of Polymer Samples.....	45

3.2.1. Preparation of varying ratio of PPy@NC.....	45
3.2.2. Incorporation of varying ratios of PPy:NC in PVA.....	46
3.3. Results and Discussion for Ratios of Polymer Samples.....	46
3.4. Experimental Procedure for All of Polymer Samples at Optimum Ratio.....	49
3.4.1. <i>In situ</i> doping preparation of PPy@NC nanohybrid from NC of Bacterial grown cellulose, Whatman filter paper, and hardwood pulp dialysed and dialysis-free, as well as neat PPy.....	49
3.4.2. Preparation of PPy@NC/PVA nanocomposites from NC of Bacterial grown cellulose, Whatman filter paper and hardwood pulp dialysed and dialysis-free.....	50
3.5. Characterisation parameters.....	50
3.6. Results and discussion for all polymer samples at optimum ratio.....	51
3.6.1. TEM images of nanohybrid samples.....	52
3.6.2. SEM-EDS of nanohybrid samples.....	55
3.6.3. FT-IR of nanohybrid samples.....	62
3.6.4. Raman spectroscopy of nanohybrid samples.....	65
3.6.5. UV-Vis analysis.....	67
3.7. References.....	68

Chapter 4

4.1. Experimental procedure for electrical testing for conductivity of the polymer samples.....	71
4.1.1. Resistivity test.....	71
4.1.2. Morphological structure analysis.....	73
4.2. Results and discussion.....	73

Chapter 5

Conclusions.....	98
Appendix.....	99

LIST OF FIGURES

Figure 1.1. The molecular structure of a cellulose polymer where the cellobios is the smallest repeating unit in the polymer.....	1
Figure 1.2. Formation of sulfate group on the nanocellulose surface, after hydrolysis reaction.....	2
Figure 1.3. Structure of pyrrole.....	7
Figure 1.4. The polymerisation of polypyrrole.....	8
Figure 2.1. TEM image of the bacteria cell from SCOBY responsible for the growth of cellulose.....	17
Figure 2.2. Image of the growth of SCOBY in a sample of Kombucha tea.....	20
Figure 2.3. SCOBY in the required medium for BC growth.....	21
Figure 2.4. The BC after 2 weeks of growth (a) and after washing and bleaching (b).....	25
Figure 2.5. SEM image of dried Bacterial cellulose.....	25
Figure 2.6. TEM image of negatively stained Bacterial cellulose.....	26
Figure 2.7. SEM image of (a) Bacterial nanocrystalline cellulose; (b) Whatman filter paper nanocrystalline cellulose and (c) Hardwood pulp nanocrystalline cellulose with corresponding EDS.....	29
Figure 2.8. SEM image of (a) Bacterial nanofibrous cellulose; (b) Whatman filter paper nanofibrous cellulose and (c) Hardwood pulp nanofibrous cellulose with corresponding EDS.....	30
Figure 2.9. FT-IR spectra of a) Bacterial nanocrystalline cellulose; (b) Whatman filter paper nanocrystalline cellulose and (c) hardwood pulp nanocrystalline cellulose.....	31
Figure 2.10. FT-IR spectra of (a) Bacterial nanofibrous cellulose; (b) Whatman filter paper nanofibrous cellulose and (c) hardwood pulp nanofibrous cellulose.....	32
Figure 2.11. Raman spectra of (a) NCC and (b) NFC from bacterial cellulose; (c) NCC	

and (d) NFC from Whatman filter paper; (e) NCC and (f) NFC from hardwood pulp.....	34
Figure 2.12. TEM images of negatively stained (a) Bacterial nanocrystalline cellulose and (b) Bacterial nano-fibrous cellulose.....	36
Figure 2.13. Histogram representing the distribution of average length (a) width (b) and aspect ratio (c) of NCC from bacterial cellulose.....	36
Figure 2.14. Histogram representing the distribution of length (a) width (b) and aspect ratio (c) of NFC from bacterial cellulose.....	37
Figure 2.15. TEM image of negatively stained Whatman filter paper <i>via</i> dialysis-free method.....	37
Figure 2.16. Histogram representing the distribution of length (a) width (b) and aspect ratio (c) of NCC of dialyzed WFP.....	38
Figure 2.17. Histogram representing the distribution of length (a) width (b) and aspect ratio (c) of NFC of dialysis-free WFP.....	38
Figure 2.18. HR-TEM image of negatively stained hardwood pulp nanocrystals produced <i>via</i> dialysis-free method.....	39
Figure 2.19. Histogram representing the distribution of length (a) width (b) and aspect ratio (c) of NCC of dialyzed hardwood pulp.....	39
Figure 2.20. Histogram representing the distribution of length (a) width (b) and aspect ratio (c) of NFC of un-dialyzed hardwood pulp.....	40
Figure 3.1. Digital picture of varying ratios of PPy:NC (L-R: (a) 0:1; (b) 1:2; (c) 1:1; (d) 2:1 and (e) 1:0) when left to settle for 30 minutes.....	48
Figure 3.2. TEM image of neat polypyrrole.....	52
Figure 3.3. TEM images for PPy@NCC from BC- dialysis method.....	53
Figure 3.4. TEM images for PPy@NFC from BC- dialysis-free method.....	53
Figure 3.5. TEM images for PPy@NCC from Whatman filter paper- dialysis method.....	53
Figure 3.6. TEM images for PPy@NFC from Whatman filter paper – dialysis-free method.....	54
Figure 3.7. TEM images for PPy@NCC from hardwood pulp- dialysis method.....	54
Figure 3.8. TEM images for PPy@NFC from hardwood pulp- dialysis-free method.....	54
Figure 3.9. SEM-EDS image of neat polypyrrole.....	55

Figure 3.10. SEM image of (a) PPy@NCC from dialyzed bacterial cellulose with (b) SEM-EDS elemental analysis of a specific cross section.....	56
Figure 3.11. SEM image of (a) PPy@NFC from dialysis-free bacterial cellulose with (b) SEM-EDS elemental analysis of a specific cross section.....	57
Figure 3.12. SEM image of (a) PPy@NCC from dialyzed Whatman filter paper with (b) SEM-EDS elemental analysis of a specific cross section.....	57
Figure 3.13. SEM image of (a) PPy@NFC from dialysis-free Whatman filter paper with (b) SEM-EDS elemental analysis of a specific cross section.....	58
Figure 3.14. SEM image of (a) PPy@NCC from dialyzed hardwood pulp with (b) SEM-EDS elemental analysis of a specific cross section.....	58
Figure 3.15. SEM image of (a) PPy@NFC from dialysis-free hardwood pulp with (b) SEM-EDS elemental analysis of a specific cross section.....	59
Figure 3.16. SEM image of polypyrrole in PVA.....	60
Figure 3.17. SEM image of PPy@NCC in PVA from BC- <i>via</i> dialysis method.....	60
Figure 3.18. SEM image of PPy@NFC in PVA from BC- <i>via</i> dialysis-free method.....	61
Figure 3.19. SEM image of PPy@NCC in PVA from Whatman filter paper- <i>via</i> dialysis method.....	61
Figure 3.20. SEM image of PPy@NFC in PVA from Whatman filter paper- <i>via</i> dialysis-free method.....	61
Figure 3.21. SEM image of PPy@NCC in PVA from Hardwood pulp- <i>via</i> dialysis method.....	62
Figure 3.22. SEM image of PPy@NFC in PVA from Hardwood pulp- <i>via</i> dialysis-free method.....	62
Figure 3.23. FT-IR spectra for neat Polypyrrole.....	63
Figure 3.24. FT-IR spectra for PPy@NCC nanohybrid from Bacterial cellulose (dialyzed).....	63
Figure 3.25. FT-IR spectra for PPy@NFC from Bacterial cellulose (dialysis-free).....	64
Figure 3.26. FT-IR spectra for PPy@NCC nanohybrid from Whatman filter paper (dialyzed).....	64
Figure 3.27. FT-IR spectra for PPy@NFC nanohybrid from Whatman filter paper (dialysis-free).....	64
Figure 3.28. FT-IR spectra for PPy@NCC nanohybrid from hardwood pulp (dialyzed).....	65
Figure 3.29. Raman spectra of neat polypyrrole.....	65

Figure 3.30. Raman spectra for (a) PPy@NCC from bacterial cellulose (dialyzed) and (b) PPy@NFC from bacterial cellulose (dialysis-free).....	66
Figure 3.31. Raman spectra for (a) PPy@NCC from Whatman filter paper (dialyzed) and (b) PPy@NFC from Whatman filter paper (dialysis-free).....	66
Figure 3.32. Raman spectra for (a) PPy@NCC from hardwood pulp (dialyzed) and (b) PPy@NFC from hardwood pulp (dialysis-free).....	66
Figure 3.33. UV-Vis spectra of Polypyrrole, NCC (dialyzed) and nanohybrid from BC, WFP and HWP.....	67
Figure 3.34. UV-Vis spectra of Polypyrrole, NFC (dialysis-free) and nanohybrid from BC, WFP and HWP.....	68
Figure 4.1. Sample of an etched copper clad board used to set sample for resistivity test.....	71
Figure 4.2. Sample set up for resistivity test.....	72
Figure 4.3. Copper plate with neat PVA (ratio PPy:NC (a) 0:0).....	73
Figure 4.4. Copper plate with ratio PPy:NC (b) 0:1 using bacterial nanofibrous cellulose (dialysis-free).....	74
Figure 4.5. The empty copper plate and the copper plate with ratio PPy:NC (c) 1:2 using bacterial nanofibrous cellulose (dialysis-free).....	74
Figure 4.6. The empty copper plate and the copper plate with ratio PPy:NC (d) 1:1 using bacterial nanofibrous cellulose (dialysis-free).....	74
Figure 4.7. The empty copper plate and the copper plate with ratio PPy:NC (e) 2:1 using bacterial nanofibrous cellulose (dialysis-free).....	75
Figure 4.8. The empty copper plate and the copper plate with ratio PPy:NC (f) 1:0, Neat PPy.....	75
Figure 4.9. TEM image of polyvinyl alcohol (PVA).....	76
Figure 4.10. TEM image of nanofibrous cellulose from bacterial cellulose (dialysis-free) in PVA.....	76
Figure 4.11. TEM image of ratio 1:2 polypyrrole to nanocellulose in PVA.....	77
Figure 4.12. TEM image of ratio 1:1 polypyrrole to nanocellulose in PVA.....	77
Figure 4.13. TEM image of ratio 2:1 polypyrrole to nanocellulose in PVA.....	78
Figure 4.14. TEM image of polypyrrole in PVA.....	78
Figure 4.15. Linear relationship based on Ohm's law for sample ratio 0:0 showing the change in current as voltage is applied.....	81
Figure 4.16. Linear relationship based on Ohm's law for sample ratio 0:1 showing the	

change in current as voltage is applied.....	81
Figure 4.17. Linear relationship based on Ohm's law for sample ratio 1:2 showing the change in current as voltage is applied.....	82
Figure 4.18. Linear relationship based on Ohm's law for sample ratio 1:1 showing the change in current as voltage is applied.....	82
Figure 4.19. Linear relationship based on Ohm's law for sample ratio 2:1 showing the change in current as voltage is applied.....	83
Figure 4.20. Linear relationship based on Ohm's law for sample ratio 1:0 showing the change in current as voltage is applied.....	83
Figure 4.21. Sem image of PVA with ratio 0:0 (a) before applied voltage and (b) after applied voltage.....	86
Figure 4.22. Sem image of PVA with ratio 0:1 nanofibrous cellulose from dialysis-free bacterial cellulose (a) before applied voltage and (b) after applied voltage.....	86
Figure 4.23. Sem image of Ratio 1:2 PPy@NFC of dialysis-free bacterial cellulose in PVA (a) before applied voltage and (b) after applied voltage.....	86
Figure 4.24. Sem image of Ratio 1:1 PPy@NFC of dialysis-free bacterial cellulose in PVA (a) before applied voltage and (b) after applied voltage.....	87
Figure 4.25. Sem image of Ratio 2:1 PPy@NFC of dialysis-free bacterial cellulose in PVA (a) before applied voltage and (b) after applied voltage.....	87
Figure 4.26. Sem image of Ratio 1:0 PPy@NFC of dialysis-free bacterial cellulose in PVA (a) before applied voltage and (b) after applied voltage.....	87
Figure 4.27. The empty copper plate and the copper plate with ratio 1:1 PPy@NCC in PVA for dialyzed hardwood pulp.....	88
Figure 4.28. The empty copper plate and the copper plate with ratio 1:1 PPy@NFC in PVA for dialysis-free hardwood pulp.....	88
Figure 4.29. The empty copper plate and the copper plate with ratio 1:1 PPy@NCC in PVA for dialyzed Whatman filter paper.....	88
Figure 4.30. The empty copper plate and the copper plate with ratio 1:1 PPy@NFC in PVA for dialysis-free Whatman filter paper.....	89
Figure 4.31. The empty copper plate and the copper plate with ratio 1:1 PPy@NCC in PVA for dialyzed bacterial cellulose.....	89
Figure 4.32. The empty copper plate and the copper plate with ratio 1:1 PPy@NFC in PVA for dialysis-free bacterial cellulose.....	89
Figure 4.33. TEM images of (1) PPy@NCC from dialyzed hardwood pulp, (2)	

PPy@NFC from dialysis-free hardwood pulp, (3) PPy@NCC from dialysed Whatman filter paper, (4) PPy@NFC from dialysis-free Whatman filter paper, (5) PPy@NCC from dialysed bacterial cellulose and (6) PPy@NFC from dialysis-free bacterial cellulose.....90

Figure 4.34. Linear relationship based on Ohm’s law for all sample showing the change in current as voltage is applied.....92

Figure 4.35. SEM image of PPy@NCC of dialysed hardwood pulp in PVA with ratio 1:1 (a) before applied voltage and (b) after applied voltage for resistivity testings.....95

Figure 4.36. SEM image of PPy@NFC of dialysis-free hardwood pulp in PVA with ratio 1:1 (a) before applied voltage and (b) after applied voltage for resistivity testings.....95

Figure 4.37. SEM image of PPy@NCC of dialysed Whatman filter paper in PVA with ratio 1:1 (a) before applied voltage and (b) after applied voltage for resistivity testings.....95

Figure 4.38. SEM image of PPy@NFC of dialysis-free Whatman filter paper in PVA with ratio 1:1 (a) before applied voltage and (b) after applied voltage for resistivity testings.....96

Figure 4.39. SEM image PPy@NCC of dialysed bacterial cellulose in PVA with ratio 1:1 (a) before applied voltage and (b) after applied voltage for resistivity testings.....96

Figure 4.40. SEM image of PPy@NFC of dialysis-free bacterial cellulose in PVA with ratio 1:1 (a) before applied voltage and (b) after applied voltage for resistivity testings.....96

LIST OF SCHEMES

Scheme 1.1. Schematic representation of the cellulose fibre with crystalline and non-crystalline regions.....2

Scheme 3.1. Schematic illustration for the *in-situ* doping synthesis of conductive PPy@NC nanohybrid.....46

Scheme 4.1. Schematic diagram showing the illustrated 3-dimensional sections of the film.....84

LIST OF TABLES

Table 2.1. The average concentration for all nanocellulose samples.....27

Table 2.2. Summary of average length, width and aspect ratio distribution with standard deviation for each sample.....35

Table 3.1. Quantity of materials used for varying ratio of polypyrrole to nanocellulose.....45

Table 3.2. Mass of sample obtained for various ratios.....47

Table 3.3 Quantity of materials used for all samples polypyrrole: nanocellulose at ratio 1:1.....49

Table 3.4. Mass of PPy@NC at ratio 1:1 sample obtained.....51

Table 4.1. Quantities of mass, volume, density and thickness of varying ratios.....80

Table 4.2. The resistivity calculations for ratios 0:0, 0:1, 1:2, 1:1, 2:1 and 1:0.....85

Table 4.3. Calculations of mass volume and density of all samples.....91

Table 4.4. The resistivity calculations for all variations of samples.....93

CHAPTER 1

1. INTRODUCTION

The cellulose (Latin: rich in small cells) polymer is a linear homo-polysaccharide consisting of D-anhydroglucopyranose units (AGU) linked together by β -1,4-glycosidic bonds.^[1] Every other AGU is rotated by 180° with respect to its neighbour and the two AGUs next to each other form a cellobios unit. The smallest repeating unit in the polymer is shown in Figure 1.1 where the reducing end group can be either a free hemiacetal or an aldehyde.

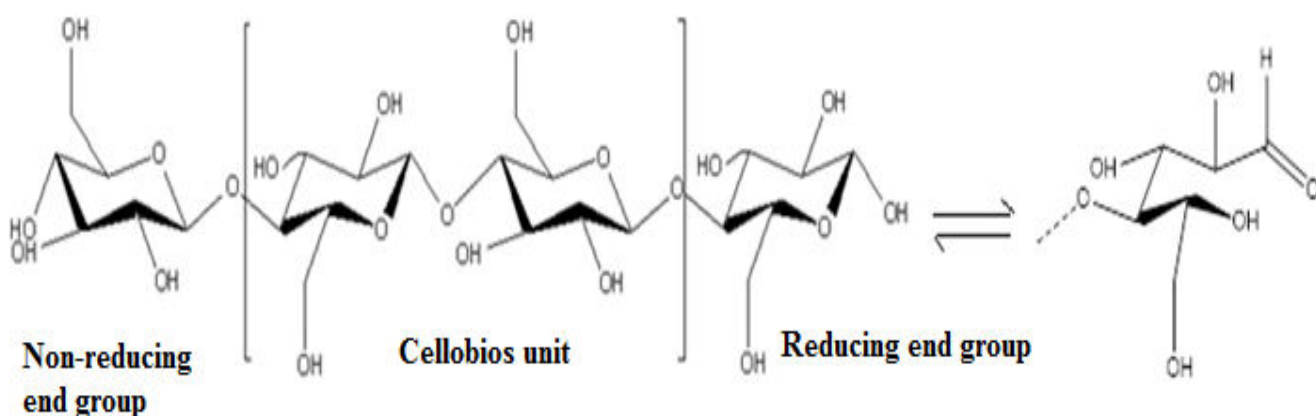
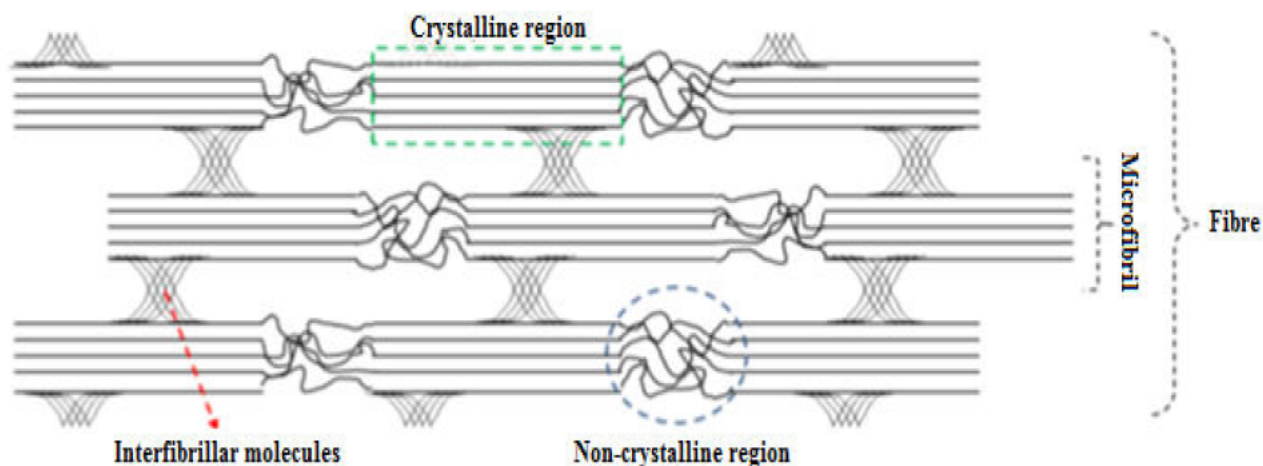


Figure 1.1. The molecular structure of a cellulose polymer where the cellobios is the smallest repeating unit in the polymer.^[1]

Cellulose is readily available, renewable, and does not compete with the food supply. Cellulose is not soluble in most solvents and is very resistant to chemical and biological transformations.^[2] Due to the hierarchical structure of cellulose, nanoparticles can be extracted from this naturally occurring polymer.^[3] When hydrolysed, cellulose yields a nano-structured cellulose, or so-called nanocellulose (NC), also variously termed nanocrystals, -whiskers, -rods, -fibrils, or nanofibers, loosely defined as when the cellulose fibre or crystal that has at least one dimension under 100 nanometres (nm).^[4,5] Scheme 1.1 is a representation of part of a cellulose fibre where the crystalline and non-crystalline regions are shown.



Scheme 1.1. Schematic representation of the cellulose fibre with crystalline and non-crystalline regions.^[1]

Acid hydrolysis is a process in which a protic acid is used to catalyse the cleavage of a chemical bond by a nucleophilic substitution reaction, with the addition of the elements of water.^[6] Upon acid hydrolysis on cellulose, Figure 1.2, sulphate groups form on the nanocellulose surface following the hydrolysis reaction.^[7] The nanocellulose suspensions form a chiral nematic ordered phase beyond a critical concentration, whereby the suspensions transform from an isotropic to an anisotropic chiral nematic liquid crystalline phase.^[3] Nano-fibrous cellulose (NFC) are unlike nanocrystalline cellulose (NCC) in terms of size and shape. When cellulose is subjected to dialysis treatment, it produces a nanocrystalline phase of cellulose, while NFC preserves the non-crystalline parts as longer length of the fibrils. NFC molecules are stabilized by hydrogen bonds between the hydroxyl groups in the cellulose polymer.

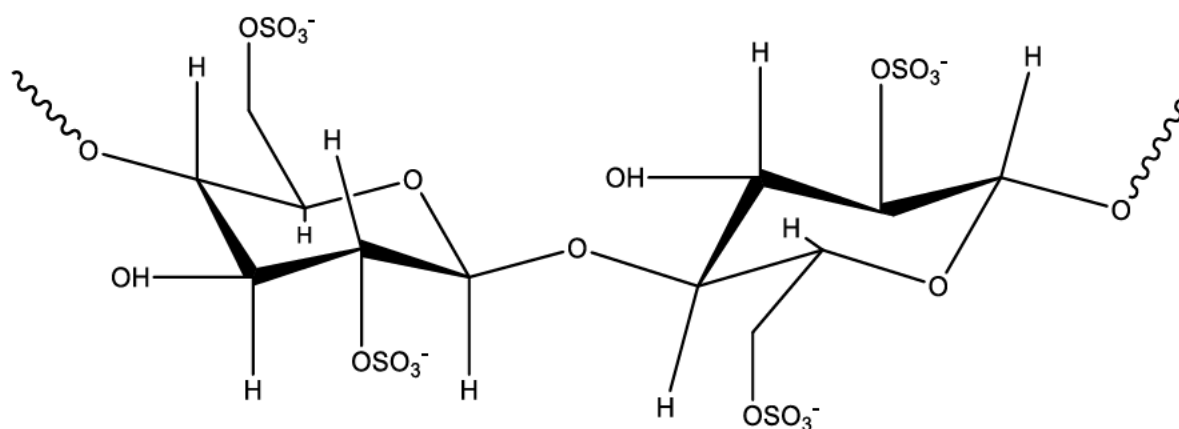


Figure 1.2. Formation of sulphate group on the nanocellulose surface, after hydrolysis reaction.

Due to the high natural abundance, high strength and stiffness, low weight and biodegradability, nano-scale cellulose fibre materials; micro-fibrillated cellulose, and bacterial cellulose serve as promising candidates for producing bio-nanocomposites.^[8] When subjected to acid hydrolysis, cellulose microfibrils undergo transverse cleavage along the amorphous regions and upon sonication a rod-like material, referred to as cellulose whiskers form.^[9] The almost perfect crystalline arrangement of cellulose whiskers, the nanocellulose has a high modulus and therefore significant potential as a reinforcing material.^[8]

Today, various renewable biomass resources are no longer waste material but have commercial value when used as nanomaterial. Work conducted on fruit shells were found to have nanocellulose content that could be used as nanomaterials.^[10] Bamboo cellulose was also previously used as a source of nanocellulose with individual bamboo nanorods having a 30% yield.^[11] The preparation of cellulose nanocrystals from wastepaper was also reported as an environmental friendly approach of source material, which can be a high availability and low-cost precursor for cellulose nanomaterial processing. Alkali and bleaching treatments were used for the extraction of cellulose particles followed by controlled-conditions of acid hydrolysis for the isolation of NC.^[12] Discarded cigarette filter shows great cellulose content where the main chemical constituent in the cigarette filter is plasticized cellulose acetate from which nanocellulose can be isolated.^[13] NC is currently a highly sought after biopolymeric nanomaterial which can be isolated from plant, animal and bacterial sources.^[14] There is great economic benefits in using nanocellulose for various applications due to the distinctive properties it possess such as biocompatibility, biodegradation, high strength, specific surface area, high crystallinity index, low toxicity and density.^[15-19]

Wood is one of the most commonly used sources of nanocellulose. The crystalline section of the semi-crystalline cellulose chains found in the plant cell walls have high potential as reinforcing agents for polymers.^[20] The mechanical extraction of nanofibers from wood dates back to the 1980s when micro-fibrillated cellulose from wood pulp was produced using cyclic mechanical treatment in a high-pressure homogenizer.^[21-23] The homogenization process resulted in fragmentation of the wood pulp and a material in which the fibres were opened into their sub-structural microfibrils.^[24] The resulting gels consisted of strongly entangled and disordered networks of cellulose nanofiber.^[25] A potential source of cellulose is hardwood pulp due to its high cellulose content.^[26] Cellulose fibres are present in all plant cell walls as

hemicelluloses, lignin, and extractives.^[27] There are two types of wood species viz. hard- and softwoods, with difference in their anatomical features.^[28] The main difference being that the failure strain for cellulose films made from soft woods increase during the processing whilst remaining constantly low for hardwood cellulose films, making hardwood pulp more desirable.^[29] The use of hardwood as a source for nanocellulose shows positive benefits to the economy and to the environment since the reusing and recycling of material conserves the available natural resources, saves energy, reduces greenhouse gas emissions, and free up landfill space. One other commonly known use of such networks is laboratory Whatman filter paper which is easily available. Filter paper shows richness in cellulose content that is easily extracted. It has been previously proven that cellulose nanoparticles from filter paper could be used as fillers to improve mechanical and barrier properties of biocomposites.^[30] Paper based nanocellulose was strategically re-engineered for its cellulose fibres to be applied as advanced energy storage systems and electronic devices.^[31] This research describes the extraction of NC from both filter paper and hardwood pulp due to the high yielding cellulosic source.

In addition to plant sources, cellulose fibers are secreted extracellularly by certain bacteria belonging to the genera *Acetobacter*, *Agrobacterium*, *Alcaligenes*, *Pseudomonas*, *Rhizobium*, or *Sarcina*.^[32,33] The most efficient producer of bacterial cellulose (BC) is *Acetobacter xylinum* (*Gluconacetobacter xylinus*), a gram-negative strain of acetic-acid-producing bacteria.^[34] BC is secreted as a ribbon-shaped fibril, less than 100 nm wide, which is composed of much finer 2–4 nm nanofibrils.^[34,35] In contrast to the existing methods for obtaining nanocellulose through mechanical or chemo-mechanical processes, BC is produced by bacteria through cellulose biosynthesis and the building up of bundles of microfibrils.^[36] These microfibril bundles have excellent intrinsic properties due to its high crystallinity which can reach up to 84–89%,^[37] with a reported elastic modulus of 78 GPa.^[38] Compared to plant based cellulose, BC also possesses higher water holding capacity, higher degree of polymerization (up to 8,000), and a finer web-like network.^[39-41] In addition, BC is produced as a highly hydrated and relatively pure cellulose membrane and therefore no chemical treatments are needed to remove lignin and hemicelluloses, as is the case for plant cellulose.^[42] This is a more environmentally friendly process as well as being more cost effective. Bacterial cellulose has various benefits due to the highly pure nanoparticle material. Bacterial cellulose has shown great benefits in drug delivery and wound dressing in the healthcare sector where the cellulose is used as a membrane system to administer antibiotics and antiseptic drugs.^[43-45] Also, bacterial nanocellulose paper was used as a supercapacitor which demonstrated high flexibility, desirable

electrochemical properties, as well as improved mechanical integrity by exploitation of bacterial cellulose unique properties.^[46] For this study, the use of Kombucha tea and its culture to produce natural pure cellulose has been utilized.^[47] Kombucha is a fermented lightly effervescent sweetened black or green tea drink. It is commonly intended as functional beverages for its proposed health benefits. Kombucha is produced by fermenting tea using a "symbiotic 'colony' of bacteria and yeast" (SCOBY).^[48] Contributing microbial populations in SCOBY cultures may vary, but the yeast component generally includes *Saccharomyces* and other species, and the bacterial component *Gluconacetobacter xylinus* to oxidize yeast-produced alcohols to acetic and other acids.^[49] Using the SCOBY produced from kombucha tea one may simply convert a simple sugar solution to pure cellulose whereby, when dried possessing a 'leather-like' textile known as a microbial cellulose leather.

Nanocellulose is an interesting building block for functional materials with mechanical robustness, large surface area and biodegradability.^[50] NC is a valuable renewable nanomaterial and offers great promise in varying applications, including valuable chemicals, as polymer reinforcement, as enzyme immobilization, catalyst support, and more.^[51-54] Through the modification of NC, a wide range of differing functionalities with outstanding properties, and improved properties can exist. This makes NC a versatile and exciting material to work with. Due to its nanoscale dimensions and fundamental physicochemical properties, NC is a renewable biomaterial that can be used as a supporting component in various high-performance nanocomposites.^[55] New nanocomposite materials with desirable properties can be obtained by incorporating NC into natural and even synthetic polymeric matrices. Simple chemical modification on NC surface improves its ability to disperse in different solvents and expand the utilisation in nano-applications, such as drug delivery, protein immobilisation, and as an inorganic reaction template.^[56]

The enriched surface active groups, aspect ratio and specific surface area, water dispersibility, strong, lightweight, and most importantly the environmental sustainability are the most desirable properties of NC.^[57] Acid hydrolysis for bulk production of cellulose to NC was developed in the 1950s, and this method was the most viable process for producing NC due to the convenience and controlled treatment.^[58] The nanoparticles are stabilised in aqueous suspension by negative charges on the surface produced from the acid hydrolysis process.^[9] During the controlled acid hydrolysis process, the amorphous region of cellulose is susceptible to hydrolysis.^[59] It is hydrolysed into soluble sugars with small molecular weight, leaving the crystalline regions intact, which is the NCC. The nanomaterials are isolated from the waste

hydrolysate *via* centrifugation and dialysis to remove the soluble sugars and residual acids. However, one drawback of this method is that the dialysis process is both time and water consuming, making this process less environmentally friendly, and raising production costs.^[60] Furthermore, a safe procedure for the disposal of the residual hydrolysis acid is yet to be found making large scale production of NCC and its nanocomposites derivatives restricted. Therefore, the need for a dialysis-free method of producing NCC should be investigated as an alternative production method. Hence the development for an economic and ecological friendly attempt to synthesise NC *via* a dialysis-free method is sought. A sustainable and eco-friendly source for obtaining cellulose has always been a challenge. In this research a new method of producing the nano-scaled fibres from cellulose without the dialysis step was achieved and a comparison to the conventional nanocellulose synthesis was performed. An application was needed whereby the excess sulphuric acid moieties on the surface of the cellulose do not negatively affect the characteristics of the material, but rather enhances its properties.

The nanocellulose samples were characterized mainly by FT-IR analysis, SEM-EDS and TEM. The negatively charged nanocellulose rods present challenges for characterisation of particle size distribution and surface area.^[61] TEM imaging was used in conjunction with ImageJ software where the average length and width distribution was measured from 250 random nanoparticles images taken. The average dimensions, and aspect ratio can thus be calculated as shown in Equation (1).

$$\text{Aspect ratio} = \frac{\text{Length}}{\text{width}} \quad (1)$$

An area of interest for nanocellulose is in composite materials applications where the high aspect ratio and flexible fibrils are suitable for use as reinforcement in a polymer matrix. For example, in the production of Polypyrrole-Nanocellulose (PPy@NC) composite synthesized from NCC and NFC was prepared for electrical conductivity and was compared. This involves pyrrole as a monomer which allows for electrical conductance upon polymerization. Pyrrole is five-membered heterocyclic aromatic organic compound with the formula C₄H₄NH as seen in Figure 1.3. It is a colourless, volatile liquid that darkens readily upon exposure to air.

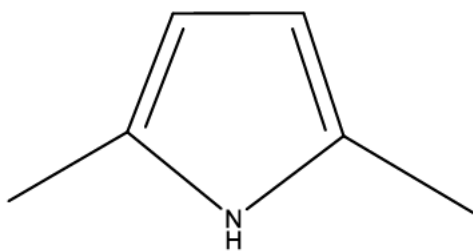


Figure 1.3. Structure of pyrrole.

PPy is a conjugated conducting polymer due to the electrons moving along the polymer chains and across the inter-chains due to the conjugated backbone.^[62, 63] The electronic conductivity of PPy switches between the conducting and the insulating states through doping and undoping cycles.^[64] PPy can be prepared by chemical or electrochemical oxidation in an aqueous media or in an organic solvent with various electrolytes.^[65] Thus, PPy shows a variety of physical and spectroscopic characteristics which can be easily obtained by changing its preparation conditions. It was found that the decrease of the electrical conductivity in air of polypyrroles show a decrease due to oxidative degradation which follow a first-order kinetics.^[64] The decrease of the conductivity is larger for the chemically synthesized polypyrrole than for the electrochemically synthesized one because of the larger surface area of the polymer particles in the former. Extensive effort, time and dedication has been invested in finding a novel, reproducible method for improving the stability of PPy. One way in which the stability can be enhanced is by forming a nanohybrid using nanocellulose.^[66] This incorporation enhances the stability of PPy in mechanical structure and conductivity.

PPy has exhibited potential applications as energy-storage devices,^[67] biomaterials,^[68] conducting films,^[69] and optical pH indicators.^[57, 70] Fortunately, the poor mechanical strength, processability, dispersibility and the low surface area of polypyrrole are significantly improved by incorporation of nanocellulose. Nanocellulose is a good template for the polymerization of a pyrrole monomer forming a connected network.^[71] Nanocellulose acts as a biotemplate and direct the growth of the nanohybrid with high aspect ratio and excellent dispersity^[60] which enable the fabrication of a 3D hierarchical multiscale conductive structure in polyvinyl alcohol (PVA) matrix. There exists excellent suspension stability of the composite in a medium such as polyvinyl alcohol, which facilitate the construction of continuous PPy@NC conductive network in the matrix. This polymer was suspended in polyvinyl alcohol (PVA) as a medium to be effectively utilized in its application. Polypyrrole polymer is formed by the polymerization of pyrrole by ferric trichloride as seen in Figure 1.4.^[72] The synthesized PPy@NC was *in situ* doped

by the residual hydrolysis acid to obtain the PPy@NC nanohybrid electrical conductivity.^[57] The PPy@NC nanohybrid was easily isolated from the polymerization products due to the decreased surface charge.

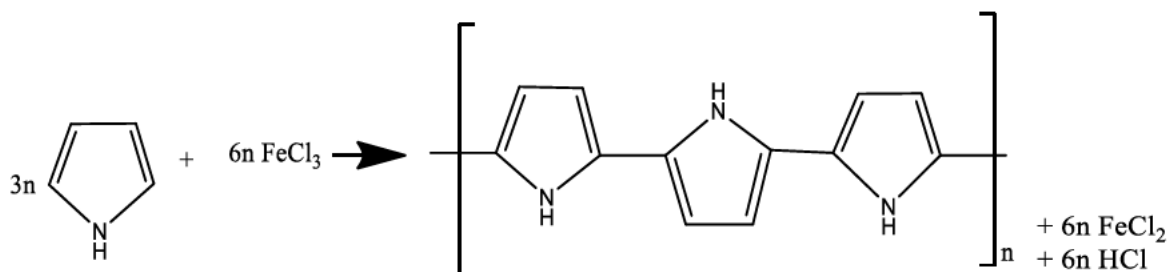


Figure 1.4. The polymerisation of polypyrrole.

A four-point probe is generally used to test for resistivity.^[73] Too often a four-point probe is not easily available for many laboratories use. An alternate method to successfully measure the resistance is thus required. It was found that simply measuring the current with an amp meter and the voltage by a volt meter, the resistance can be determined. To verify this method as an acceptable use, the samples will also be tested using a four-point probe and the results will be compared. The resistivity, also known as the specific electrical resistance, is a measure of how strongly a material opposes the flow of electric current. The lower the resistivity, the more readily the sample allows the flow of electric current. The electrical resistance of the sample is defined as the ratio of the voltage applied to the electrical current which flows, given by Equation (2):

$$R = \frac{V}{I} \quad (2)$$

where R is the resistance, V the voltage and I the current. When the resistance is constant over a range of voltage, it obeys Ohm's law whereby $I = \frac{V}{R}$ can be used to predict the behaviour of the sample. Whether the sample does obey Ohm's law or not, its resistance can be described in terms of its bulk resistivity where resistivity is temperature dependant. Polypyrrole has ohmic conductor properties,^[74] where the electronic conductivity of PPy switches between the conducting and the insulating states through doping and undoping cycles.^[64, 75]

1.1. Problem identification

The problem identified in this nanocellulose study was i) finding a source of cellulose that is fully renewable and eco-friendly, ii) removing the time- and water consuming dialysis step; dialysis made the process less environmentally friendly and raised costs. The need for research in exploiting the characteristics of dialysis-free NC is highlighted. Furthermore, a safe procedure for the disposal of the residual hydrolysis acid is yet to be found making large scale production of NCC and its nanocomposites derivatives restricted. Therefore, the need for a dialysis-free method of producing NC becomes necessary.

1.2. Purpose of the study

Cellulose is an inexhaustible raw material derived from nature with a biomass of 1.5 tera tons per year.^[57] NC comes from natural cellulose fibers by controlled acid hydrolysis. This has attracted much attention due to its versatile and unique properties such as enriched active groups, high aspect ratios and specific surface area, good water dispersibility, outstanding mechanical properties such as strength whilst being light weight. For these reasons one of the main attractions in this study is its sustainable and environmentally friendly protocols. This makes NC widely used in numerous applications such as polymer reinforcement, enzyme immobilization, catalytic support, drug delivery and much more.^[57] Therefore, the need for such novel design is in demand, and this project will utilize nanocellulose in combination with polymers to obtain novel composites with unique electrical properties.

1.3. Aims of the study

1. The aims of this study are to: Investigate the possibilities of an environmentally sustainable, low-cost and scalable approach to synthesize nanocellulose from a variety of sources.
2. To form polymer@nanocellulose nanohybrids from renewable resources.
3. To compare a dialysis method to a dialysis-free method in the production of nanocellulose composites.
4. To use the composite for application in *in situ* doping and measure conductive properties.

1.4. The objectives of this project are as follows:

1. The main objective of this project was to form nanocellulose from two methods described in literature, i.e. dialysis method and a dialysis free method.
2. Nanocellulose was isolated from renewable resources such as bacterial cellulose, filter paper and hardwood pulp making this design sustainable and eco-friendly.
3. Avoided the time-consuming dialysis step (4-6 days) formed an important part of the study. The comparative alternate route taken for this formation avoids the dialysis step, whereby the nanocrystalline cellulose was obtained *via* a dialysis-free method.
4. Further reactions was performed for surface modification whereby an *in situ* doping of polypyrrole using nanocellulose as a stabilizer was synthesized for a more connective network with improved dispersal of the polymer which thus enhances the electrical conductivity outcome.
5. Also, for the investigation of electrical properties of the composite using PVA as a medium to form a constructive, rigid network.

1.5. Important research questions to be addressed include:

- What are the various renewable resources and methods that can be employed to obtain cellulose that meets required standards?
- Can a dialysis-free synthesis method be successfully developed for NC?
- Can the NC be modified to give measurable and improved electrical properties?

1.6. Overview

This dissertation has been separated into separate chapters 2-5 each containing an Introduction, Experimental procedure, Results and discussion and References with regards to the appropriate topics covered.

Chapter 2 describes the three sources of cellulose studied: Bacterial grown cellulose, Whatman filter paper and hardwood pulp. These three sources are then sub divided into two

methods used in literature, dialysis and a dialysis-free method. All characterizations and comparisons are described for each source of cellulose.

Chapter 3 describes the production of the polypyrrole and nanocellulose hybrid with all characterizations.

And Chapter 4 describes the distribution of the nanohybrid in PVA as a continuous network with all electrical testing.

With Chapter 5 as an overall conclusion and summation.

1.7. References

1. Börjesson, M., Westman, G., *Crystalline Nanocellulose — Preparation, Modification, and Properties*, in *Cellulose - Fundamental Aspects and Current Trends*, 2015, InTech: Rijeka.
2. Rinaldi, R. Schüth, F., *Acid hydrolysis of cellulose as the entry point into biorefinery schemes*. *ChemSusChem*, 2009, **2**, 1096-1107.
3. Dufresne, A., *Nanocellulose: a new ageless bionanomaterial*. *Materials Today*, 2013, **16**, 220-227.
4. Chirayil, C.J., L. Mathew. L., Thomas, S., *review of recent research in nano cellulose preparation from different lignocellulosic fibers*. *Reviews on advanced materials science*, 2014. **37**.
5. Charreau, H., M. L Foresti, M. L., Vázquez. A., *Nanocellulose patents trends: a comprehensive review on patents on cellulose nanocrystals, microfibrillated and bacterial cellulose*. *Recent patents on nanotechnology*, 2013, **7**, 56-80.
6. Fan, L., Gharpuray. M. M., Lee. Y. H., *Acid hydrolysis of cellulose*, in *Cellulose Hydrolysis*, Springer, 1987, 121-148.
7. Mandal, A., Chakrabarty. D., *Isolation of nanocellulose from waste sugarcane bagasse (SCB) and its characterization*. *Carbohydrate Polymers*, 2011, **86**, 1291-1299.
8. Siró, I., Plackett, D., *Microfibrillated cellulose and new nanocomposite materials: a review*. *Cellulose*, 2010, **17**, 459-494.
9. Elazzouzi-Hafraoui, S., *The shape and size distribution of crystalline nanoparticles prepared by acid hydrolysis of native cellulose*. *Biomacromolecules*, 2007, **9**, 57-65.

10. Bano, S., Negi, Y. S., *Studies on cellulose nanocrystals isolated from groundnut shells*. Carbohydrate polymers, 2017, **157**, 1041-1049.
11. Brito, B.S., *Preparation, morphology and structure of cellulose nanocrystals from bamboo fibers*. Cellulose, 2012, **19**, 1527-1536.
12. Danial, W.H., *The reuse of wastepaper for the extraction of cellulose nanocrystals*. Carbohydrate polymers, 2015, **118**, 165-169.
13. Ogundare, S.A., Moodley, V., van Zyl, W. E., *Nanocrystalline cellulose isolated from discarded cigarette filters*. Carbohydrate polymers, 2017, **175**, 273-281.
14. Wei, H., *Environmental science and engineering applications of nanocellulose-based nanocomposites*. Environmental Science: Nano, 2014, **1**, 302-316.
15. Cowie, J., *Market projections of cellulose nanomaterial-enabled products*. Tappi Journal, 2014, **13**.
16. Lin, N., Huang, J., Dufresne, A., *Preparation, properties and applications of polysaccharide nanocrystals in advanced functional nanomaterials: a review*. Nanoscale, 2012, **4**, 3274-3294.
17. Habibi, Y., *Key advances in the chemical modification of nanocelluloses*. Chemical Society Reviews, 2014, **43**, 1519-1542.
18. Moon, R.J., *Cellulose nanomaterials review: structure, properties and nanocomposites*. Chemical Society Reviews, 2011, **40**, 3941-3994.
19. Habibi, Y., Lucia, L. A., Rojas, O. J., *Cellulose nanocrystals: chemistry, self-assembly, and applications*. Chemical reviews, 2010, **110**, 3479-3500.
20. Ng, H.-M., *Extraction of cellulose nanocrystals from plant sources for application as reinforcing agent in polymers*. Composites Part B: Engineering, 2015, **75**, 176-200.
21. Herrick, F.W., *Microfibrillated cellulose: morphology and accessibility*. in *J. Appl. Polym. Sci.: Appl. Polym. Symp.:(United States)*, ITT Rayonier Inc., Shelton, WA, 1983.
22. Turbak, A.F., Snyder, F. W., Sandberg. K. R., *Microfibrillated cellulose, a new cellulose product: properties, uses, and commercial potential*. in *J. Appl. Polym. Sci.: Appl. Polym. Symp.:(United States)*. ITT Rayonier Inc., Shelton, WA. 1983.
23. Klemm, D., *Nanocelluloses: a new family of nature-based materials*. Angewandte Chemie International Edition, 2011, **50**, 5438-5466.
24. Andresen, M., *Properties and characterization of hydrophobized microfibrillated cellulose*. Cellulose, 2006, **13**, 665-677.

25. Pääkkö, M., *Enzymatic hydrolysis combined with mechanical shearing and high-pressure homogenization for nanoscale cellulose fibrils and strong gels*. *Biomacromolecules*, 2007, **8**, 1934-1941.
26. Laka, M., S. Chernyavskaya, S., *Obtaining of microcrystalline cellulose from softwood and hardwood pulp*. *BioResources*, 2007, **2**, 583-589.
27. Pérez, J., *Biodegradation and biological treatments of cellulose, hemicellulose and lignin: an overview*. *International Microbiology*, 2002, **5**, 53-63.
28. Guillén, F., *Biodegradation of lignocelluloses: microbial, chemical, and enzymatic aspects of the fungal attack of lignin*. *International Microbiology*, 2005, **8**, 195-204.
29. Stelte, W., Sanadi, A. R., *Preparation and characterization of cellulose nanofibers from two commercial hardwood and softwood pulps*. *Industrial & engineering chemistry research*, 2009, **48**, 11211-11219.
30. Siqueira, G., Bras, J., Dufresne, A., *Cellulosic bionanocomposites: a review of preparation, properties and applications*. *Polymers*, 2010, **2**, 728-765.
31. Zheng, G., *Nanostructured paper for flexible energy and electronic devices*. *MRS bulletin*, 2013, **38**, 320-325.
32. El-Saied, H., Basta, A. H., Gobran, R. H., *Research progress in friendly environmental technology for the production of cellulose products (bacterial cellulose and its application)*. *Polymer-Plastics Technology and Engineering*, 2004, **43**, 797-820.
33. Deinema, M.H., Zevenhuizen, L., *Formation of cellulose fibrils by gram-negative bacteria and their role in bacterial flocculation*. *Archiv für Mikrobiologie*, 1971, **78**, 42-57.
34. Brown, E.E., Laborie, M. P. G., *Bioengineering bacterial cellulose/poly (ethylene oxide) nanocomposites*. *Biomacromolecules*, 2007, **8**, 3074-3081.
35. Iguchi, M., Yamanaka, S., Budhiono, A., *Bacterial cellulose—a masterpiece of nature's arts*. *Journal of materials science*, 2000, **35**, 261-270.
36. Nakagaito, A., Iwamoto, S., Yano, H., *Bacterial cellulose: the ultimate nano-scalar cellulose morphology for the production of high-strength composites*. *Applied Physics A*, 2005, **80**, 93-97.
37. Czaja, W., Romanovicz, D., Malcolm Brown, R., *Structural investigations of microbial cellulose produced in stationary and agitated culture*. *Cellulose*, 2004, **11**, 403-411.
38. Guhados, G., Wan, W., Hutter, J. L., *Measurement of the elastic modulus of single bacterial cellulose fibers using atomic force microscopy*. *Langmuir*, 2005, **21**, 6642-6646.

39. Klemm, D., *Nanocelluloses as innovative polymers in research and application*, in *Polysaccharides Ii*. Springer, 2006, 49-96.
40. Wan, W., *Bacterial cellulose and its nanocomposites for biomedical applications*, ACS Publications, 2006.
41. Barud, H.S., *Self-supported silver nanoparticles containing bacterial cellulose membranes*. *Materials Science and Engineering: C*, 2008, **28**, 515-518.
42. Barud, H., *Thermal characterization of bacterial cellulose–phosphate composite membranes*. *Journal of Thermal Analysis and Calorimetry*, 2007, **87**, 815-818.
43. Moritz, S., *Active wound dressings based on bacterial nanocellulose as drug delivery system for octenidine*. *International journal of pharmaceutics*, 2014, **471**, 45-55.
44. Abeer, M.M., *A review of bacterial cellulose-based drug delivery systems: their biochemistry, current approaches and future prospects*. *Journal of Pharmacy and Pharmacology*, 2014, **66**, 1047-1061.
45. Müller, A., *The biopolymer bacterial nanocellulose as drug delivery system: investigation of drug loading and release using the model protein albumin*. *Journal of pharmaceutical sciences*, 2013, **102**, 579-592.
46. Kang, Y.J., *All-solid-state flexible supercapacitors fabricated with bacterial nanocellulose papers, carbon nanotubes, and triblock-copolymer ion gels*. *ACS nano*, 2012, **6**, 6400-6406.
47. Nguyen, V.T., *Characterization of cellulose production by a *Gluconacetobacter xylinus* strain from Kombucha*. *Current microbiology*, 2008, **57**, 449.
48. Kozyrovska, N.O., Reva, O. M., Goginyan, V. B., *Kombucha microbiome as a probiotic: a view from the perspective of post-genomics and synthetic ecology*. *Biopolymers and cell*, 2012, 103-113.
49. Jonas, R.F., Luiz F., *Production and application of microbial cellulose*. *Polymer Degradation and Stability*, **59**, 101-106.
50. Kumar, V., *Comparison of nano-and microfibrillated cellulose films*. *Cellulose*, 2014, **21**, 3443-3456.
51. Wu, X., *A novel reagentless approach for synthesizing cellulose nanocrystal-supported palladium nanoparticles with enhanced catalytic performance*. *J. Mater. Chem. A*, 2013, **1**, 8645-8652.
52. Benaissi, K., *Synthesis of platinum nanoparticles using cellulosic reducing agents*. *Green Chem.*, 2010, **12**, 220-222.

53. Rezayat, M., *Green One-Step Synthesis of Catalytically Active Palladium Nanoparticles Supported on Cellulose Nanocrystals*. ACS Sustainable Chem. Eng., 2014, **2**, 1241-1250.
54. Zhou, Z., *Cellulose nanocrystals as a novel support for CuO nanoparticles catalysts: facile synthesis and their application to 4-nitrophenol reduction*. RSC Adv., 2013, **3**, 26066-26073.
55. Youssef Habibi, L.A., *Cellulose Nanocrystals: Chemistry, Self-Assembly, and Applications*. pubs.acs, 2010, **110**, 3479–3500.
56. Peng, B.L., *Chemistry and applications of nanocrystalline cellulose and its derivatives: A nanotechnology perspective*. The Canadian Journal of Chemical Engineering, 2011, **89**, 1191-1206.
57. Zhang, X., *Dialysis-Free and in Situ Doping Synthesis of Polypyrrole@Cellulose Nanowhiskers Nanohybrid for Preparation of Conductive Nanocomposites with Enhanced Properties*. ACS Sustainable Chemistry & Engineering, 2015, **3**, 675-682.
58. Mukherjee, S. M. W., *X-ray and electron microscope studies of the degradation of cellulose by sulphuric acid*. Biochim. Biophys. , 2014, **Acta 1953**, 499–511.
59. Satyamurthy, P., *Preparation and characterization of cellulose nanowhiskers from cotton fibres by controlled microbial hydrolysis*. Carbohydrate Polymers, 2011, **83**, 122-129.
60. Zhang, X., *Dialysis-free and in situ doping synthesis of polypyrrole@ cellulose nanowhiskers nanohybrid for preparation of conductive nanocomposites with enhanced properties*. ACS Sustainable Chemistry & Engineering, 2015, **3**, 675-682.
61. Brinkmann, A., *Correlating cellulose nanocrystal particle size and surface area*. Langmuir, 2016, **32**, 6105-6114.
62. Liu, Y. C., Hwang, B. J., *Enhancement of conductivity stability of polypyrrole films modified by valence copper and polyethylene oxide in an oxygen atmosphere*. Thin Solid Films, 2000, **360**, 1-9.
63. Erlandsson, R., *XPS and electrical characterization of BF₄⁻-doped polypyrrole exposed to oxygen and water*. Synthetic metals, 1985, **10**, 303-318.
64. Chen, X., *The stability of polypyrrole electrical conductivity*. European polymer journal, 1994, **30**, 809-811.
65. Satoh, M., Kaneto, K., Yoshino, K., *Dependences of electrical and mechanical properties of conducting polypyrrole films on conditions of electrochemical polymerization in an aqueous medium*. Synthetic metals, 1986, **14**, 289-296.

66. Srivastav, S., *Understanding ionic transport in polypyrrole/nanocellulose composite energy storage devices*. *Electrochimica Acta*, 2015, **182**, 1145-1152.
67. Razaq, A., *Paper-Based Energy-Storage Devices Comprising Carbon Fiber-Reinforced Polypyrrole-Cladophora Nanocellulose Composite Electrodes*. *Advanced Energy Materials*, 2012, **2**, 445-454.
68. Gelmi, A., Higgins, M. J., Wallace, G. G., *Physical surface and electromechanical properties of doped polypyrrole biomaterials*. *Biomaterials*, 2010, **31**, 1974-1983.
69. Holdcroft, S., Funt, B. L., *Preparation and electrocatalytic properties of conducting films of polypyrrole containing platinum microparticulates*. *Journal of electroanalytical chemistry and interfacial electrochemistry*, 1988, **240**, 89-103.
70. de Marcos, S. Wolfbeis, O. S., *Optical sensing of pH based on polypyrrole films*. *Analytica chimica acta*, 1996, **334**, 149-153.
71. Tang, L., *Flexible conductive polypyrrole nanocomposite membranes based on bacterial cellulose with amphiphobicity*. *Carbohydrate polymers*, 2015, **117**, 230-235.
72. Shinde, S.S., *Morphological modulation of polypyrrole thin films through oxidizing agents and their concurrent effect on supercapacitor performance*. *Electrochimica Acta*, 2014, **119**, 1-10.
73. Smits, F., *Measurement of sheet resistivities with the four-point probe*. *Bell Labs Technical Journal*, 1958, **37**, 711-718.
74. Malhotra, U., Maity, S., Chatterjee, A., *Polypyrrole-silk electro-conductive composite fabric by in situ chemical polymerization*. *Journal of Applied Polymer Science*, 2015, **132**.
75. Panero, S., *Characteristics of Electrochemically Synthesized Polymer Electrodes VI. Kinetics of the Process of Polypyrrole Oxidation*. *Journal of The Electrochemical Society*, 1989, **136**, 3729-3734.

CHAPTER 2

2.1. Background

2.1.2. Bacterial grown cellulose

Present day research endeavours aim to utilize processes that reduce both environmental impact and production cost. Bacterial cellulose (BC), also called microbial cellulose, or biocellulose,^[1] show positive outcomes in these areas. BC has remarkable mechanical properties even though it contains up 99% water.^[2] Kombucha tea is used for the growth of the "symbiotic 'colony' of bacteria and yeast" (SCOBY)^[3] which produces pure cellulose in a Hestrin- Schramm (HS) medium.^[4] In SCOBY, the yeast component generally includes *Saccharomyces*, and the bacterial component consists of *Gluconacetobacter xylinus*, which is used to oxidize yeast-produced alcohols to acetic and other acids.^[5] Acetic acid bacterium such as *G. xylinum* can assimilate several sugars. BC is an extracellular polysaccharide secreted by the rod-shaped, aerobic gram-negative bacterium *Gluconacetobacter xylinus*.^[6] Figure 2.1 is a TEM image captured of the bacteria microorganism colony that facilitates the growth of the cellulose used in this study, which has a distinct nanofibrillar structure.

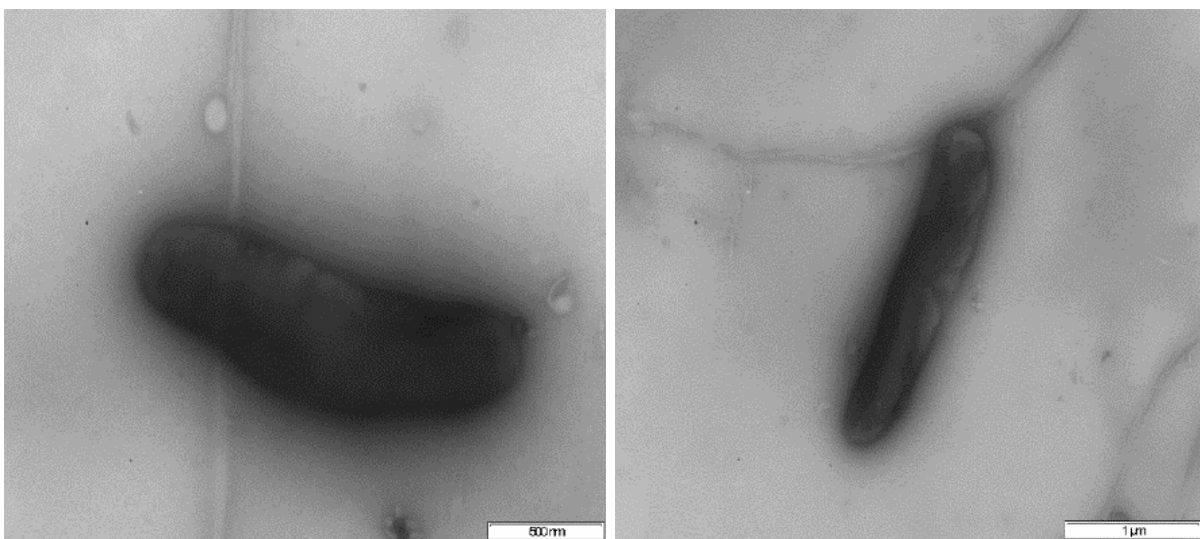


Figure 2.1. TEM image of the bacteria cells, *Gluconacetobacter xylinus*, from SCOBY responsible for the growth of cellulose.

The growth of NC from BC is a ‘bottom-up’ approach whereby the BC is being built up from the molecular level, rather than ‘top-down’ approach, i.e. broken down from another material. The BC has a dense surface on the air-exposed side, and a gelatinous layer on the aqueous-interaction side.^[7] Isolated BC is pure and does not contain lignin and hemicellulose like cellulose derived from plant matter.^[8] This is a positive characteristic since it makes BC a highly pure source of cellulose and reduces cost and time for purification yielding higher concentrations of nanocellulose compared to plant base cellulose. BC is also different from the plant equivalent due to a higher crystallinity index (above 60 %) and a different degree of polymerization (DP), usually between 2000 and 6000.^[6] Due to its unique properties, BC is being employed as biological material in many applications, such as the food industry,^[9] as wound-dressing materials,^[10] artificial skin,^[11] vascular grafts,^[12] scaffolds for tissue engineering,^[13] artificial blood vessels,^[14] and dental implants and is ever-growing in application.^[6] In BC the cellulase is a multicomponent enzyme which hydrolyze cellulose into smaller fragments, oligosaccharides, cellobiose or glucose, depending on a variety of parameters.^[15] This process starts with a random cleavage of the amorphous regions of the long cellulose microfibrils and give rise to several fractions of hydrolysis products.^[16] The crystalline regions of cellulose are more resistant to hydrolysis due to the presence of strong hydrogen bonding when compared to the less compacted amorphous regions.^[17] Bacterial cellulose and nanocellulose derivatives show remarkable mechanical properties, purity and straightforwardness in production, which has gained much interest over the years.

2.1.3. Whatman filter paper

Highly crystalline cellulose are found in renewable resources which are easily available, such as laboratory Whatman filter paper.^[18] Studies have shown that cellulose nanoparticles from Whatman filter paper could be used as fillers to improve mechanical and barrier properties of biocomposites.^[19] In previous studies, paper based nanocellulose was strategically re-engineered for its cellulose fibers to be applied to advanced energy storage systems and optoelectronic devices.^[20] Nanocellulose is emerging as a sustainable biomaterial with exceptional physicochemical properties^[21] by overcoming many obstacles that are commonly faced, such as time-consuming preparation procedures with very low yield, a highly hydrophilic surface, unavailability, poor dispersion due to the tendency to agglomerate, low thermal stability and most importantly higher cost through expensive sources.^[22] The use of Whatman filter paper as

a primary source of NC helps develop strategies that support the mechanical properties at the cost of eco-compatibility.^[22]

2.1.4. Hardwood pulp

The major component of wood from a deciduous (hardwood) tree consists of libriform fibers^[23] which can achieve good stiffness and bulking ability. Cellulose fibers are present in all plant cell walls as hemicelluloses, lignin, and extractives.^[24] Cellulose nanofibers can be isolated from wood pulps. Previously, nanocellulose was produced from hardwood pulp by combining refining and high-pressure homogenization techniques.^[25] There are two types of wood species viz. hard- and softwoods, with differences in their anatomical features.^[26] This difference is that the failure strain for cellulose films made from soft woods increased during the processing whilst it remained constantly low for hardwood cellulose films, making hardwood pulp more desirable.^[27] Hardwood fibers have a more rigid structure as compared to softwoods because of their higher Runkel ratios.^[27, 28] In this study, hardwood pulp was used as a source of nanocellulose. Hardwoods are more complex and heterogeneous in structure compared to softwoods and have specialized vessel elements.^[27] The present study utilizes this hardwood pulp as a primary source of cellulose and study the impact of mechanical fibrillation on the morphology the cellulose fibers to produce nanocellulose.

2.2. Experimental Procedure for Preparation of Nanocellulose

2.2.1. PREPARATION OF NANOCELLULOSE FROM BACTERIAL CELLULOSE

2.2.1.1. PREPARATION OF SCOBY

In a 600 mL sterilised beaker, 400 mL of Kombucha tea (bought from a health shop) was added (manufactured date: 14/03/2017). The beaker was covered with an air/water permeable cloth and left to develop for 10 days, Figure 2.2.



Figure 2.2. Image of the growth of SCOBY in a sample of Kombucha tea.

2.2.1.2. PREPARATION OF BACTERIAL CELLULOSE (BC) USING SCOBY

To a sterilised dish, 1 L of boiling H₂O was added followed by two Five Roses Green tea teabags. The solution was left to brew for 15 minutes and the teabags were then removed. White sugar (200 g) was added and stirred until dissolved. The temperature was monitored within the range 20-30° C. Apple cider vinegar (200 mL) was added followed by the SCOBY culture. The tray was covered with an air/water permeable cloth and left to develop for 14 days, see Figure 2.3, until most water content evaporated. The cellulose layer formed uniformly over the surface. The cellulose was washed with deionised water and bleach.

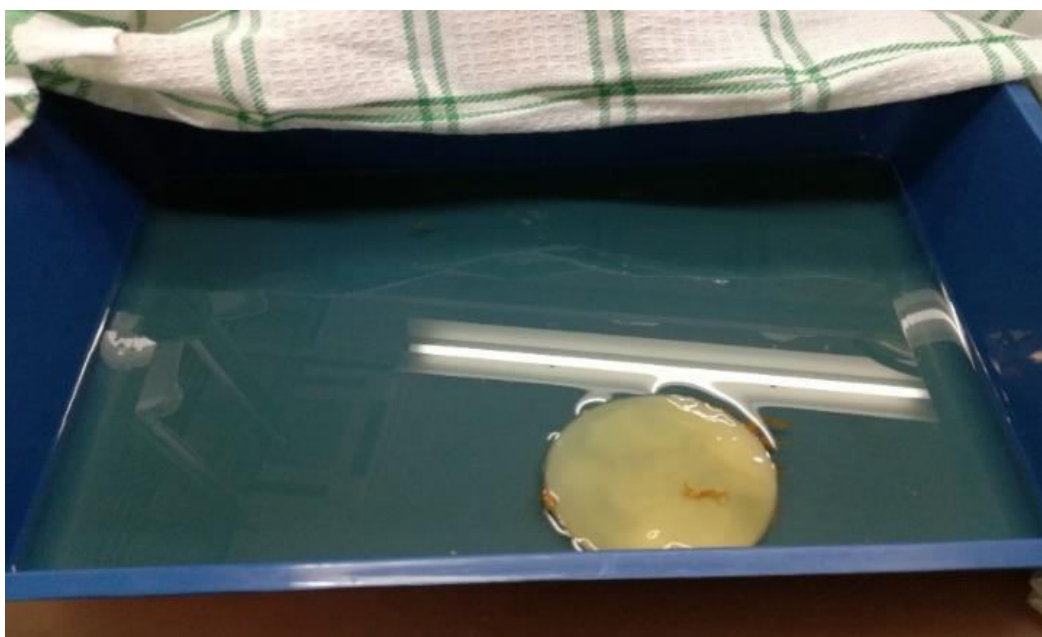


Figure 2.3. SCOBY in the required medium for BC growth.

2.2.1.3. PREPARATION OF BACTERIAL NANOCELLULOSE

The bacterial cellulose was easier to be broken down through hydrolysis when wet rather than when dry. Therefore, the wet sample's water mass was needed to give approximately 10 g of dry sample.

A mass of 1.013 g of wet bacterial cellulose was placed in a petri dish to dry overnight. Upon re-weighing, the mass of dry sample was 0.512 g indicating approximately 49.46% water in a gram of wet sample according to Equation (3):

$$\text{Percentage of water content} = \frac{\text{mass of wet sample} - \text{mass of dry sample}}{\text{mass of wet sample}} \times 100\% \quad (3)$$

A sample with wet mass of 20.01 g was cut into the size of approximately 10 mm × 10 mm × 10 mm, (9.90 g dry bacterial cellulose) and was washed under running water to remove any acetic acid that was previously added for preservation. To remove the bacterial cell debris, the BC was boiled in a 1 wt. % NaOH (1 g NaOH in 100 mL water) aqueous solution for 2 h and then washed with water, this procedure was repeated twice. BC was then neutralized with 0.2% acetic acid. Purified BC was homogenized using a pestle and mortar and then mixed with sulfuric acid to a

final sulfuric acid concentration of 60 wt. % (89.82 mL sulfuric acid in 110.18 mL water) using an acid-to-cellulose ratio of 20 mL/g; it was then stirred at 40 °C for 1 h and left to sit overnight. Thereafter the hydrolysis was stopped using 400 mL ddH₂O, two layers formed where the cellulose layer separated into the upper portion whilst an acidic yellow discoloured layer settled to the bottom. The upper layer was decanted and centrifuged at 4000 rpm for 5 mins and washed 3 times. The sample was sonicated for 30 min at room temperature and the suspension was then dialyzed to remove residual acid and hydrolysate of cellulose in the suspension whereby a dialysis sock was cut to size and the sample was filled in the tube. The result was monitored by checking the neutrality of the dialysate. After a five-day pH testing and water changing period, the water was measured to have a pH 6.38 and the dialysis was stopped. The average concentration of the NCC was measured where 2 mL of each sample was syringed onto a petri dishes and left to dry overnight.

2.2.1.4. PREPARATION OF NANOCELLULOSE FROM BACTERIAL CELLULOSE: DIALYSIS- FREE METHOD

Following the same procedure, a wet mass of 20.12 g (9.95% dry bacterial cellulose) was similarly subjected to hydrolyzation but instead of dialysing the sample. The hydrolysis product was centrifuged five times at 4000 rpm for 5 min. The average mass of the NFC was measured where 2 mL of each sample was syringed onto a petri dishes and left to dry overnight.

2.2.2. PREPARATION OF NANOCELLULOSE FROM WHATMAN FILTER PAPER

2.2.2.1. PREPARATION OF NANOCELLULOSE FROM WHATMAN FILTER PAPER- DIALYSIS METHOD

NCC were prepared by controlled acid hydrolysis of Whatman filter paper. A mass of 10.29 g Whatman filter paper (Qualitative circles 150 mm Cat No. 1001-150, Capital Lab Supplies cc) was shredded in a blender until it had the consistency of wool. The filter paper was mixed with sulfuric acid solution 64 wt.% (2 x 49 mL of H₂SO₄ was made to mark of 200 mL double distilled water). The mixture was stirred vigorously with a stirring bar on a magnetic heating mantle over an oil bath and heated to 45°C for 45 min. The suspension was diluted in 800 mL ddH₂O in a 1 L flask to stop the hydrolysis. The sample was centrifuged and washed with ddH₂O followed by

sonication for 30 min at room temperature. The suspension was then dialyzed to remove residual acid and hydrolysate of the cellulose in the suspension whereby a dialysis sock was cut to size and filled with the sample. The system was monitored by checking the neutrality of the dialysate. After a five-day period of pH testing and water changing, the water was measured to have a pH 6.45 and the dialysis was stopped. The average mass of the NCC was measured where 2 mL of each sample was syringed onto petri dishes and left to dry overnight.

2.2.2.2. PREPARATION OF NANOCELLULOSE FROM WHATMAN FILTER PAPER-DIALYSIS-FREE METHOD

For the dialysis-free method, the exact procedure was followed, a mass of 10.37 g was similarly subjected to hydrolyzation, but instead of dialyzing the sample, the hydrolysis product was centrifuged five times at 4000 rpm for 5 min. The average mass of the NFC was measured where 2 mL of each sample was syringed onto a petri dishes and left to dry overnight.

2.2.3. PREPARATION OF NANOCELLULOSE FROM HARDWOOD PULP

2.2.3.1. PREPARATION OF NANOCELLULOSE FROM HARDWOOD PULP-DIALYSIS METHOD

NCC were prepared by controlled acid hydrolysis of hardwood pulp. A mass of 10.11 g was shredded in a blender until it formed a consistency of wool. The filter paper was mixed with sulfuric acid solution 64 wt.% where 2 x 49 mL of H₂SO₄ was made to mark of 200 mL double distilled water. The mixture was stirred vigorously with a stirring bar on a magnetic heating mantle over an oil bath and heated to 45 °C for 45 min. The suspension was diluted in 800 mL ddH₂O in a 1 L flask to stop the hydrolysis immediately after hydrolysis. The sample was then centrifuged and washed four times with ddH₂O. The sample was then sonicated for 30 min. The suspension was then dialyzed to remove residual acid and hydrolysate of cellulose in the suspension whereby a dialysis sock was cut to size and the sample was filled in the tube. The result was monitored by checking the neutrality of the dialysate. After a five-day pH testing and water changing period, the water was measured to have a pH 4.60 and the dialysis was stopped.

The average mass of the NCC was measured where 2 mL of each sample was syringed onto two petri dishes and left to dry overnight.

2.2.3.2. PREPARATION OF NANOCELLULOSE FROM WHATMAN FILTER PAPER-DIALYSIS- FREE METHOD

For the dialysis-free method, following the exact procedure, a wet mass of 10.178 g was similarly subjected to hydrolyzation but instead of dialysing the sample, the hydrolysis product was centrifuged at 4000 rpm for 5 min, five times over. The average mass of the NFC was measured where 2 mL of each sample was syringed onto a petri dishes and left to dry overnight.

2.2.4. CHARACTERISATION

Fourier transform infrared spectroscopy (FT-IR)

Analyses were carried out at room temperature using a Perkin Elmer Spectrum 100 FTIR spectrometer and was recorded in the range 380-4000 cm^{-1} at a resolution of 4 cm^{-1} fitted with a Universal Attenuated Total Reflectance (ATR) sampling accessory (Perkin Elmer, USA). The data was processed using Spectrum® software. A small amount of the sample was placed onto the ATR crystal and a pressure of 120 psi was applied to ensure contact between the crystal and the catalyst material.

Morphological structure analysis

The morphology of all nanocellulose and bacterial cellulose as well as the bacteria of SCOBY was established with the aid of electron microscopic studies. For the TEM study, a JEOL-JEM 1010 (Japan) operating at 100 kV was used. TEM images of the sample were acquired using 5 μL of a 0.01 w/w% suspension of the sample deposited on a copper (Cu) TEM-grid. The deposited crystals on the TEM-grid were negatively stained after drying with 5 μL of 2 wt. % uranyl acetate for 5 minutes in the dark. The excess uranyl acetate solution was wicked off with the tip of filter paper and the stained crystals on the TEM-grid were dried. The dimensions of 250 randomly selected samples representing NC from the TEM micrographs were measured using ImageJ 1.42 software and the obtained data were processed on Origin® 9 software where the particle length, width and aspect ratio with respective standard deviation were generated.

For the SEM study, a Zeiss Ultra Plus field emission gun scanning electron microscope (FEGSEM) equipped with energy dispersive X-ray Spectroscopy (EDS) detector (Germany) was used. The samples for SEM images were deposited separately on conductive carbon tape stuck to aluminium stubs. Each sample was coated with gold with the aid of sputter coater to minimize charging.

Raman Spectroscopy

Raman spectra were measured using a Delta Nu Advantage 532 instrument fitted with a 532 nm laser source (green) and operated by NuSpec® software. Laser intensity, polarization and the integration time of the scans were varied until each sample gave clear and reproducible spectra. All analyses were carried out at room temperature with the powdered sample loaded in quartz tubes.

2.3. Results and Discussion

The grown bacterial cellulose consisted of a highly crystalline cellulose structure. The growth of the cellulose (Figure 2.3. a) showed a uniformity that could be manipulated by the shape of the container that held it. The width of the cellulose layer was measured to be 2.53 cm and expanded across the area of the container. The SCOBY could easily be removed and reused for growth in another sample. Since this BC grew in a tea based medium, it was slightly discoloured, but after bleaching in commercial detergent and multiple washes under cold running water, the BC possessed a bright white colour (Figure 2.4. b). The SEM images taken of the dried bacterial cellulose showed (Figure 2.5) that the dried cellulose has a uniform network.

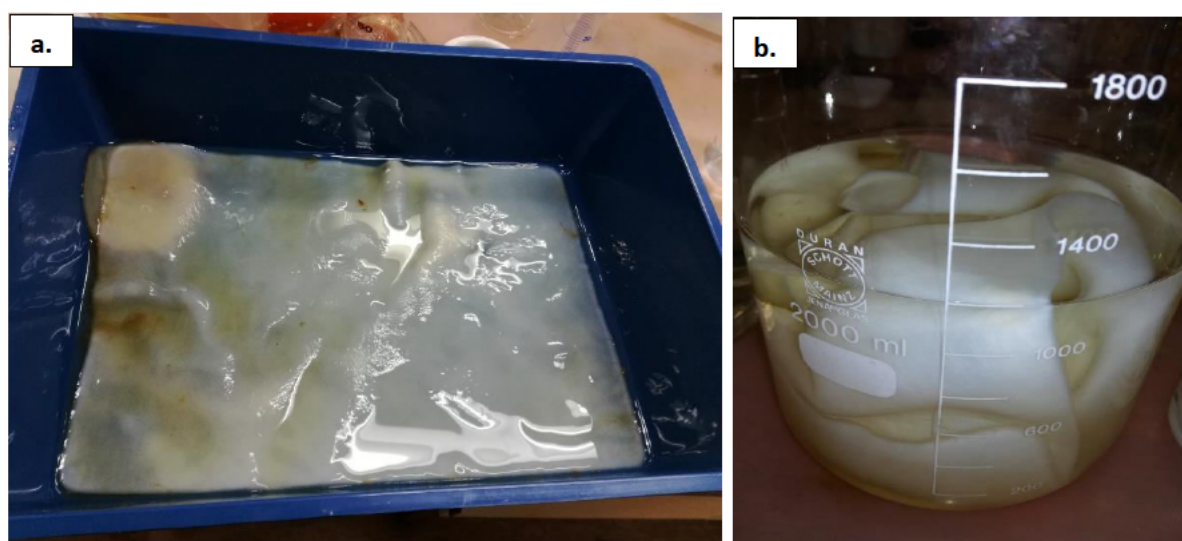


Figure 2.4. The BC after 2 weeks of growth (a) and after washing and bleaching (b).

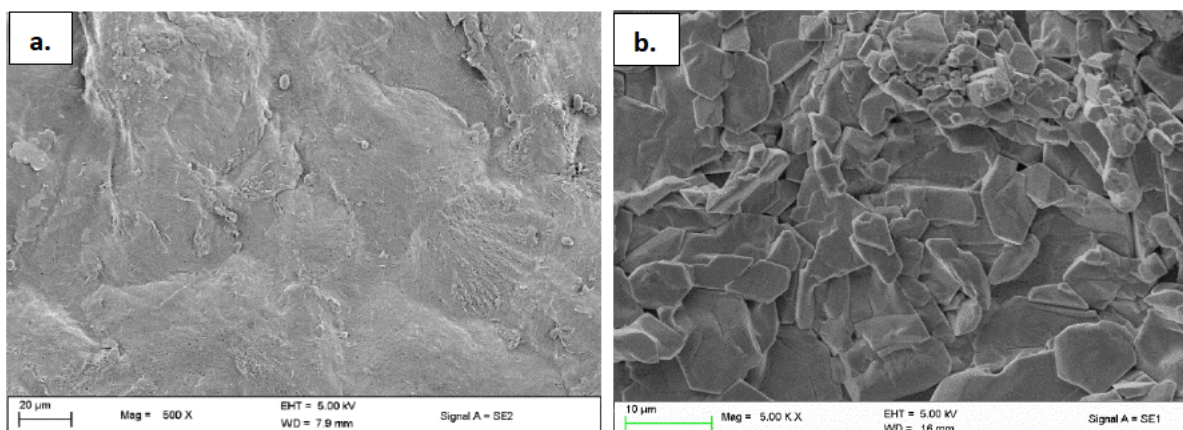


Figure 2.5. SEM image of dried Bacterial cellulose at 500 X magnification (a) and 5.00K X magnification (b).

The TEM images taken for the bacterial grown cellulose (Figure 2.6) indicated that the sample was the desired size and shape of cellulose and the experimental procedure induced growth of BC. The fibres seen under imaging were of unmeasurable length within the frame of the micrographs, even at low magnification. This result indicated that the cellulose fibres require additional modification to fit the desired nano-scale length and was thus subjected to acid hydrolysis.

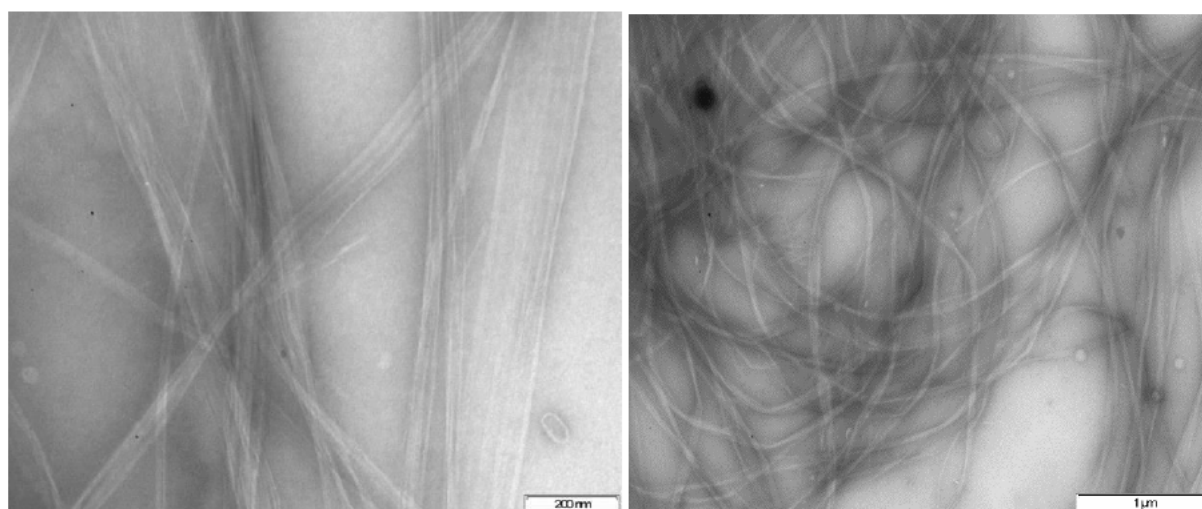


Figure 2.6. TEM image of negatively stained Bacterial cellulose.

It was noted that upon hydrolysis of the Bacterial cellulose, the rate of hydrolysis was much lower than that of other plant-based sources of cellulose. This was presumably due to the presence of strong hydrogen bonding that exists between bacterial cellulose fibres which prevent faster enzymatic hydrolysis. During this process, the enzyme slowly penetrates the inner layers of cellulose network and hydrolyse the amorphous regions of cellulose chains.

2.3.1. Average concentration of dialyzed and dialysis-free nanocellulose from bacterial grown cellulose, Whatman filter paper and hardwood pulp.

Upon drying a sample of 2 mL (x 2) NCC and 2 mL (x 2) NFC for each source, an average concentration was calculated as follows.

Average concentration of NCC from bacterial cellulose that was subjected to dialysis:

Mass of petri dish + NCC (1) /g : 47.6014

Mass of petri dish (1) /g: 47.5510

Mass of NCC (1) /g : 0.0504

Mass of petri dish + NCC (2) /g : 48.3840

Mass of petri dish (2) /g: 48.3195

Mass of NCC (2) /g : 0.0645

Average mass of NCC: $\frac{(0.0504+0.0645)\text{g}}{2} = 0.0575 \text{ g in } 2 \text{ mL}$

= 0.0288 g. mL⁻¹

= 28.80 mg. mL⁻¹

In the same way, the average concentration was calculated for the remaining samples summarized in Table 2.1.

Table 2.1. The average concentration for all nanocellulose samples.

Sample	Concentration mg.mL ⁻¹
Bacterial NCC	28.80
Bacterial NFC	29.30
Whatman paper NCC	28.50
Whatman paper NFC	28.60
Hardwood pulp NCC	24.50
Hardwood pulp NFC	26.30

It was evident that the concentration of NFC for bacterial nanocellulose, 29.30 mg. mL⁻¹ was higher than that of the concentration of NCC at 28.80 mg. mL⁻¹. The concentration of NFC for Whatman filter paper was calculated to be 28.60 mg.mL⁻¹, and was higher than that of the concentration of NCC at 28.50 mg.mL⁻¹. For hardwood pulp, the concentration of NFC, 26.30 mg. mL⁻¹, was higher than that of the concentration of NCC which 24.50 mg.mL⁻¹. These results are within similar ranges for the same standard of nanocellulose. It was noted that upon drying, the NFC (dialysis-free) did not form a crystalline film-like NCC (which was dialyzed). For all three sources, the NFC was a sticky substance that required to be scraped off the petri dish to be retrieved. The NCC, however, formed a transparent, flexible uniform layer that lifted off the petri dish easily. This is consistent with the characteristics of NC that is subjected to dialysis as compared to dialysis-free NC which still contains significant amount of sulfuric acid.

2.3.2. SEM-EDS imaging of dialyzed and dialysis-free nanocellulose from bacterial grown cellulose, Whatman filter paper and hardwood pulp.

A neat film of nanocrystalline cellulose from dialyzed bacterial cellulose, Whatman filter paper and hardwood pulp was observed where a well distributed layer was found, Figures 2.7. The film was readily removed from the petri dish, was strong enough to be analysed, but also flexible, and could bend. This was a positive characteristic for the sample since good mechanical strength was desired for polymer amalgamation. Under SEM imaging of the films, Figure 2.8., individual nano-whiskers were not well distinguished since the nanocellulose was tightly packed in a uniform crystalline layer. According to the SEM-EDS analysis, there was only carbon and oxygen present. The nanofibrous cellulose grown from bacterial cellulose, Whatman filter paper and hardwood pulp, not subjected to dialysis, dried as a mucilage with no crystalline structure and demonstrated the lack of uniformity. The nano-fibres were visible in the structure and according to the SEM-EDS, there was trace amounts of sulfur present due to sulfonate groups present on the surface of the nanocellulose.

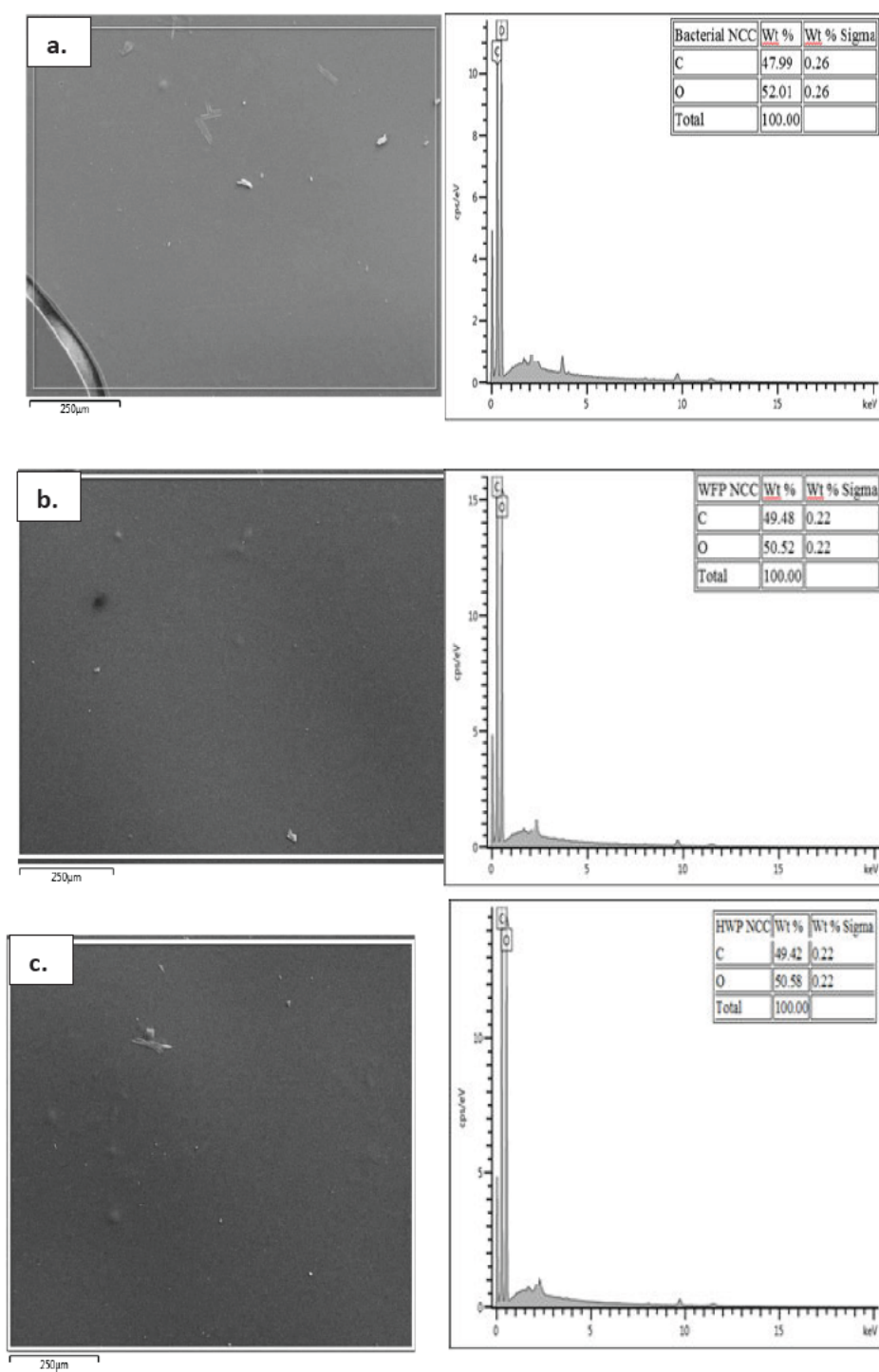


Figure 2.7. SEM image of (a) Bacterial nanocrystalline cellulose; (b) Whatman filter paper nanocrystalline cellulose and (c) Hardwood pulp nanocrystalline cellulose with corresponding EDS showing a neat well-constructed film with no disturbances.

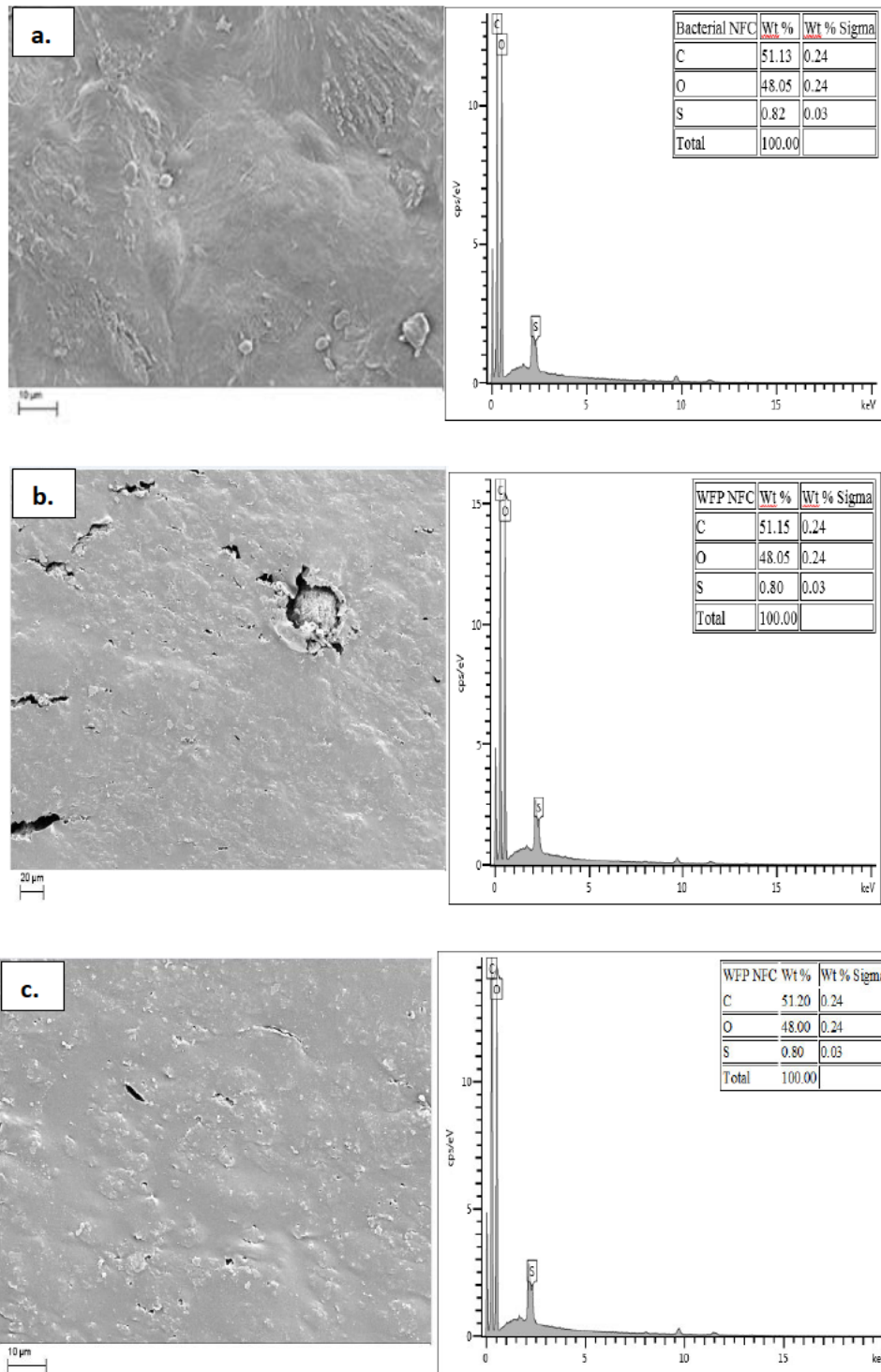


Figure 2.8. SEM image of (a) Bacterial nanofibrous cellulose; (b) Whatman filter paper nanofibrous cellulose and (c) Hardwood pulp nanofibrous cellulose with corresponding EDS.

2.3.3. FT-IR spectra for dialyzed and dialysis-free nanocellulose grown from bacterial cellulose, Whatman filter paper and hardwood pulp

The characterisation of nanocellulose by FT-IR, Figure 2.9. from (a) bacterial cellulose, (b) Whatman filter paper and (c) hardwood pulp was confirmed. For the dialyzed nanocrystalline cellulose from bacterial cellulose, characteristic bands of cellulose were found showing a broad band at 3292 cm^{-1} assigned to the O-H bending stretch, at 3334 cm^{-1} for Whatman filter paper and 3324 cm^{-1} for hardwood pulp. A medium band at 2897 cm^{-1} of the C-H asymmetrical stretch was observed for bacterial cellulose, 2902 cm^{-1} for Whatman filter paper and at 2900 cm^{-1} for hardwood pulp. The band at 1647 cm^{-1} was associated with the bending of the absorbed water moisture for bacterial cellulose, at 1652 cm^{-1} for Whatman filter paper and at 1650 cm^{-1} for hardwood pulp. The broad band at 1031 cm^{-1} , 1029 cm^{-1} and 1051 cm^{-1} was attributed to the pyranose backbone vibration, respectively.

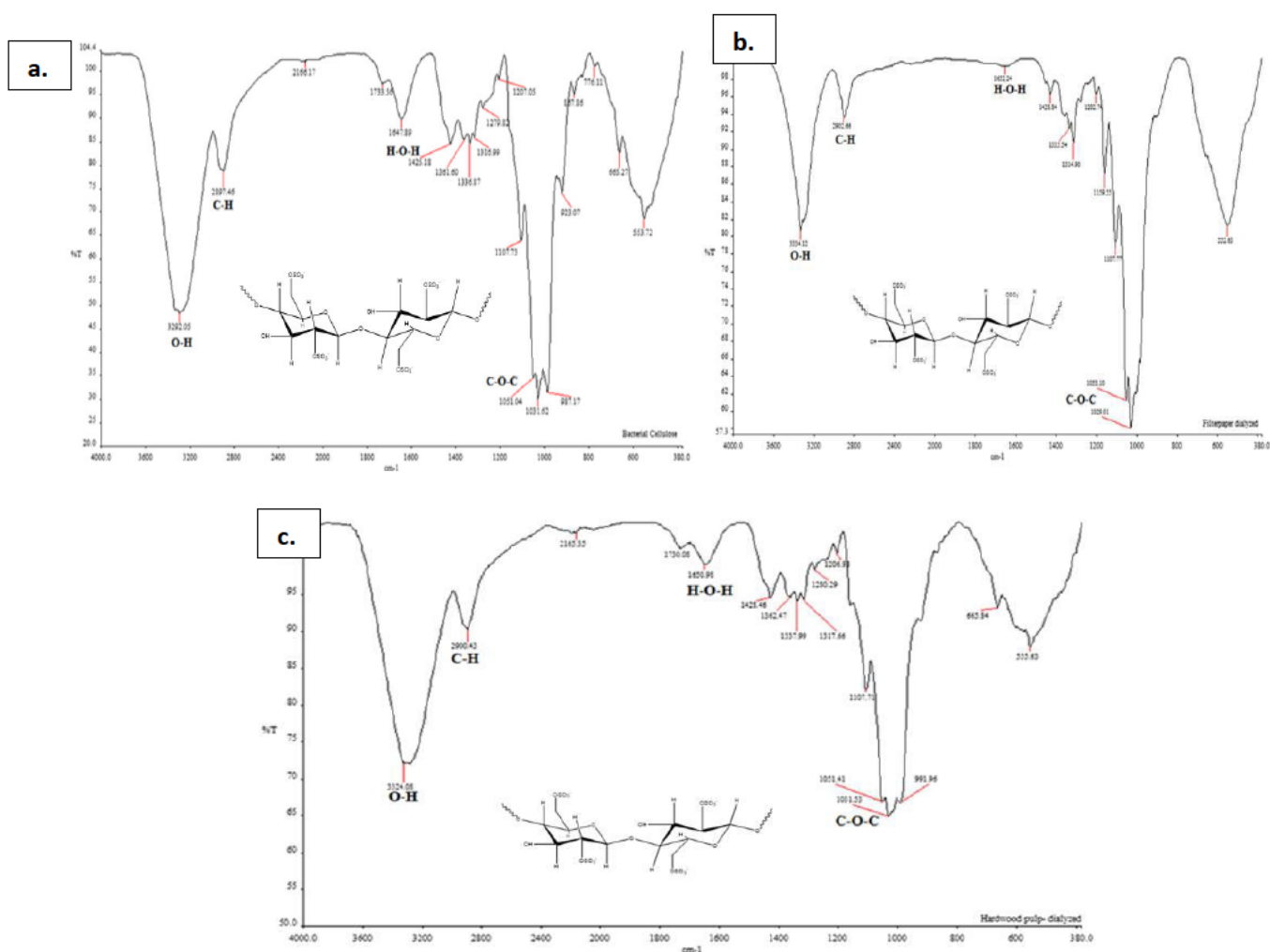


Figure 2.9. FT-IR spectra of (a) Bacterial nanocrystalline cellulose; (b) Whatman filter paper nanocrystalline cellulose and (c) hardwood pulp nanocrystalline cellulose.

Similarly, in Figure 2.10., the FT-IR from the nanofibrous cellulose produced by the dialysis-free method, confirmed the peaks showing a broad band at 3296 cm^{-1} assigned to the O-H bend for the NFC from bacterial cellulose, a band at 3337 cm^{-1} for Whatman filter paper and 3337 cm^{-1} for hardwood pulp. A medium band at 2898 cm^{-1} , 2900 cm^{-1} and 2901 cm^{-1} of the C-H asymmetrical stretch was assigned to bacterial cellulose, Whatman filter paper and hardwood pulp, respectively. The band found at 1639 cm^{-1} is associated with the bending of the absorbed water moisture for bacterial cellulose, 1714 cm^{-1} for Whatman filter paper and 1705 cm^{-1} for hardwood pulp. The broad band at 1034 cm^{-1} was attributed to the pyranose backbone vibration for bacterial cellulose and 1030 cm^{-1} for both Whatman filter paper and hardwood pulp.

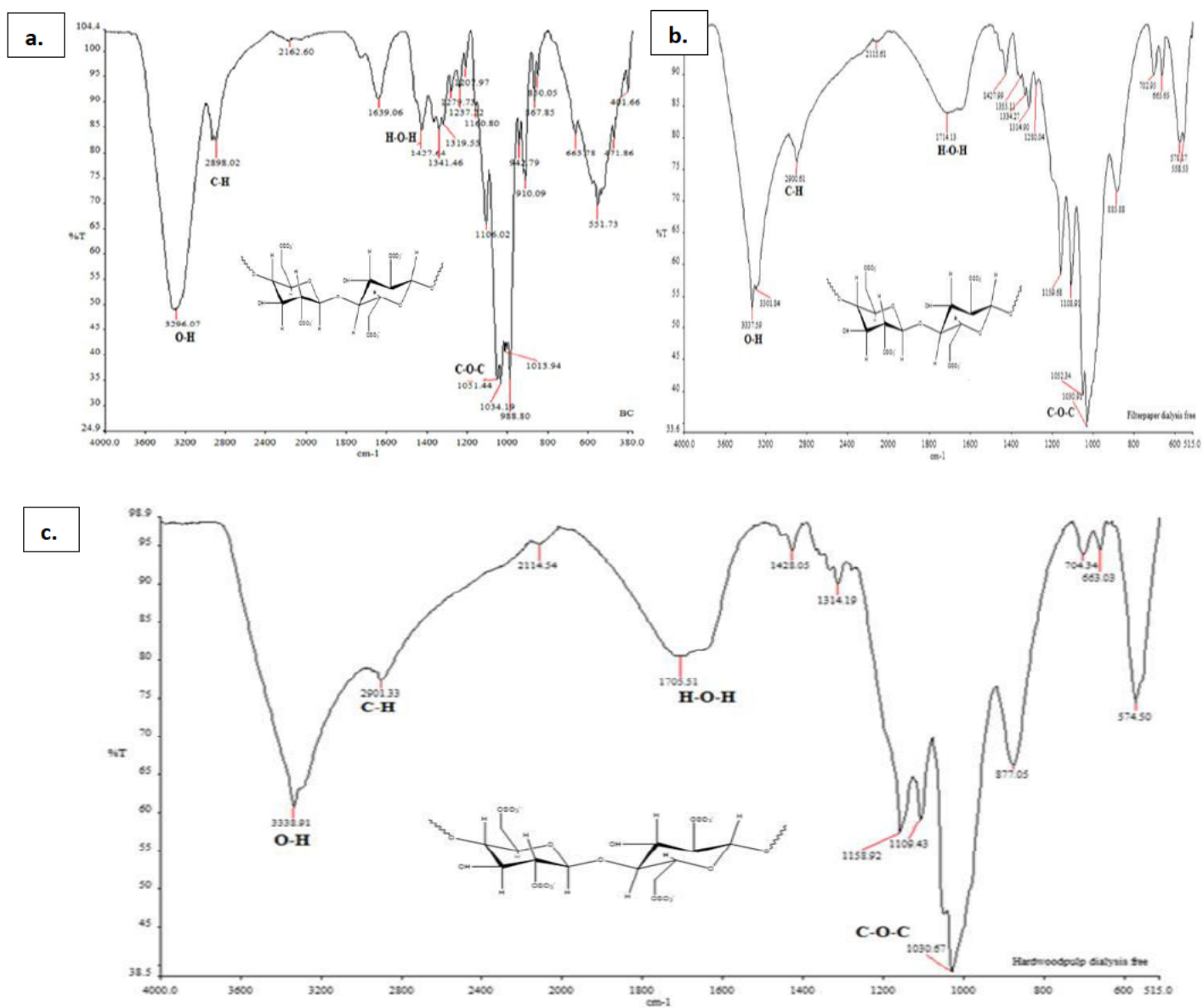


Figure 2.10. FT-IR spectra of (a) Bacterial nanofibrous cellulose; (b) Whatman filter paper nanofibrous cellulose and (c) hardwood pulp nanofibrous cellulose.

All peaks for nanocellulose were consistent with reported values in the region assigned (v/cm^{-1}) as: 3320 (O-H), 2900 (C-H asym), 1646 (H-O-H bend), 1437 CH_2 symm), 1371 (C-H asym bend), 1018 (C-O-C) and 898 (C-H deform) modes of the β -glycosidic linkage (4C1) between the anhydroglucose rings.^[29] These results were consistent with the cellulose structure which suggests that the method of growing pure cellulose as well as the production and isolation of nanocellulose from bacterial cellulose and extraction of nanocellulose from Whatman filter paper and hardwood pulp, was successful.

2.3.4. Raman spectra for dialyzed and dialysis-free nanocellulose from bacterial grown cellulose, Whatman filter paper and hardwood pulp.

Raman spectroscopy was performed for both nanocrystalline cellulose and nanofibrous cellulose to determine if there were any differences in Raman shift, but it turned out there was no significant difference. In Figures 2.11. (a) to (f) a sharp 2D band was found around 1100 cm^{-1} and 2900 cm^{-1} which is characteristic for cellulose.^[30]

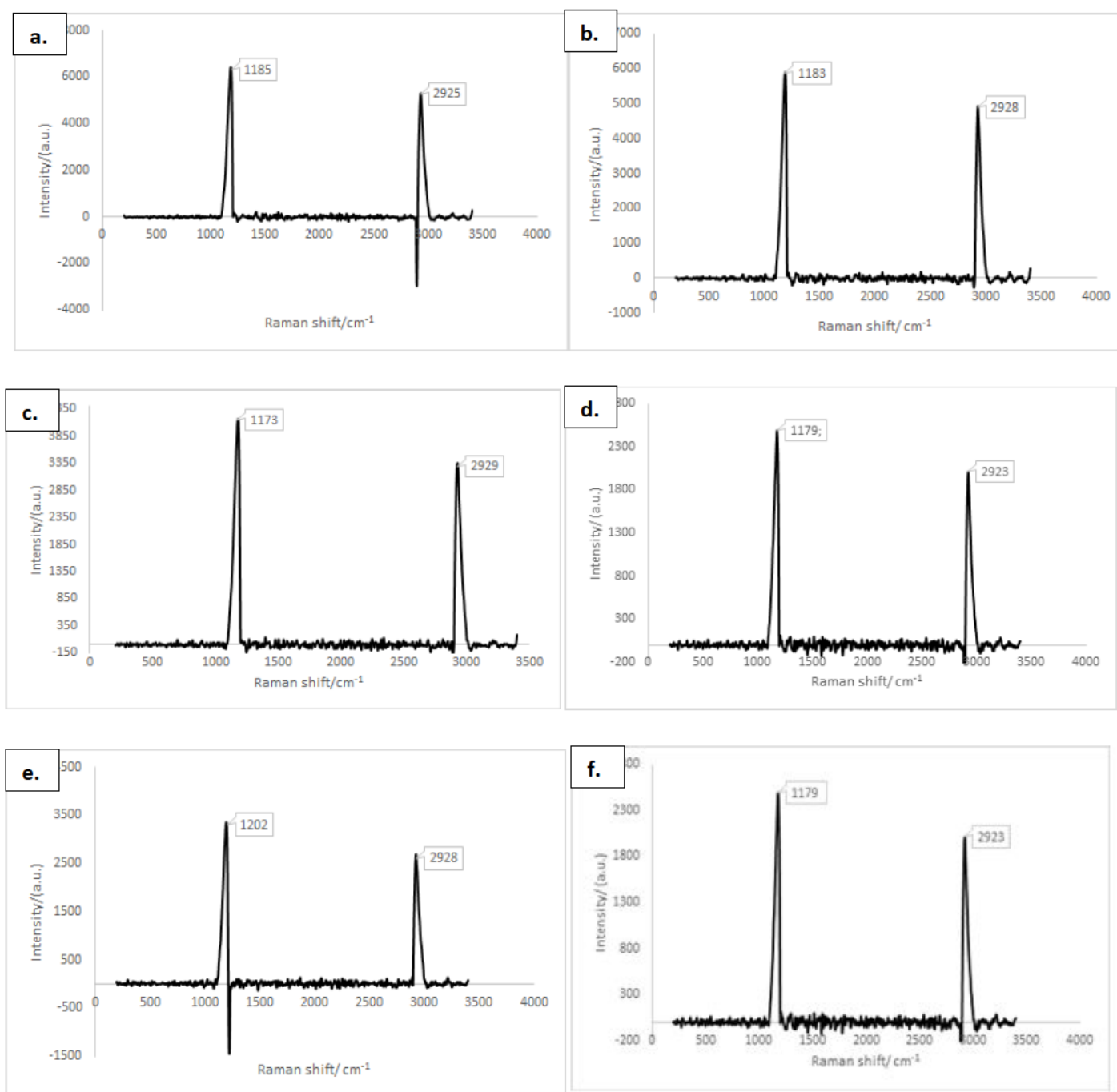


Figure 2.11. Raman spectra of (a) NCC and (b) NFC from bacterial cellulose; (c) NCC and (d) NFC from Whatman filter paper; (e) NCC and (f) NFC from hardwood pulp.

2.3.5. TEM imaging with calculated aspect ratio for dialyzed and dialysis-free nanocellulose from bacterial grown cellulose, Whatman filter paper, and hardwood pulp

TEM imaging was used to investigate the microstructures of the produced nanocellulose. In Figures 2.12; 2.15; and 2.18 all nanocellulose samples showed distinct needle-like nanowhiskers, which were expected. From 250 randomly selected nanocellulose structures from each sample source, the average length and width distribution, as well as aspect ratio was calculated as shown in Table 2.2.

Table 2.2. Summary of average length, width and aspect ratio distribution with standard deviation for each sample.

Source of nanocellulose	Average length/nm	Average width/nm	Aspect ratio
Bacterial NCC	109.79 ± 64.35	9.00 ± 3.47	8.96 ± 4.66
Bacterial NFC	130.00 ± 30.99	15.00 ± 3.05	9.03 ± 3.38
Whatman filter paper NCC	130.00 ± 33.54	15.00 ± 3.07	6.91 ± 4.15
Whatman filter paper NFC	138.41 ± 45.06	15.83 ± 6.4	7.50 ± 0.34.
Hardwood pulp NCC	70.00 ± 32.04	17.50 ± 4.37	5.85 ± 3.03
Hardwood pulp NFC	81.65 ± 32.21	9.00 ± 3.13	6.50 ± 4.42

The length and width distribution of nanocellulose from Whatman filter paper and bacterial cellulose proves to be larger than that of hardwood pulp. The high standard deviation of the dimensions showed that the nanoparticles were polydispersed, as shown by the distributions of the dimension. The high standard deviation of the dimensions showed that the nanoparticles were polydispersed as revealed by the distributions of the dimensions. The minimum aspect ratio required for ideal stress transfer within the interaction between fibres and matrix is 10. The isolated NC from bacterial cellulose dialysis-free and dialysed have aspect ratio closest to 10. The NC from bacterial cellulose show greater potential to provide strong reinforcement and mechanical stability irrespective of the percentage added when included in polymer composites. Whatman filter paper aspect ratio for both NCC and NFC fall far below the minimum and hardwood pulp is almost half the requirement for ideal reinforcement.

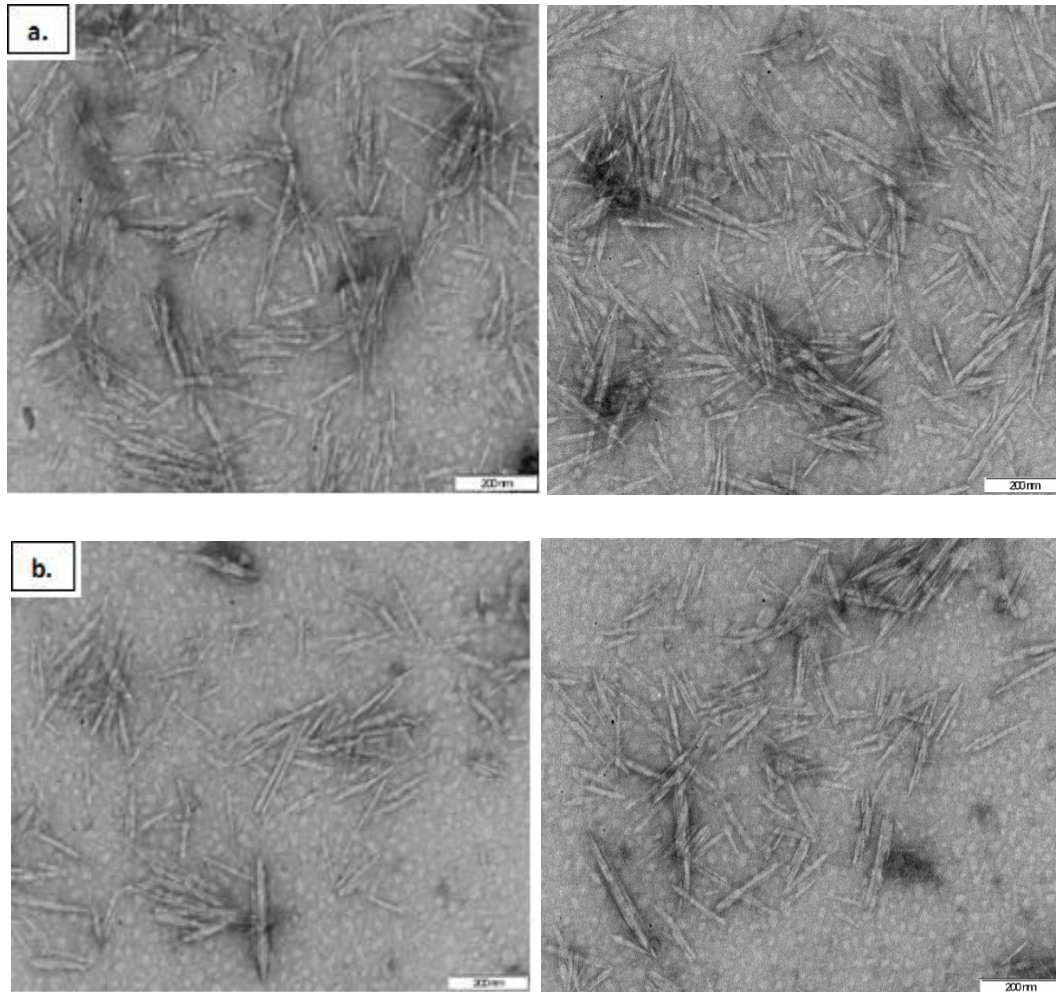


Figure 2.12. TEM images of negatively stained (a) Bacterial nanocrystalline cellulose (dialyzed) and (b) Bacterial nano-fibrous cellulose *via.* dialysis-free.

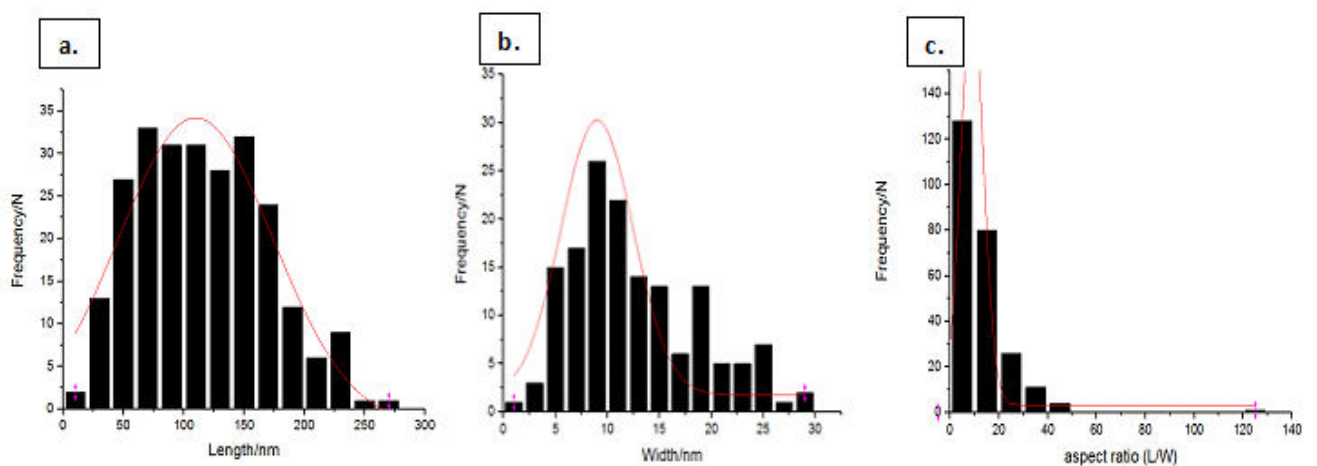


Figure 2.13. Histogram representing the distribution of average length (a), width (b), and aspect ratio (c) of NCC from bacterial cellulose (dialysed).

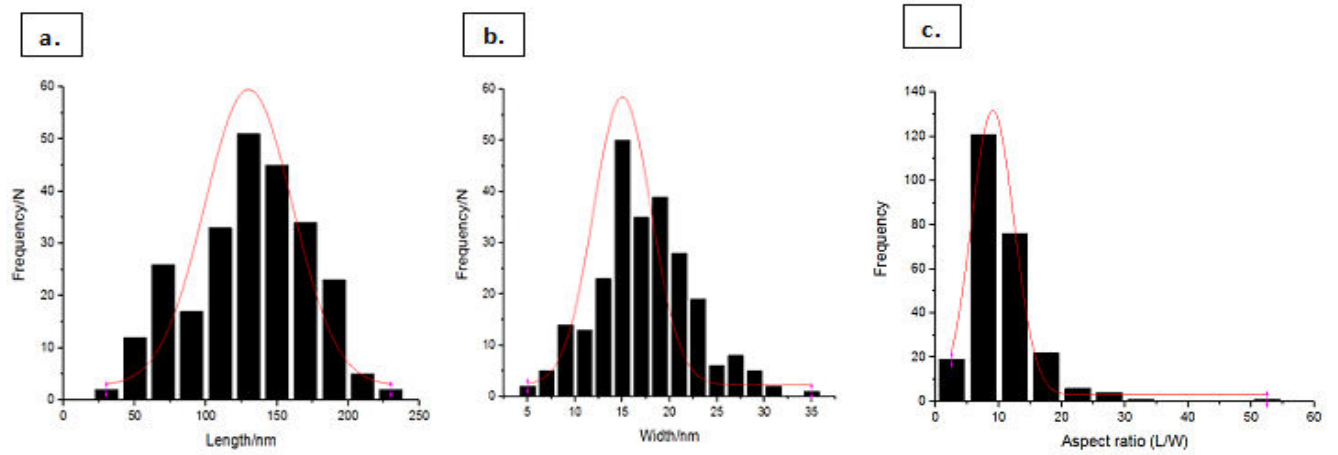


Figure 2.14. Histogram representing the distribution of length (a), width (b), and aspect ratio (c) of NFC from bacterial cellulose *via* dialysis-free.

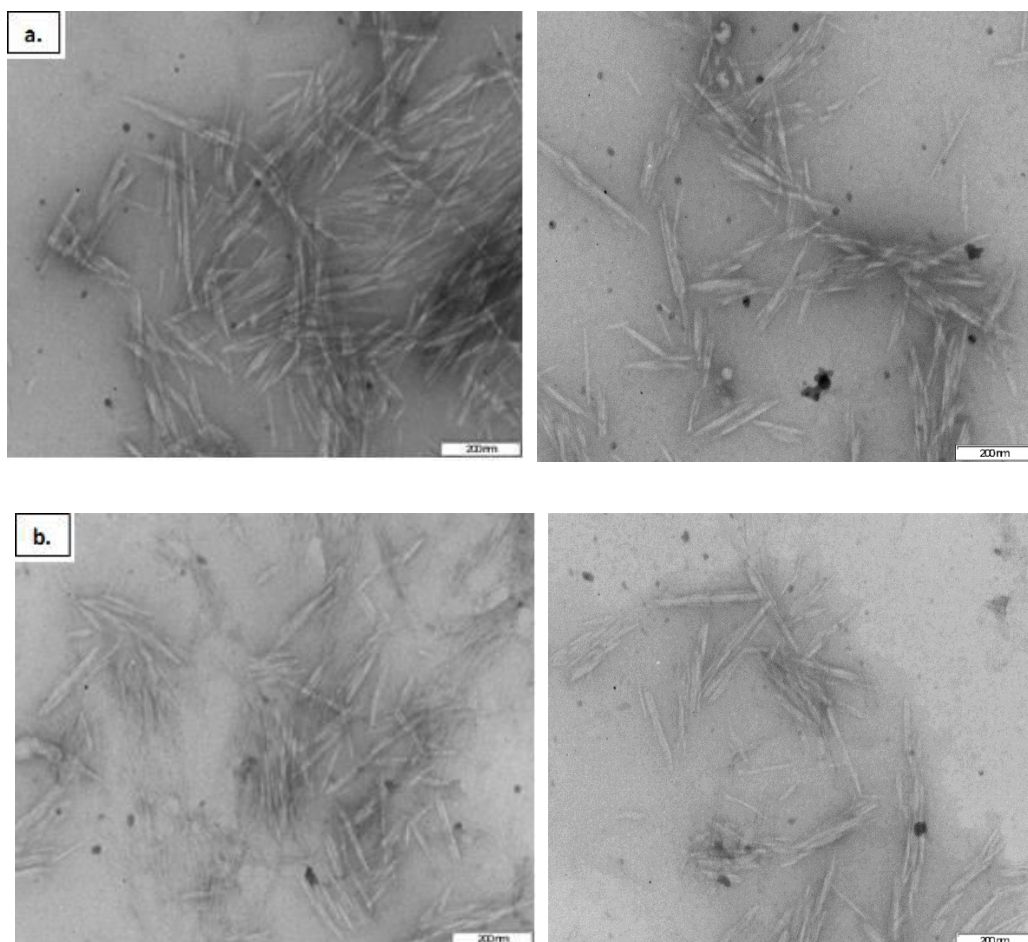


Figure 2.15. TEM image of negatively stained Whatman filter paper *via* dialysis-free method.

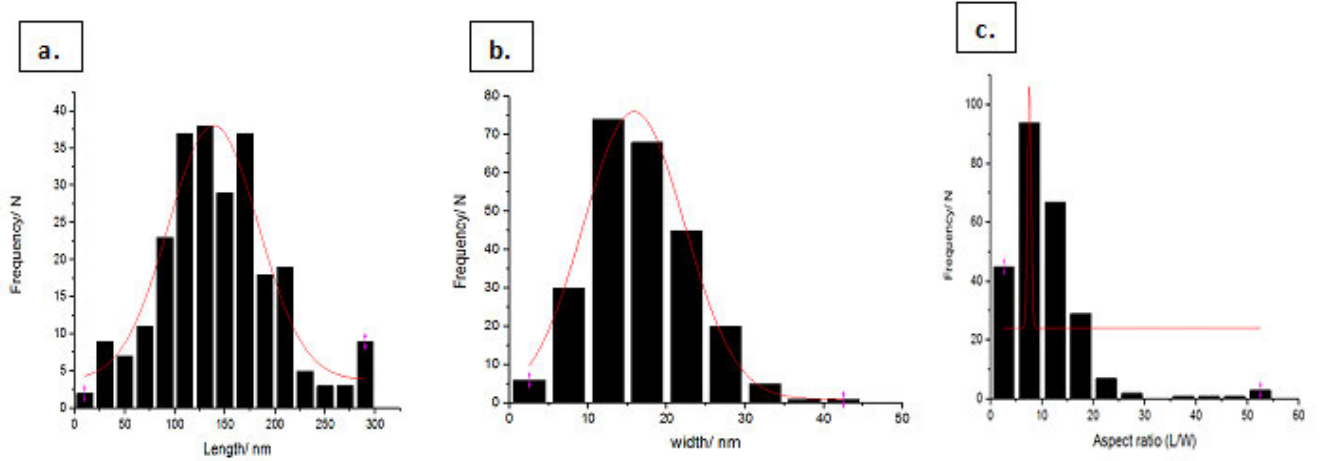


Figure 2.16. Histogram representing the distribution of length (a), width (b), and aspect ratio (c) of NCC of dialyzed WFP.

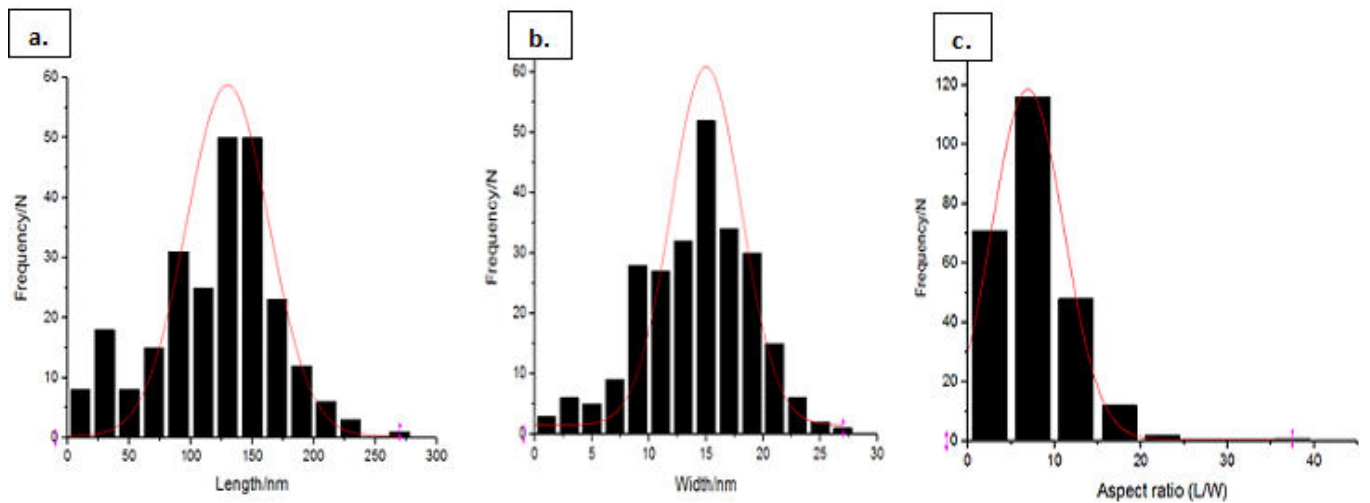


Figure 2.17. Histogram representing the distribution of length (a), width (b), and aspect ratio (c) of NFC of dialysis-free WFP.

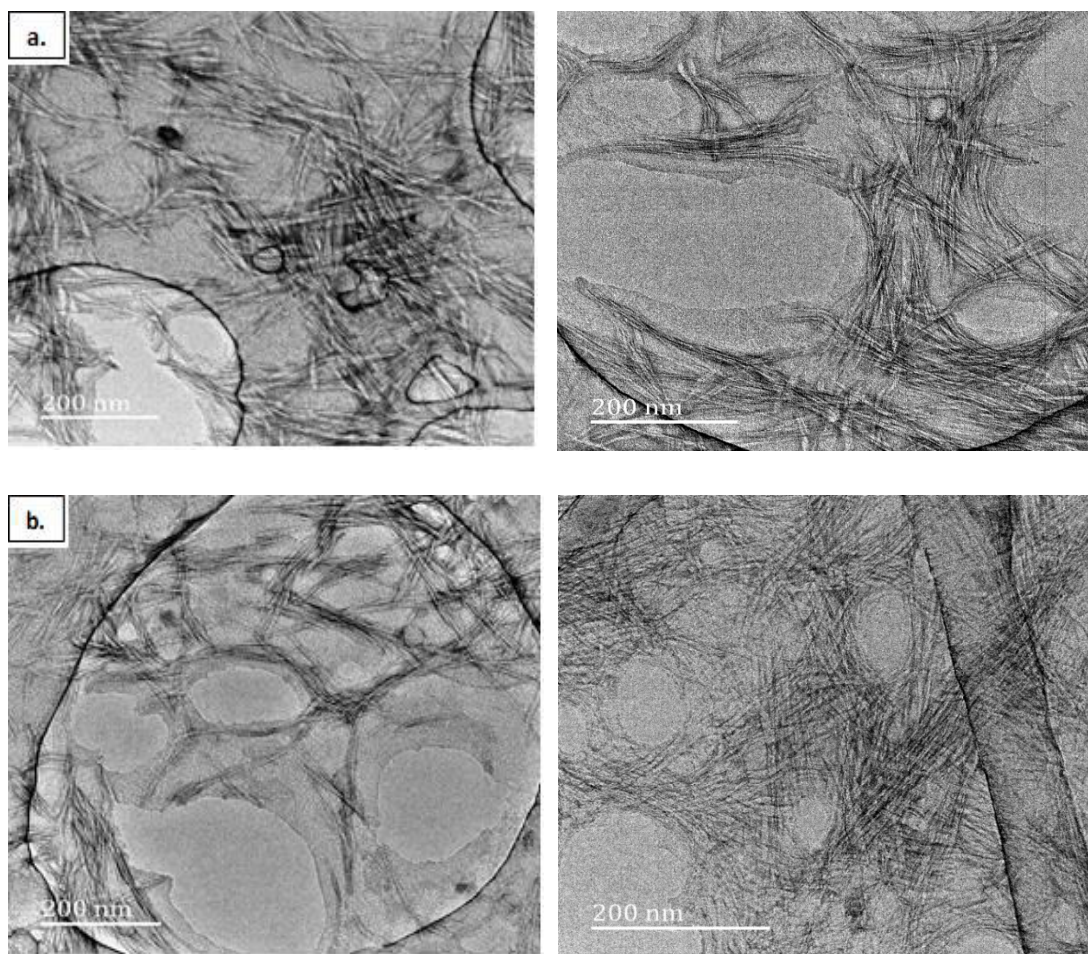


Figure 2.18. HR-TEM image of negatively stained hardwood pulp nanocrystals produced via dialysis-free method.

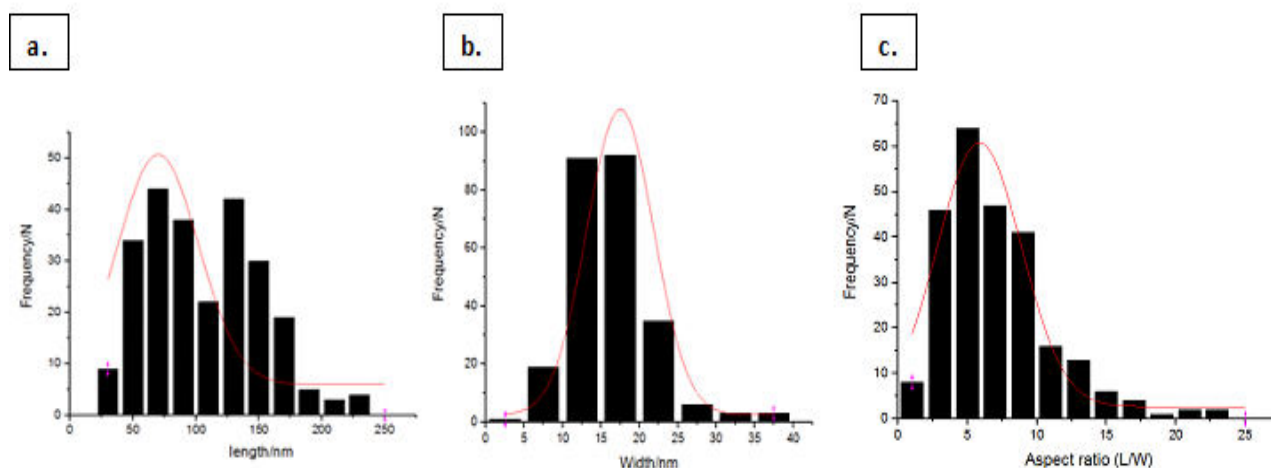


Figure 2.19. Histogram representing the distribution of length (a) width (b) and aspect ratio (c) of NCC of dialyzed hardwood pulp.

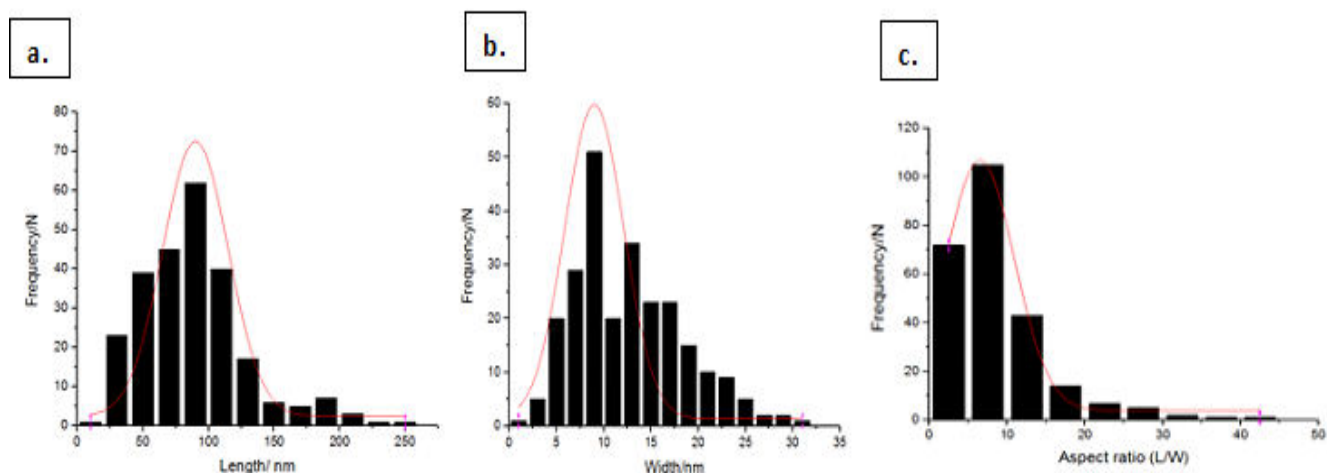


Figure 2.20. Histogram representing the distribution of length (a) width (b) and aspect ratio (c) of NFC of un-dialyzed hardwood pulp.

From these results, it was evident that bacterial cellulose was successfully grown by SCOBY, and subsequently converted to nanocellulose by acid hydrolysis. By following the same hydrolysis synthetic methodology, Whatman filter paper and hardwood pulp was also converted into nanocellulose. The nanocrystalline cellulose was effectively converted into a nanocrystalline cellulose film through the dialysis method and nanofibrous cellulose *via* the dialysis-free method. However, both these types of nanocellulose showed no difference in morphologic characteristics since both methods produced the nano-whisker type cellulose. The only chemical difference was the presence of residual sulfur and soluble sugars on the surface of the nanofibrous cellulose which affected the physical characteristics upon drying. The nanocellulose from bacterial cellulose was like nanocellulose from Whatman filter paper and hardwood pulp with minor differences in concentration and length and width distribution.

2.4. References

1. Klemm, D., *Nanocelluloses: A new family of nature-based materials*. Angewandte Chemie International Edition, 2011. **50**, 5438-5466.
2. Gatenholm, P.D., *Bacterial nanocellulose as a renewable material for biomedical applications*. MRS bulletin, 2010. **35**, 208-213.

3. Kozyrovska, N.O., Reva O.M., Goginyan V.B., *Kombucha microbiome as a probiotic: a view from the perspective of post-genomics and synthetic ecology*. Biopolymers and cell, 2012, **28**, 103-113.
4. Hestrin, S., Schramm. M., *Synthesis of cellulose by Acetobacter xylinum. 2. Preparation of freeze-dried cells capable of polymerizing glucose to cellulose*. Biochemical Journal, 1954. **58**, 345.
5. Jonas, R.F., Luiz F., *Production and application of microbial cellulose*. Polymer Degradation and Stability, **59**, 101-106.
6. Jozala, A.F., *Bacterial cellulose production by Gluconacetobacter xylinus by employing alternative culture media*. Applied microbiology and biotechnology, 2015. **99**, 1181-1190.
7. Nge, T.T., Sugiyama, J., Bulone, V., *Bacterial cellulose-based biomimetic composites*, in *Biopolymers*, In Tech, 2010.
8. Khan, A., *Nanocellulose-based composites and bioactive agents for food packaging*. Critical reviews in food science and nutrition, 2014, **54**, 163-174.
9. Shi, Z., *Utilization of bacterial cellulose in food*. Food Hydrocolloids, 2014, **35** 539-545.
10. Maneerung, T., Tokura, S., and Rujiravanit, R., *Impregnation of silver nanoparticles into bacterial cellulose for antimicrobial wound dressing*. Carbohydrate polymers, 2008, **72**, 43-51.
11. Farah, L.F., *Process for the preparation of cellulose film, cellulose film produced thereby, artificial skin graft and its use*, 1990.
12. Schumann, D.A., *Artificial vascular implants from bacterial cellulose: preliminary results of small arterial substitutes*. Cellulose, 2009, **16**, 877-885.
13. Svensson, A., *Bacterial cellulose as a potential scaffold for tissue engineering of cartilage*. Biomaterials, 2005, **26**, 419-431.
14. Klemm, D., *Bacterial synthesized cellulose—artificial blood vessels for microsurgery*. Progress in Polymer Science, 2001, **26**, 1561-1603.
15. Johnsy George, K.V.R., Bawa, A.S., *Bacterial cellulose nanocrystals exhibiting high thermal stability and their polymer nanocomposites*. International Journal of Biological Macromolecules, 2011, **48**, 50-57.
16. George, J., Ramana, K., Bawa. A., *Bacterial cellulose nanocrystals exhibiting high thermal stability and their polymer nanocomposites*. International Journal of Biological Macromolecules, 2011, **48**, 50-57.

17. Puri, V.P., *Effect of crystallinity and degree of polymerization of cellulose on enzymatic saccharification*. Biotechnology and Bioengineering, 1984, **26**, 1219-1222.
18. Sadeghifar, H., *Production of cellulose nanocrystals using hydrobromic acid and click reactions on their surface*. Journal of materials science, 2011, **46**, 7344-7355.
19. Siqueira, G., J. Bras, A., *Cellulosic bionanocomposites: A review of preparation, properties and applications*. Polymers, 2010, **2**, 728-765.
20. Zheng, G., *Nanostructured paper for flexible energy and electronic devices*. MRS bulletin, 2013, **38**, 320-325.
21. Sanga Pachuau, L., *Plant-based nanocellulose: production, sources, modifications and its potential in drug delivery applications*. Medicinal chemistry, 2015, **15**, 543-552.
22. Pandey, J.K., Nakagaito. A.N., Takagi. H., *Fabrication and applications of cellulose nanoparticle-based polymer composites*. Polymer Engineering & Science, 2013, **53**, 1-8.
23. Fujita, M., Harada. H., *Ultrastructure and formation of wood cell wall*. Wood and cellulosic chemistry, 2000, 1-49.
24. Pérez, J., *Biodegradation and biological treatments of cellulose, hemicellulose and lignin: An overview*. International Microbiology, 2002, **5**, 53-63.
25. Spence, K.L., *The effect of chemical composition on microfibrillar cellulose films from wood pulps: Mechanical processing and physical properties*. Bioresource technology, 2010, **101**, 5961-5968.
26. Guillén, F., *Biodegradation of lignocellulosics: microbial, chemical, and enzymatic aspects of the fungal attack of lignin*. International Microbiology, 2005, **8**, 195-204.
27. Stelte, W. Sanadi. A.R., *Preparation and characterization of cellulose nanofibers from two commercial hardwood and softwood pulps*. Industrial & engineering chemistry research, 2009, **48**, 11211-11219.
28. Ververis, C., *Fiber dimensions, lignin and cellulose content of various plant materials and their suitability for paper production*. Industrial crops and products, 2004, **19**, 245-254.
29. Ogundare, S.A., Moodley. V., Van Zyl. W.E., *Nanocrystalline cellulose isolated from discarded cigarette filters*. Carbohydrate polymers, 2017, **175**, 273-281.
30. Kang, Y.R., *Fabrication of electric papers of graphene nanosheet shelled cellulose fibres by dispersion and infiltration as flexible electrodes for energy storage*. Nanoscale, 2012, **4**, 3248-3253.

CHAPTER 3

3.1. Background to Polypyrrole@Nanocellulose Polymer Samples

Polypyrrole (PPy) has high conductivity, fast electrochemical switching, high specific capacitance values and is environmentally stable.^[1, 2] The complex nanostructures of PPy influence the properties and the overall functionality.^[3] The variety of preparation routes influences the change in electrical and optical properties with size and shape of nanostructures.^[4] PPy is a conjugated conducting polymer and easily polymerizes with ferric trichloride.^[5] PPy has a wide range of applications in sensors,^[6] electrochromic devices,^[7] and batteries.^[8, 9] The conducting property of PPy is due to the electrons moving along the polymer chains and across the interchain, owing to the conjugated backbones.^[10, 11]

Unfortunately, neat polypyrrole have poor mechanical strength, processability, dispersibility and low surface area.^[12, 13] Recently, extensive research has been devoted to studying the properties of PPy and several methods have been developed to improve the stability. For example, an enhancement in stability can be accomplished by forming a nanohybrid using nanocellulose.^[14] This enhances the stability of PPy in mechanical structure and conductivity. The incorporation of nanocellulose into polypyrrole allows for deposition on the surface of nanocellulose forming a continuous structure and overcoming the shortcomings of neat polypyrrole.^[15] Nanocellulose is a good template for the polymerization of pyrrole monomer forming a more connected network.^[16] Nanocellulose acts as a biotemplate and directs the growth of the nanohybrid with high aspect ratio and excellent dispersity.^[17]

The electrical resistance of the prepared hybrid was tested, where resistance is a measure of the resisting power to the flow of an electric current. Ohm's law states that current flowing through a resistor is directly proportional to the voltage across the resistor at a constant temperature. Ohm's law relates to current and voltage- (the potential difference of a cell, electrical supply or electric component measured in volts, V). The current flowing through a conductor- (which allows an electrical current to pass through easily due to low resistance), is directly proportional to the voltage across the conductor, therefore the current increases as the voltage increases. Since the electrical resistivity of the sample is the measure of how strongly a material opposes the flow of electric current, a low resistivity indicates how readily the sample allows the flow of electric current. Some materials resist the flow of electrical current, while

others are better at conducting it. The resistivity enables comparisons of the way in which different materials allow or resist the flow of current. Specific units are used for resistivity to enable resistivity measurements to be meaningful, and there are formulas for calculating and relating it to the resistance (in Ohm) for a given size of material. A material that readily conducts electrical current is a conductor and has a lower resistivity, and a material that does not conduct electricity easily is an insulator which has a higher resistivity.

An ohmic conductor is a component that obeys Ohm's law. A graph of voltage on the vertical axis against current on the horizontal axis (a voltage-current graph) gives a straight line with a positive gradient, the steeper the gradient, the higher the resistance will be. In this study the voltage was independent, and the current was the effect of the voltage, using the established convention, a current vs voltage graph would have current on vertical axis and voltage on the horizontal axis. In such a case the resistances would be the reciprocal of slope, where the relationship between the current and voltage is linear, and a steeper slope indicates a lower resistance.

Polypyrrole presents ohmic conductor-like properties,^[18] where the electronic conductivity of PPy switches between the conducting and the insulating states through doping and undoping cycles.^[19, 20] The nature of this study demanded various ratios of polypyrrole to nanocellulose to be synthesized in order to determine the ideal ratio for optimal mechanical properties, being well dispersed and robust enough to hold its structural integrity after being tested for conductivity. Due to the different kinds of nanocellulose studied, only one type of ratio was varied for determining the optimum ration to be used, namely bacterial nanofibrous cellulose (dialysis-free). This optimum ratio was used to test the remaining samples. The resistivity will be studied for the polypyrrole@nanocellulose nanohybrid to determine if the nanocellulose endows electrical conductivity or hinders the flow of charge. Also, the nanocellulose in this study are made from various sources of cellulose i.e. bacterial grown cellulose, Whatman filter paper and hardwood pulp, therefore the quality of the nanocellulose was compared. In parallel, a dialysis method and a dialysis-free method was carried out for the nanocellulose and therefore the two methods can be compared to determine a less time-consuming and economical method that produces improved results. The various ratios synthesized were tested for resistivity and the optimal ratio was used to prepare the varying samples.

3.2. Experimental Procedure for Varying Ratios of Polymer Samples

3.2.1. Preparation of varying ratio of PPy@NC

Materials: Pyrrole 97%, CAS-NO: 109-97-7, China, Merck KGaA. ferric chloride hexahydrate, $\text{FeCl}_3 \cdot 6\text{H}_2\text{O}$ 98%, batch no.: 350710, SMM Chemicals (PTY) LTD. Polyvinyl alcohol (PVA), VWR Chemicals Prolabo, CAS-NO: 9002-89-5. All chemicals used as received.

Various ratios of pyrrole to nanocellulose was synthesized using only bacterial grown nanofibrous cellulose, dialysis-free, to determine the optimum ratio that will be used for the remaining samples to give excellent dispersibility. The quantity ratio is as follows in Table 3.1.

Table 3.1. Quantity of materials used for varying ratio of polypyrrole to nanocellulose.

Ratio PPy:NC	Volume of Pyrrole/ mL	Mass of Pyrrole/ g	Volume of Nanocellulose/ mL	Mass of Nanocellulose/ g	Mass of $\text{FeCl}_3 \cdot 6\text{H}_2\text{O}/$ g
0:1	0.00	0.00	34.13	1.00	0.00
1:2	1.03	1.00	68.26	2.00	2.00
1:1	1.03	1.00	34.13	1.00	2.00
2:1	2.06	2.00	34.13	1.00	4.00
1:0	1.03	1.00	0.00	0.00	2.00

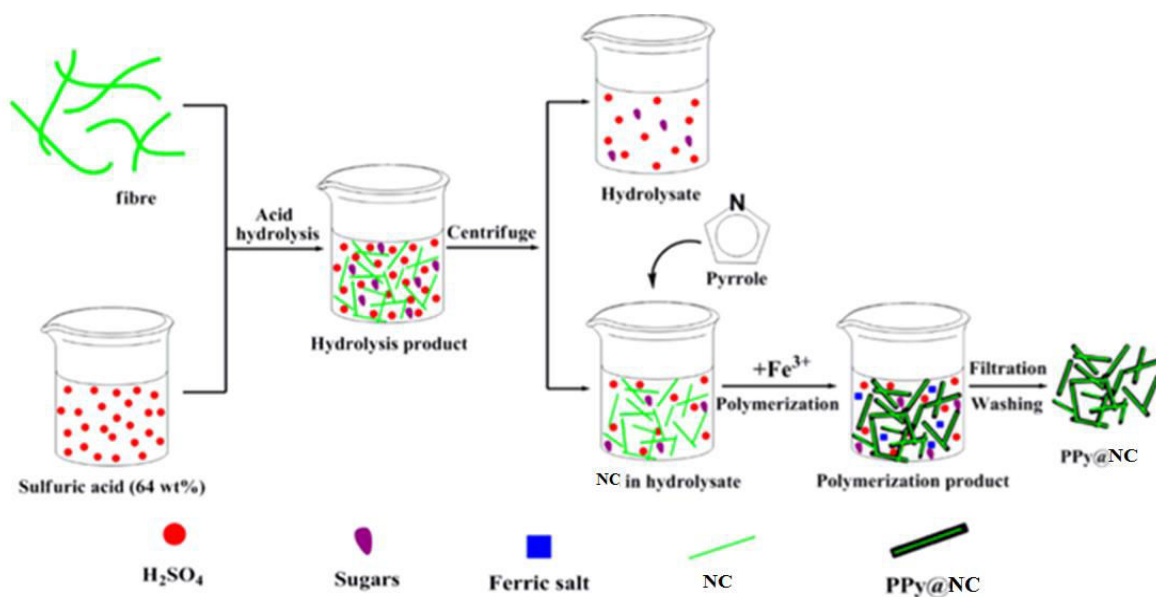
The volume of polypyrrole was stirred in ice-water for one hour with the respective volume of bacterial nanofibrous cellulose, 29.30 mg/mL, according to the ratio required, Table 3.1. Thereafter, the respective amount of $\text{FeCl}_3 \cdot 6\text{H}_2\text{O}$ was added into the mixture to initiate the polymerization. The polymerization proceeded in ice-water for 2 h. The obtained product was filtered and washed several times with distilled water to remove the remaining reagents.

3.2.2. Incorporation of varying ratios of PPy:NC in PVA

For the preparation of PPy@NC/PVA nanocomposites, 2 g for each varying ratio suspension (prepared in 3.2.1) was dispersed in 20 mL of ddH₂O and sonicated for 10 mins to disperse the aggregation. Digital images were taken to show varying dispersions. Simultaneously, 2.00 g of PVA was dissolved 20 mL of ddH₂O and heated to 200° C and stirred until dissolved. Thereafter, the 20 mL sonicated PPy@NC nanohybrid suspension and 20 mL of PVA solution were mixed together to form a homogeneous mixture and sonicated for one hour.

3.3. Results and Discussion for Ratios of Polymer Samples

To better understand the *in situ* doping of the PPy@NC nanohybrid, the experimental process is schematically illustrated in a flow diagram in Scheme 3.1.



Scheme 3.1. Schematic illustration for the *in situ* doping synthesis of conductive PPy@NC nanohybrid

Cellulose fibres were hydrolysed by H₂SO₄, yielding a hydrolysis product consisting of nanocellulose, soluble sugars, and residual acid, Scheme 3.1. The hydrolysate was treated by dialysis to yield nanocrystalline cellulose and another portion was treated by the dialysis-free method to yield nanofibrous cellulose which still contained some soluble sugars and residual acids. The hydrolysis product was used as the starting materials for the preparation of PPy@NC

nanohybrid. The dialysis-free nanofibrous cellulose had no significant effect on polymerization of pyrrole. The polymerization of pyrrole was initiated with ferric trichloride hexahydrate added into the hydrolysis product, and the generated PPy was deposited on the nanocellulose, yielding a soft, black precipitate of PPy@NC hybrid. Meanwhile, the dialysis-free nanofibrous cellulose for the synthesized PPy@NFC nanohybrid was *in situ* doped by the residual hydrolysis acid. The PPy@NC nanohybrid was easily separated from the polymerization product by filtration and washing. The separated PPy@NC nanohybrid was dried overnight, obtaining a PPy@NC powder which possessed low electrical resistance due to its precipitate form. For the dialysis-free process of producing nanofibrous cellulose, the process presented to be facile, inexpensive, and eco-friendly to synthesize PPy@NC hybrid compared to the dialysed PPy@NCC. By avoiding the time-consuming and water-consuming dialysis process of nanocellulose and utilizing the residual hydrolysis acid as doping agent, it dramatically reduced the production cost of PPy@NC and widely extend its applications producing equivalent results.

The mass obtained for polypyrrole@nanocellulose hybrid for the various ratios are recorded in Table 3.2.

Table 3.2. Mass of sample obtained for various ratios of PPy:NC

Sample PPy:NC	Mass obtained/ g
0:1	-
1:2	0.754
1:1	0.812
2:1	0.898
1:0	0.664

The ratios of polypyrrole to nanocellulose had to be varied to find the optimum ratio being well dispersed. When the optimum ratio of PPy:NC are mixed in PVA and dried, the mechanical properties was ideal, being strong enough to retain its integrity and flexible when bent without shattering. The amount of polypyrrole should be minimal in the nanohybrid. Due to the various types of nanocellulose studied, only one type of nanocellulose ratio was varied for determining the optimum ration to be used, i.e. bacterial nanofibrous cellulose (dialysis-free) and

that optimum ratio was then used to prepare the remaining hybrids made from bacterial cellulose, Whatman filter paper and hardwood pulp, both with dialysis and dialysis-free. The varying ratios of polypyrrole to bacterial nanofibrous cellulose was dispersed in water and left to settle for 30 minutes to demonstrate which ratio had the best dispersity.

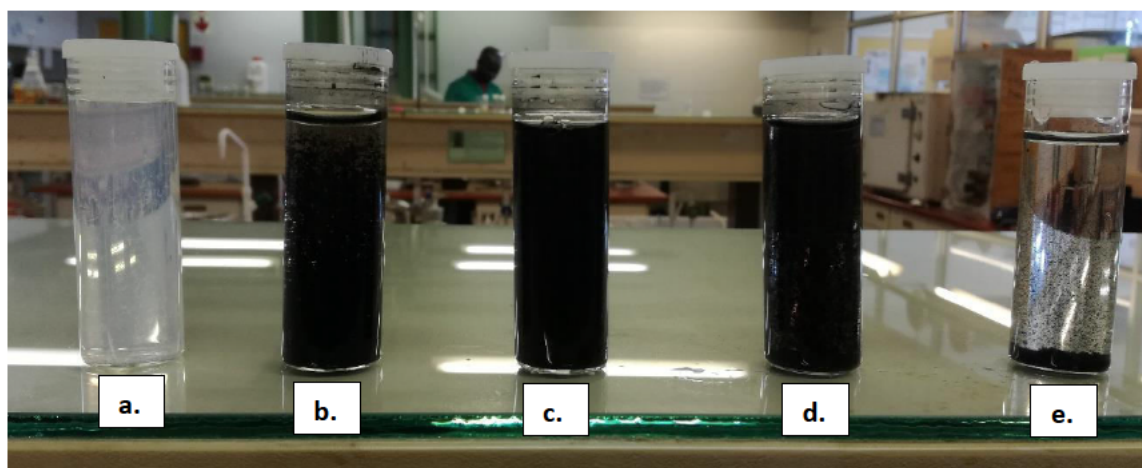


Figure 3.1. Digital picture of varying ratios of PPy:NC (L-R: (a) 0:1; (b) 1:2; (c) 1:1; (d) 2:1 and (e) 1:0) when left to settle for 30 minutes.

In Figure 3.1., from left to right, the ratio by weight of (a) 0:1, (b) 1:2, (c) 1:1, (d) 2:1 and (e) 1:0 are seen. For the ratio of 0:1, only one-part nanocellulose was dispersed in water. There was no polypyrrole added. This was used to demonstrate the suspension of nanocellulose. The solution was white and opaque as expected for nanocellulose, with excellent suspension and no separation. When dried in PVA, an even film formed. For ratio 1:2, one-part polypyrrole was polymerized with twice the amount of nanocellulose. The sample was black in colour due to the polypyrrole. After t-20 mins. of settling, polypyrrole was well dispersed but eventually after 30 mins the nanocellulose began to separate from the polypyrrole due to the excess nanocellulose present, see Figure 3.1 The denser polypyrrole settled to the bottom. When this ratio was dispersed in PVA, the sample did not dry evenly, but instead the polypyrrole was scattered within the film. The ratio of 1:1 proved to be most satisfactory whereby the polypyrrole was well dispersed. After 30 minutes there was no change in the consistency. The hybrid remained well distributed in suspension. When dried in PVA, the sample dried evenly into a smooth film that was easily removed from the petri dish. It was flexible and maintained its structural integrity when bent. Also, similar results were seen for ratio 2:1, where twice as much polypyrrole was used than nanocellulose. Over time the suspension separated slightly due to the higher amount of polypyrrole compared to NC. Unfortunately, when dried in PVA, the film was brittle and did not set in a neat film. When it was removed from the petri dish, the film was hard and brittle.

For ratio 1:0, no nanocellulose was used. As seen, the polypyrrole sank to the bottom of the vial immediately. When drying in PVA, there was no homogeneity. The polypyrrole clumped together. It had a rough texture, with no connected network. There were spaces between the polypyrrole and PVA. It had no mechanical support structure and it was clear it needed nanocellulose for stability. Therefore, ratio 1:1 showed ideal mechanical and physical properties where the polypyrrole was well dispersed by the nanocellulose. It was expected that the greater distribution would allow for improved conductivity measurement. Since the ratio 1:1 showed the most promising outcome, it was the chosen ratio used for further investigation.

3.4. Experimental Procedure for All of Polymer Samples at Optimum Ratio

3.4.1. *In situ* doping preparation of PPy@NC nanohybrid from NC of Bacterial grown cellulose, Whatman filter paper, and hardwood pulp dialysed and dialysis-free, as well as neat PPy

For all samples, pyrrole to nanocellulose was synthesized using the optimum ratio 1:1 according to Table 3.2.

Table 3.3 Quantity of materials used for all samples polypyrrole: nanocellulose at ratio 1:1.

Sample	Volume of pyrrole/ mL	Mass of pyrrole/ g	Concentration of Nanocellulose/ mg.mL ⁻¹	Volume of NC/ mL	Mass of NC/ g	Mass of FeCl ₃ ·6H ₂ O/ g
HWP-NCC	1.03	1.00	24.50	40.82	1.00	2.00
HWP-NFC	1.03	1.00	26.30	38.02	1.00	2.00
WFP-NCC	1.03	1.00	28.50	35.09	1.00	2.00
WFP-NFC	1.03	1.00	28.60	34.97	1.00	2.00
BC-NCC	1.03	1.00	28.80	34.72	1.00	2.00
BC-NFC	1.03	1.00	29.30	34.13	1.00	2.00

A mass of 1.00 g. (1.03 mL), of pyrrole was dispersed in a volume of dialyzed sample according to individual concentrations as shown in Table 2 for NCC from BC, WFP and HWP. Similarly, for the dialysis-free method, 1.00 g, (1.03 mL), pyrrole was added to the respective volumes of remaining hydrolysis product from BC, WFP and HWP (containing NC, soluble sugars, residual acid). The volume of NC and pyrrole was measured accurately using a micropipette and the mixture was stirred evenly in ice-water for 1 h. Thereafter, 4.00 g of $\text{FeCl}_3 \cdot 6\text{H}_2\text{O}$ was added into the mixture to initiate the polymerization. The polymerization proceeded in ice-water for 2 h. The obtained product was filtered and washed five times with distilled water to remove the remaining reagents.

3.4.2. Preparation of PPy@NC/PVA nanocomposites from NC of Bacterial grown cellulose, Whatman filter paper and hardwood pulp dialysed and dialysis-free

In the preparation of PPy@NC/PVA nanocomposites, the obtained PPy@NC nanohybrid was filtered and washed with ddH₂O. 2 g of each PPy@NC nanohybrid suspension was dispersed in 20 mL of ddH₂O and sonicated for 10 min to disperse the aggregation. Simultaneously, 2.00 g of PVA was dissolved 20 mL of ddH₂O and heated to 200° C stirred until dissolved. Then the 20 mL sonicated PPy@NC nanohybrid suspension and 20 mL of PVA solution were mixed together to form a homogeneous mixture and sonicated for one hour. A portion of sample was stored in a sealed vial for conductance testing and the remaining was used for characterisation tests.

3.5. CHARACTERISATION

Transmission electron microscopy (TEM)

TEM was performed using a transmission electron microscope. JEOL-JEM 1010 (Japan) operating at 100 kV was used. Diluted PPy@NC nanohybrid aqueous suspensions were sonicated for 30 min to disperse the aggregation. A copper grid was dipped in the well dispersed nanohybrid suspensions until drying and images were taken.

Scanning Electron Microscopy coupled with Energy Dispersive X-ray (SEM)

For the SEM study, a Zeiss Ultra Plus field emission gun scanning electron microscope (FEGSEM) equipped with energy dispersive X-ray (EDS) detector (Germany) was used. The samples were deposited separately on conductive carbon tapes stuck to aluminium stubs. Each sample was coated with gold with the aid of sputter coater to minimize charging.

Fourier transform infrared spectroscopy (FT-IR)

Analyses were carried out at room temperature using a Perkin Elmer Spectrum 100 FTIR spectrometer fitted with a Universal Attenuated Total Reflectance (ATR) sampling accessory. The data was processed using Spectrum® software. A small amount of the dry sample was placed onto the ATR crystal and a pressure of 120 psi was applied to ensure contact between the crystal and the catalyst material.

Raman spectroscopy

Raman spectra were measured using a Delta Nu Advantage 532 instrument fitted with a 532 nm laser source (green) and operated by NuSpec® software. Laser intensity, polarization and the integration time of the scans were varied until each sample gave clear and reproducible spectra. All analyses were carried out at room temperature with the powdered PPy and PPy@NC sample loaded in quartz tubes.

UV-vis

For UV-vis measurement the Neat PPy and PPy@NC nanohybrid suspensions were sonicated for 30 min to disperse the aggregation. The well dispersed nanohybrid suspension was placed in a quartz cuvette with an optical path of 1 cm.

3.6. Results and Discussion for All Polymer Samples at Optimum Ratio

The mass obtained for all polypyrrole@nanocellulose hybrid are recorded in Table 3.4.

Table 3.4. Mass of PPy@NC at ratio 1:1 sample obtained

Sample	Mass of PPy@NC obtained/ g
BC-NCC	0.800
BC-NFC	0.812
WFP-NCC	0.773
WFP-NFC	0.791
HWP-NCC	0.764
HWP-NFC	0.782

3.6.1. TEM images of nanohybrid samples

TEM was used to investigate the microstructures of neat polypyrrole and the various PPy@NC nanohybrids. The polymerization of the pyrrole monomer without nanocellulose was found to be nodular in structure, Figure 3.2.

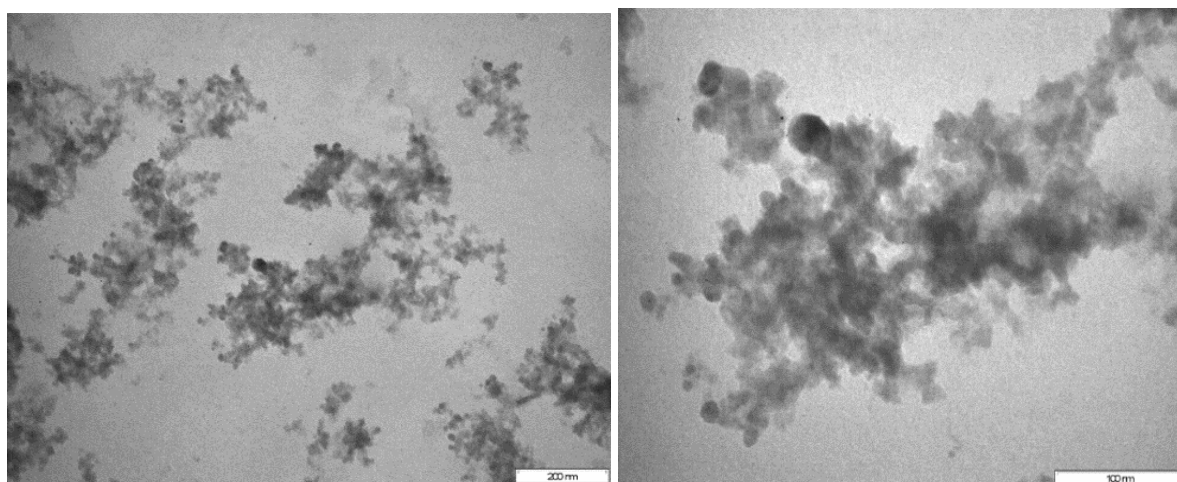


Figure 3.2. TEM image of neat polypyrrole.

Distinct nodular structures are visible for pure polypyrrole, Figure 3.2. There was no connective network existing between the particles to allow a conductive system to exist. In comparison to the nanohybrid in Figure 3.3 to Figure 3.8, there was a well-defined network in nanosheath formation. The dispersal of the nanocellulose within the nanohybrid are visible. The polypyrrole was deposited on the surface of nanocellulose forming a continuous nanosheath structure. The hydrogen bonds between imine groups of PPy and hydroxyl groups of nanocellulose served as an interaction to assist with the growing of the continuous nanosheath of PPy on NC and prevented the formation of large scale PPy aggregation.^[21] Large scale aggregation of PPy was not observed which demonstrated that nanocellulose acted as a suitable template for the polymerization of pyrrole monomer as there was a more connected network and dispersion. Moreover, the PPy@NCC nanohybrid prepared *via* conventional routes through dialysis exhibited a similar morphology as that of the PPy@NFC nanohybrid that was not subjected to dialysis as compared from Figure 3.3 to Figure 3.8.

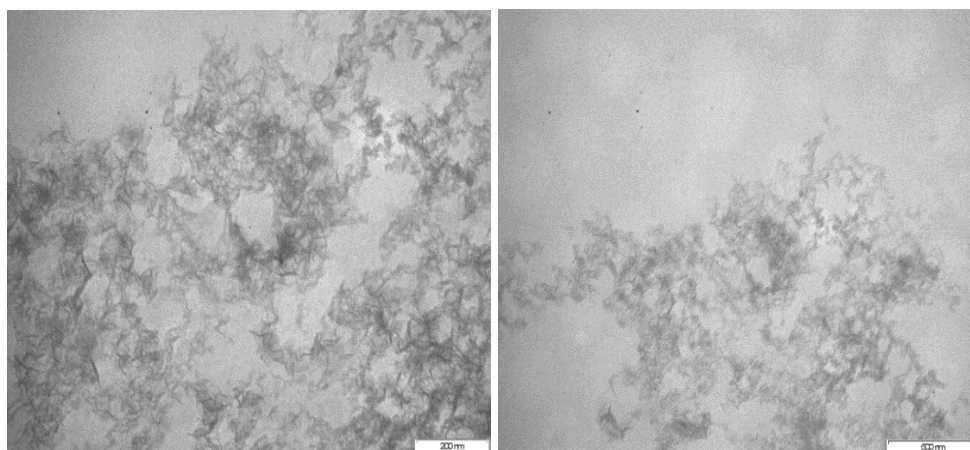


Figure 3.3. TEM images for PPy@NCC from BC- dialysis method.

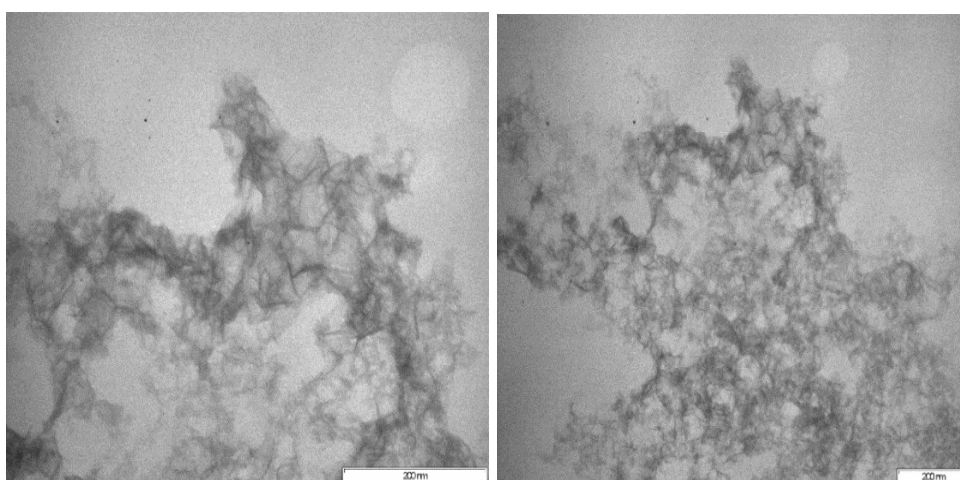


Figure 3.4. TEM images for PPy@NFC from BC- dialysis-free method.

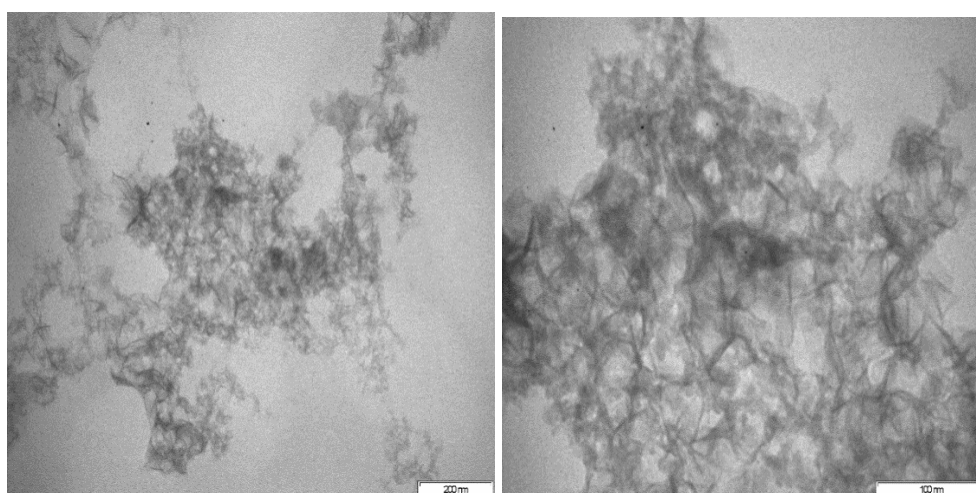


Figure 3.5. TEM images for PPy@NCC from Whatman filter paper- dialysis method.

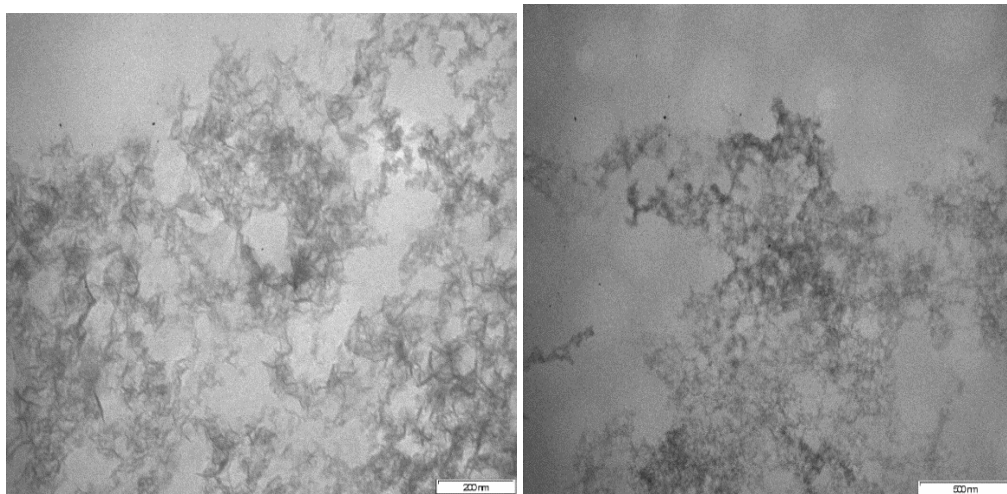


Figure 3.6. TEM images for PPy@NFC from Whatman filter paper- dialysis-free method.

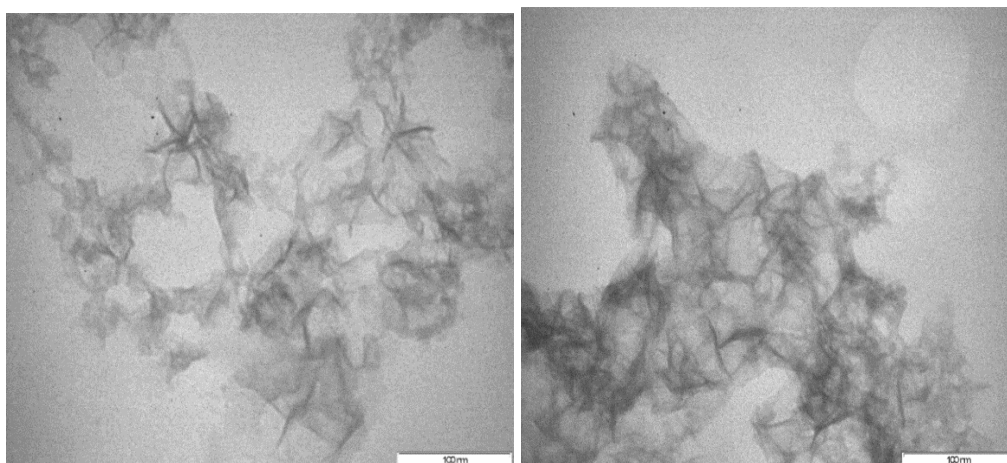


Figure 3.7. TEM images for PPy@NCC from hardwood pulp- dialysis method.

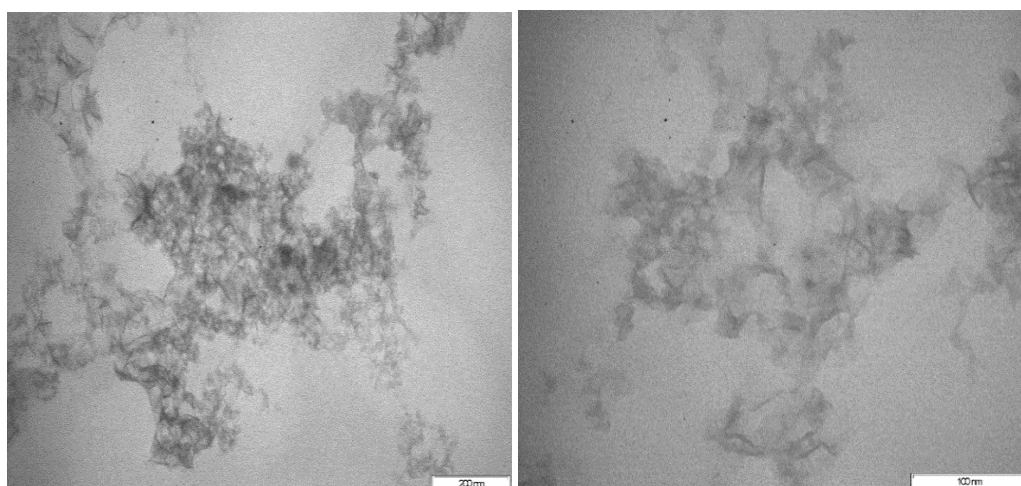


Figure 3.8. TEM images for PPy@NFC from hardwood pulp- dialysis-free method.

3.6.2. SEM-EDS of nanohybrid samples

SEM images were taken for neat polypyrrole at 1.00K magnification and 5.00K magnification (Figure 3.9.), where the micrographs reveal that the surface morphology of polypyrrole has cauliflower structures with the florets. Such porous-like nanoparticles morphological alteration exhibits the influence of oxidant on the rate of chemical polymerization, which significantly affects the growth and nucleation rate. According to the SEM-EDS elemental analysis, for neat polypyrrole, a high percentage of carbon 59.76 wt.%, nitrogen 14.81 wt.% and oxygen of 11.21 wt.% was found, which are distinctive elements for pyrrole. The elements of iron 2.54 wt.% and chlorine 11.68 wt.% are present in the sample due to the ferric trichloride used as a catalyst to initiate polymerisation. The presence and ratio of the iron to the polypyrrole sample is at minimum trace levels and bare no impact on the conductivity of the sample. The sharp chlorine peak compared to other elemental peaks are due to the higher energy absorbance of chlorine as compared to the other elements present. With further washing of the sample, it was possible to remove the last traces of ferric trichloride.

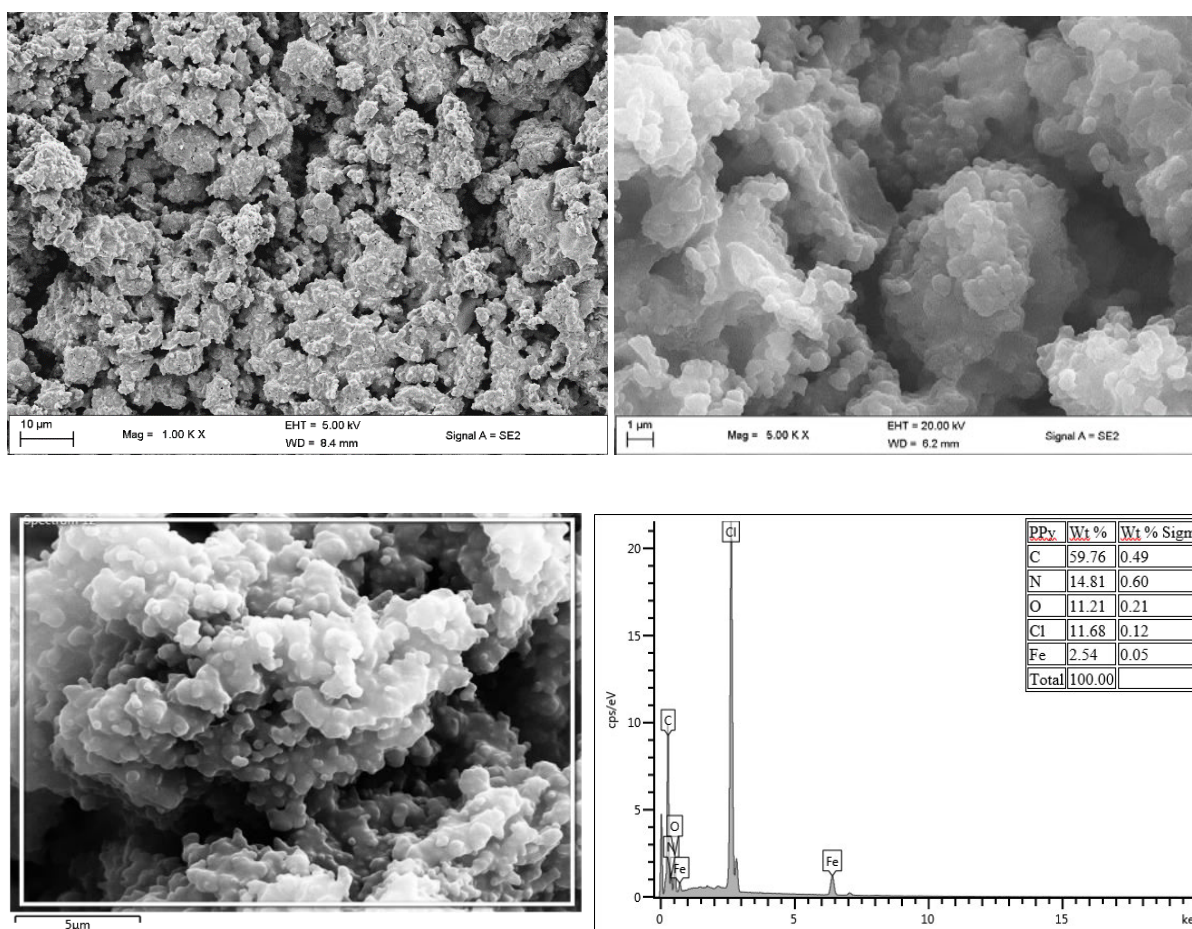


Figure 3.9. SEM-EDS image of neat polypyrrole.

The SEM images for the polypyrrole in various nanocellulose samples was taken, Figure 3.10 to 3.15. The sample was a powdery material with dispersed uniformity. According to the SEM-EDS elemental analysis, Figure 3.10, of PPy@NCC for dialysed bacterial cellulose, Figure 3.11 of PPy@NFC for dialysis-free bacterial cellulose, Figure 3.12 of PPy@NCC of dialysed Whatman filter paper, Figure 3.13 of PPy@NFC for dialysis-free Whatman filter paper, Figure 3.14 of PPy@NCC for dialysed hardwood pulp, and Figure 3.15 of PPy@NFC for dialysis-free hardwood pulp, a strong presence of carbon, nitrogen and oxygen was found. These high weight percentages are attributed to the structural component of polypyrrole as well as the nanocellulose chemical structure which contribute surplus amounts of carbon, oxygen and nitrogen. In the preparation of the polypyrrole nanohybrids, additional washing was introduced to remove as much of the ferric trichloride as possible, the wt % of the ferric trichloride decreased substantially as compared to neat polypyrrole.

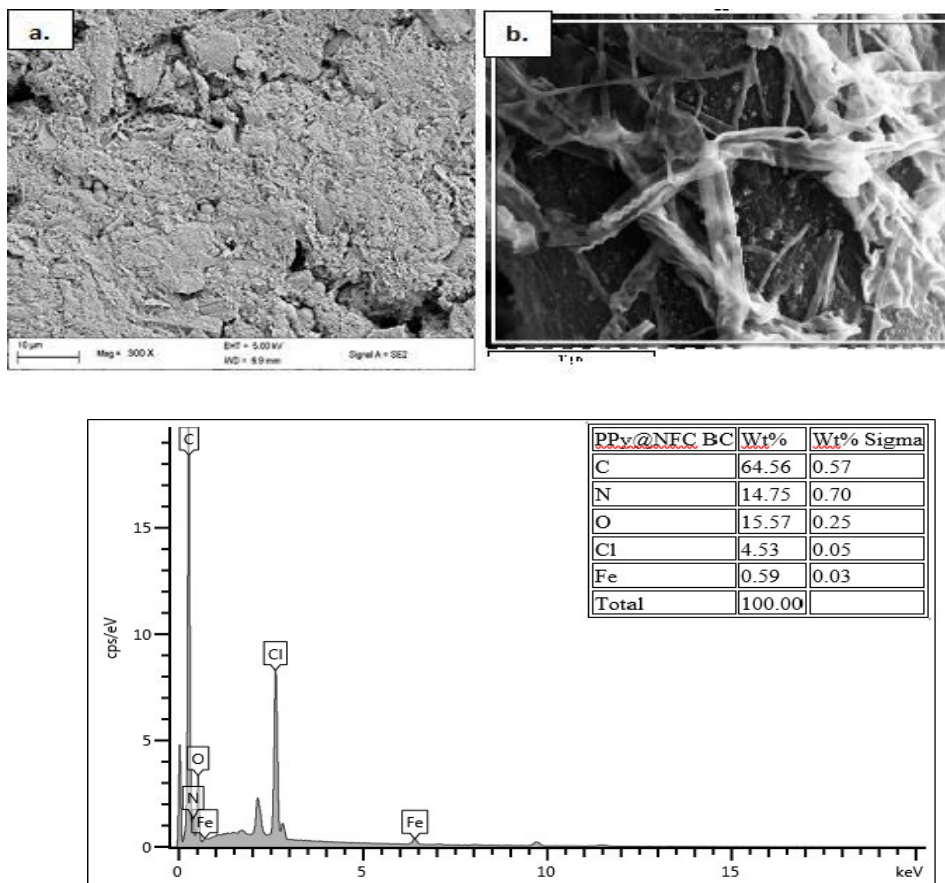


Figure 3.10. SEM image of (a) PPy@NCC from dialysed bacterial cellulose with (b) SEM-EDS elemental analysis of a specific cross section.

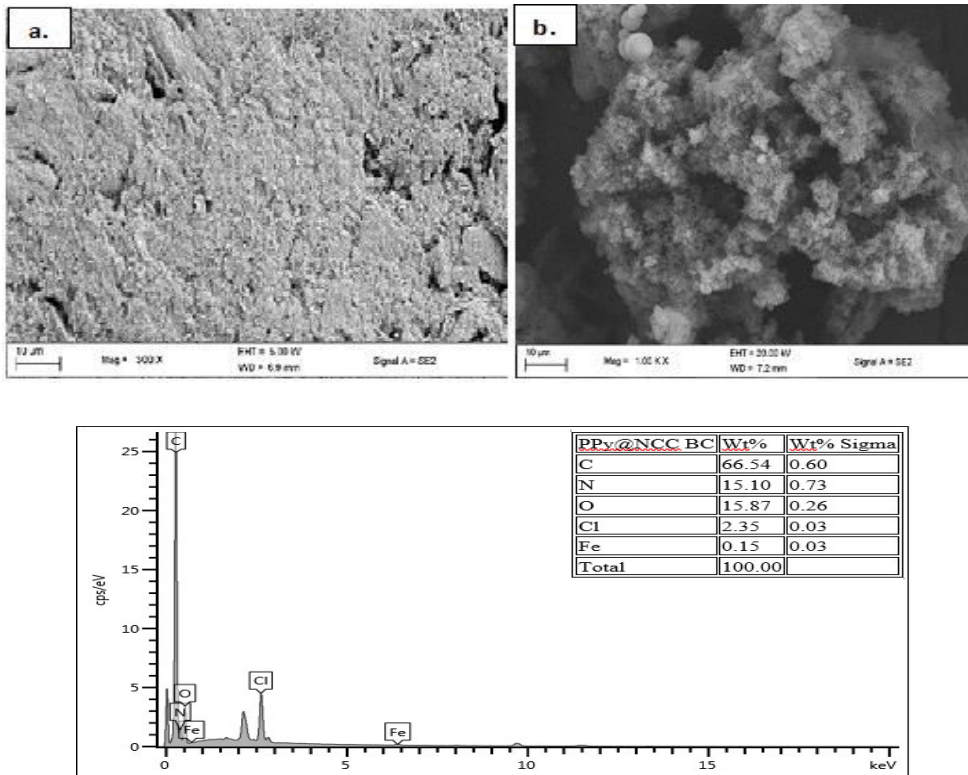


Figure 3.11. SEM image of (a) PPy@NFC from dialysis-free bacterial cellulose with (b) SEM-EDS elemental analysis of a specific cross section.

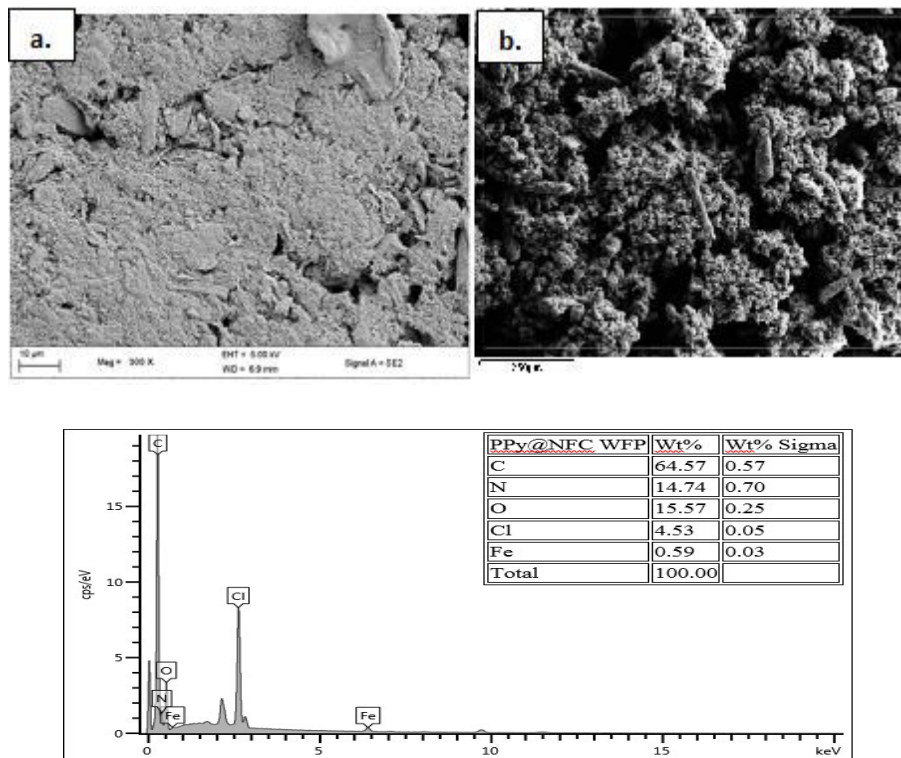


Figure 3.12. SEM image of (a) PPy@NCC from dialysed Whatman filter paper with (b) SEM-EDS elemental analysis of a specific cross section.

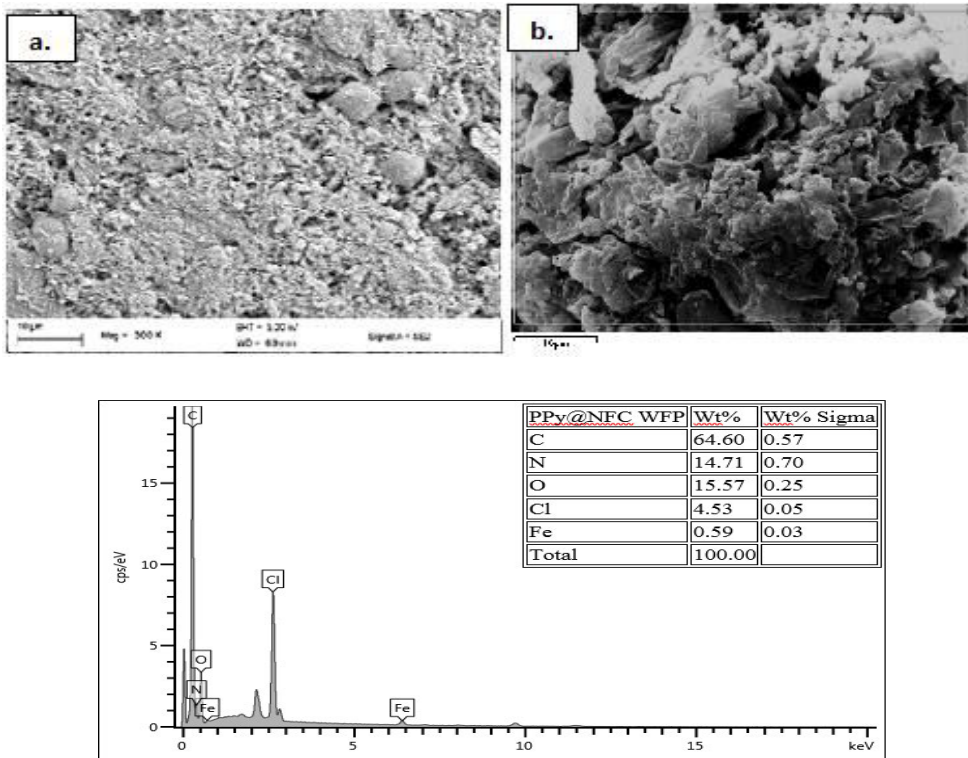


Figure 3.13. SEM image of (a) PPy@NFC from dialysis-free Whatman filter paper with (b) SEM-EDS elemental analysis of a specific cross section.

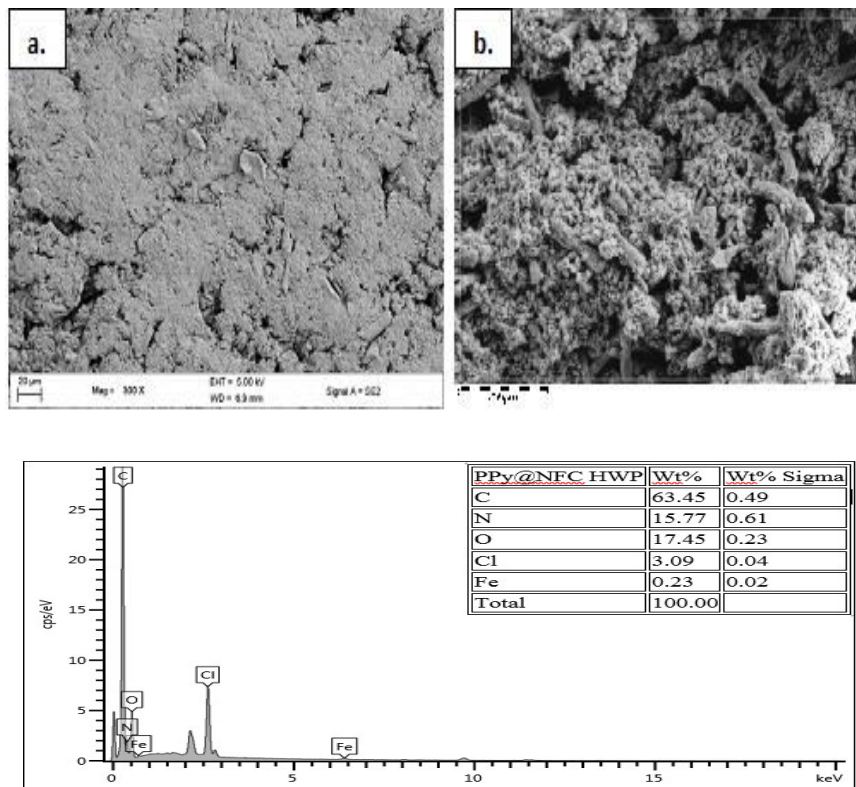


Figure 3.14. SEM image of (a) PPy@NCC from dialysed hardwood pulp with (b) SEM-EDS elemental analysis of a specific cross section.

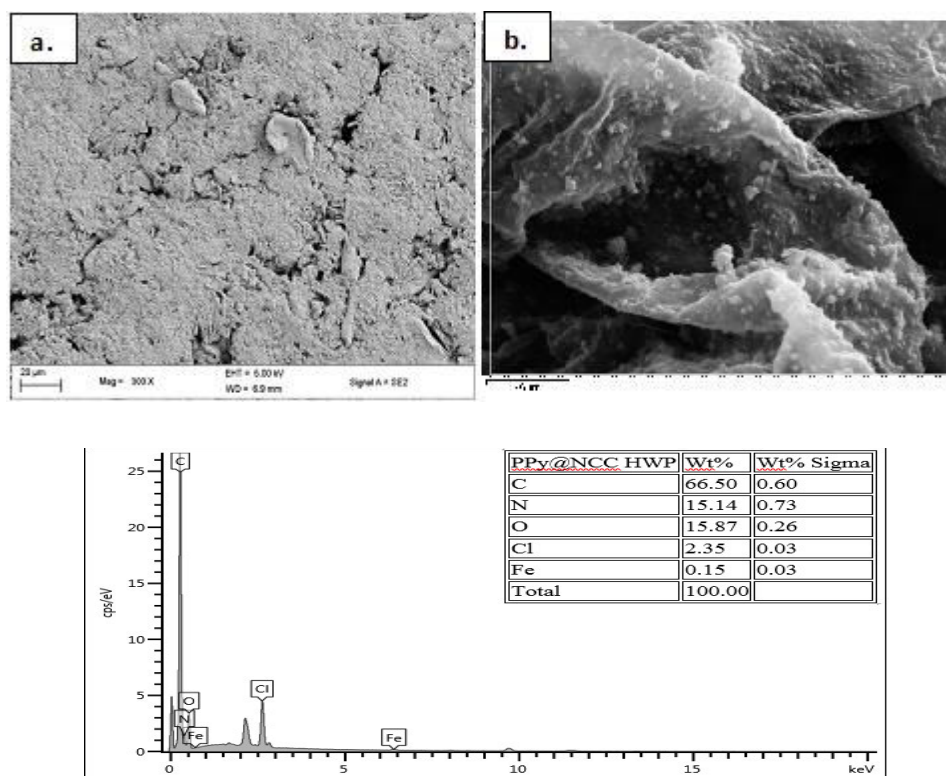


Figure 3.15. SEM image of (a) PPy@NCC from dialysis-free hardwood pulp with (b) SEM-EDS elemental analysis of a specific cross section.

To evaluate the feasibility of this PPy@NCC nanohybrid in construction of conductive polymer nanocomposites, PPy@NC/PVA, PPy@NC nanohybrid was mixed in Polyvinyl alcohol. The PPy@NC nanohybrid is found in the interstitial space between the PVA and formed a continuous network, which benefited from the good suspension property and high aspect ratio of the PPy@NC nanohybrid. The morphology of PPy@NC/PVA nanocomposite was characterized by TEM observation. The continuous network structure enhances the electrical conductivity as well as mechanical properties of the nanocomposites. To achieve higher conductivity at the same PPy content, it is expected that all the PPy participate in the fabrication of a continuously conductive network in the PVA matrix. Unfortunately, for neat PPy severe agglomeration was observed due to its poor suspension stability which made it difficult to connect with each other and form conductive networks, as seen in Figure 3.16 However, a continuous network structure of PPy@NC nanohybrid could be formed by incorporation of nanocellulose due to the remarkably enhanced stability in PVA. As a result, compared with PPy/PVA significant distribution within PVA is observed for all PPy@NC/PVA samples.

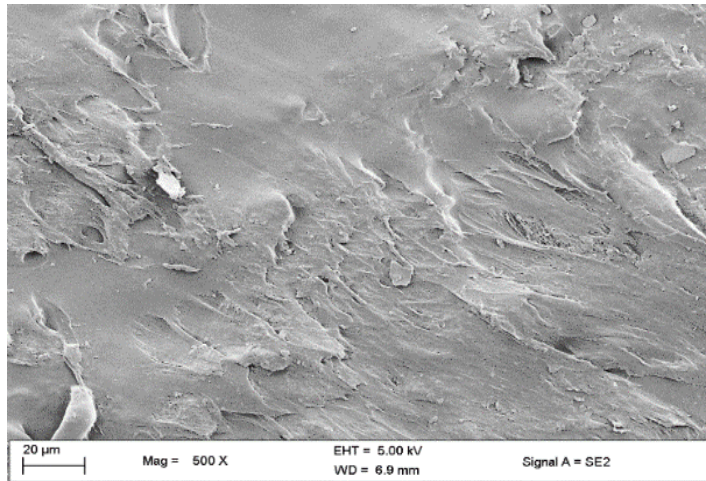


Figure 3.16. SEM image of polypyrrole in PVA.

The SEM images for PPy@NC/PVA, Figure 3.17 to Figure 3.22, show a more uniform surface structure than that of neat PPy/PVA. The nanohybrid possessed a smooth surface texture with an improved connected network. Bacterial cellulose was used as the source of the NC that was incorporated in the nanohybrid possessed the most homogeneity when incorporated in PVA where there were minimum irregularity and distortions. The samples from Whatman filter paper and hardwood pulp also had good uniformity. When comparing the samples containing the dialyzed nanocellulose (PPy@NCC/PVA) to the samples containing the dialysis-free nanocellulose (PPy@NCC/PVA) there is no visible difference. The size, morphology, and dispersion state of conductive fillers have significant effects on the mechanical properties of conductive composites. The mechanical properties of PPy@NFC/PVA nanocomposites were comparable to that of PPy@NCC/PVA nanocomposites.

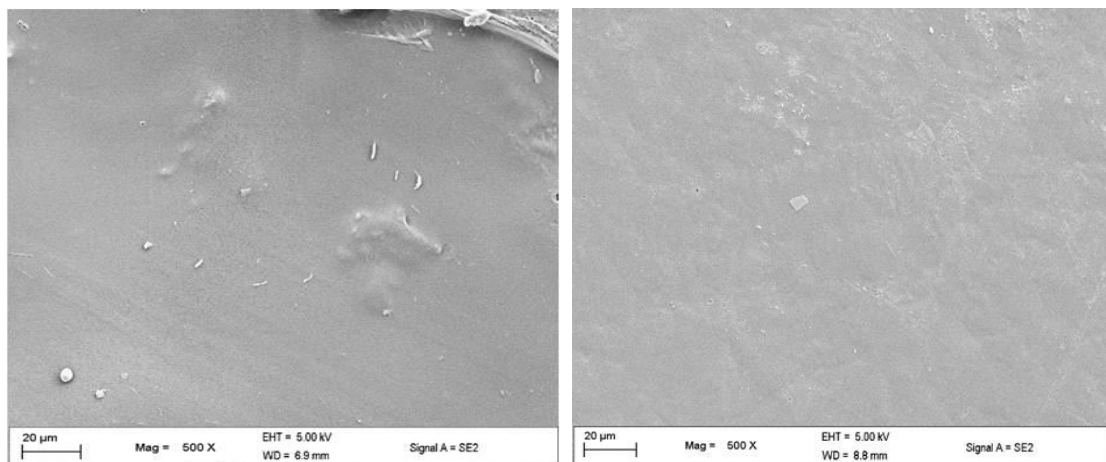


Figure 3.17. SEM image of PPy@NCC in PVA from BC- *via* dialysis method.

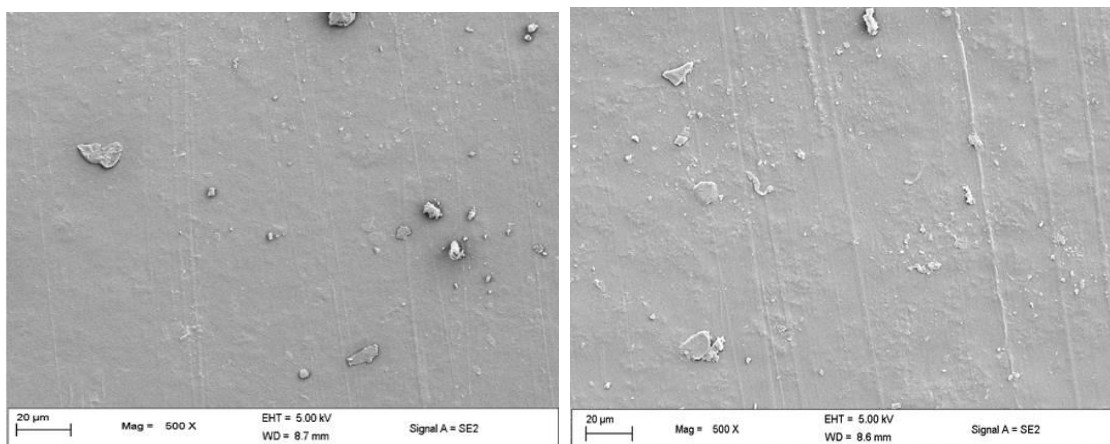


Figure 3.18. SEM image of PPy@NFC in PVA from BC- *via* dialysis-free method.

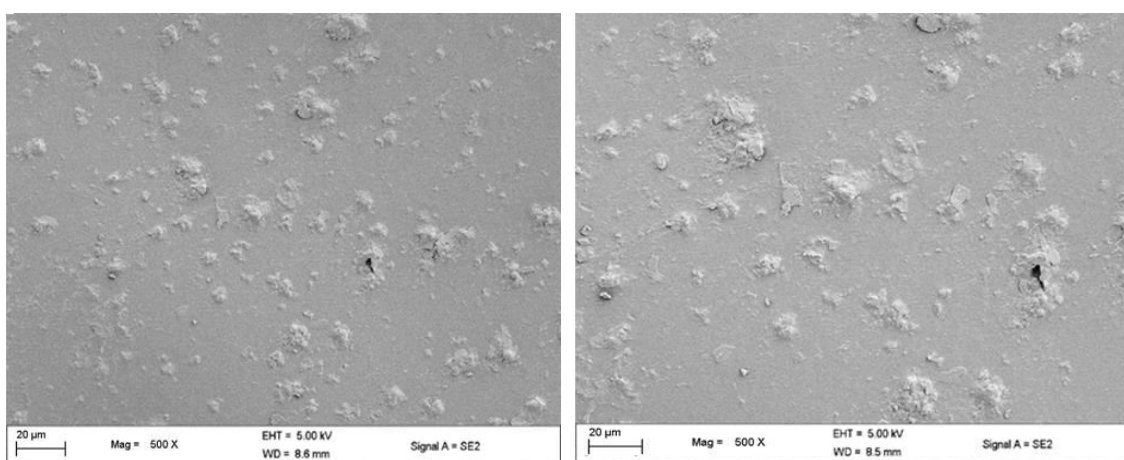


Figure 3.19. SEM image of PPy@NCC in PVA from Whatman filter paper- *via* dialysis method.

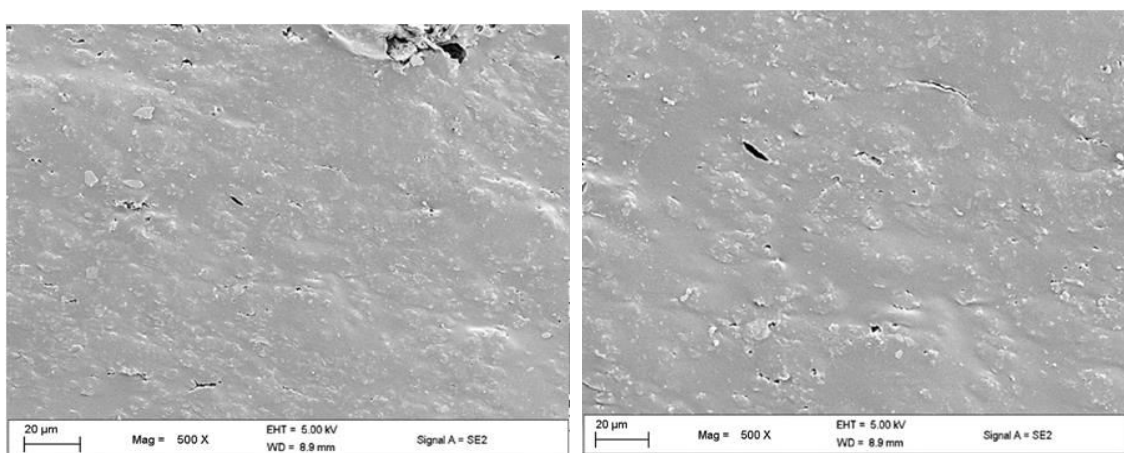


Figure 3.20. SEM image of PPy@NFC in PVA from Whatman filter paper- *via* dialysis-free method.

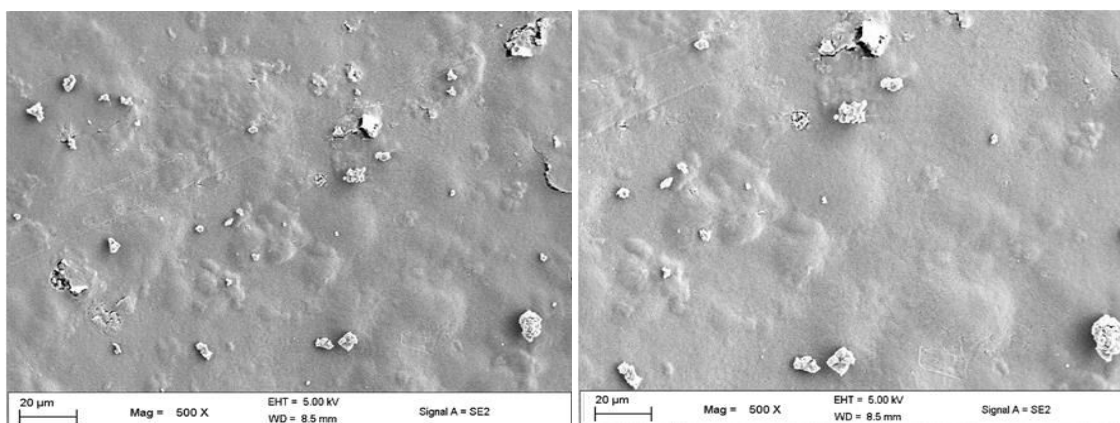


Figure 3.21. SEM image of PPy@NCC in PVA from Hardwood pulp- *via* dialysis method.

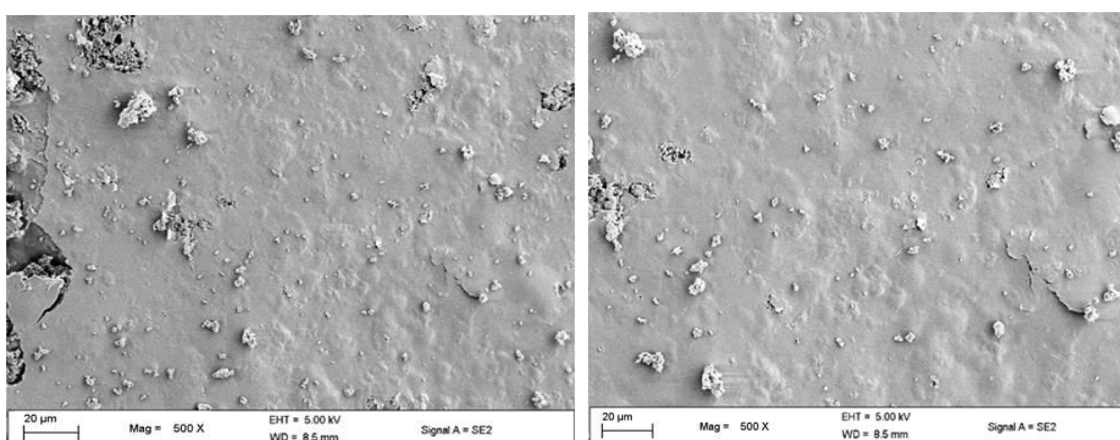


Figure 3.22. SEM image of PPy@NFC in PVA from Hardwood pulp- *via* dialysis-free method.

This superior straightforward, green, cost effective, and scalable approach to PP@NFC/PVA nanocomposites with nearly identical performance compared with PPy@NCC/PVA nanocomposites makes it more suitable and applicable for the large-scale application of nanocellulose based conductive nanocomposites.

3.6.3. FT-IR of nanohybrid samples

FT-IR analysis was carried out to analyse the chemical structure of neat Polypyrrole and PPy@NC nanohybrids. The characteristic bands of neat PPy can also be observed clearly in Figure 3.23. The bands around 3222 and 1527 cm^{-1} are responsible for the N-H stretching vibration and C-C ring stretching of the quinonoid structure in PPy. The band at 1441 cm^{-1} is attributed to C-N stretching vibration in the pyrrole ring. Additionally, bands at 1247, 1155.18,

and 1032 are ascribed to C-H on-plane vibration, and the band at 894 cm^{-1} is for C-H out-of-plane vibration. The FT-IR for all PPy@NC nanohybrid, from Figure 3.24 to Figure 3.28, exhibit a similar spectrum as that of neat PPy, however, all major peaks for PPy@NC have shifted wavenumbers with additional peaks attributed to nanocellulose, suggesting the existence of the interaction between PPy and nanocellulose. The FT-IR spectrum of PPy@NC nanohybrids appeared like a superposition of the FT-IR curves of neat polypyrrole and nanocellulose. However, the intensity of the O-H stretching band of NC and N-H stretching band of PPy decreased dramatically. On the other hand, peaks for NC and PPy in PPy@NC nanohybrids shifted to lower wavenumbers compared to the neat NC and PPy. These results all suggested that NC formed strong interfacial interactions with the polypyrrole layer. This is ascribed to the hydrogen bonding interaction between -OH of nanocellulose and -NH of polypyrrole.

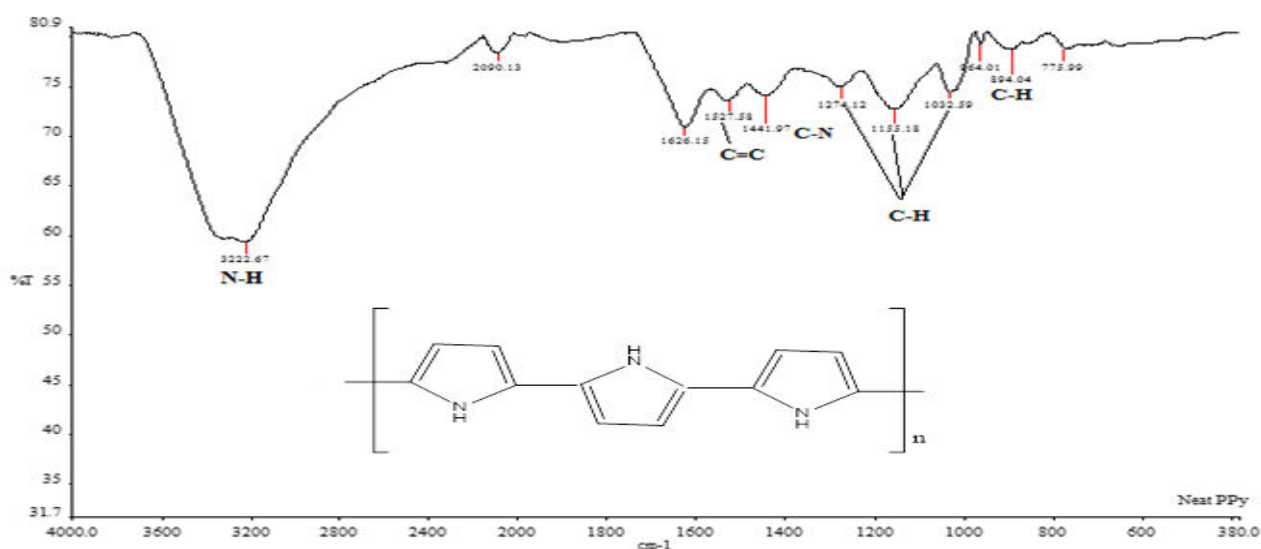


Figure 3.23. FT-IR spectra for neat polypyrrole.

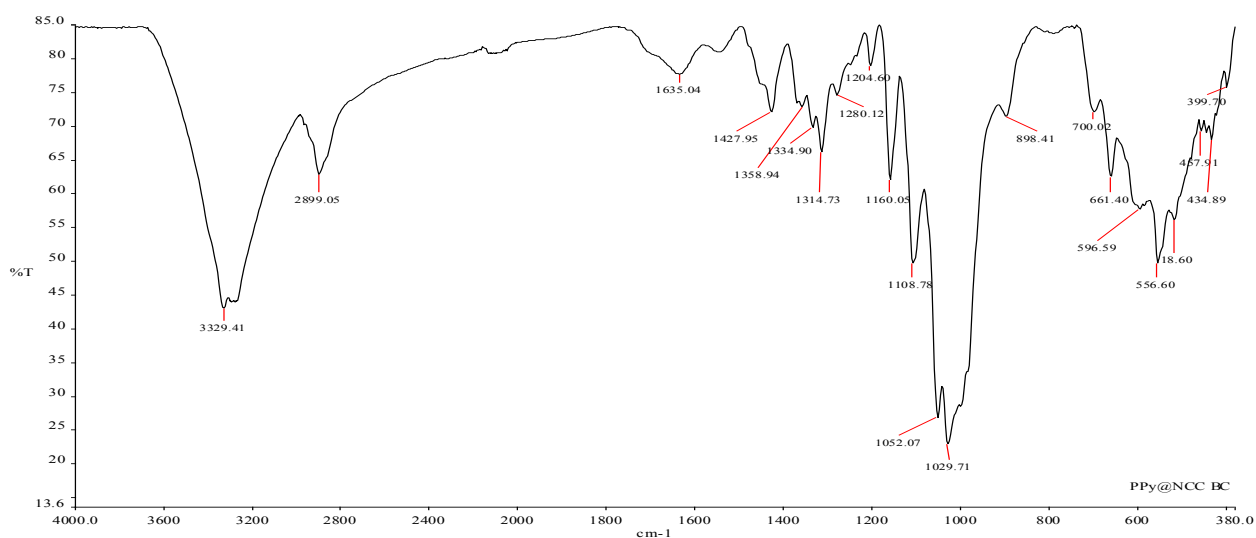


Figure 3.24. FT-IR spectra for PPy@NCC nanohybrid from Bacterial cellulose (dialyzed).

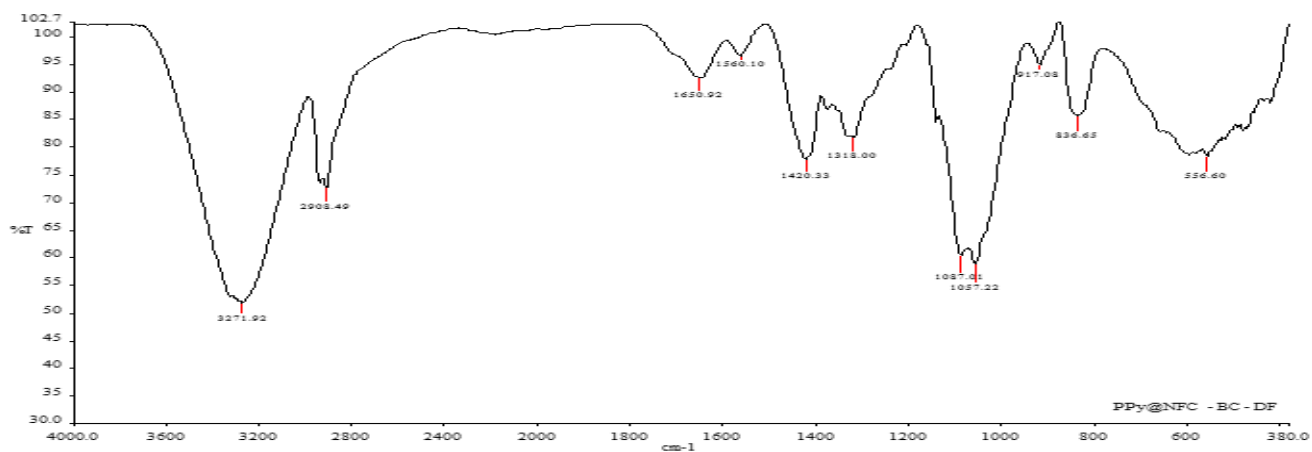


Figure 3.25. FT-IR spectra for PPy@NFC from Bacterial cellulose (dialysis-free).

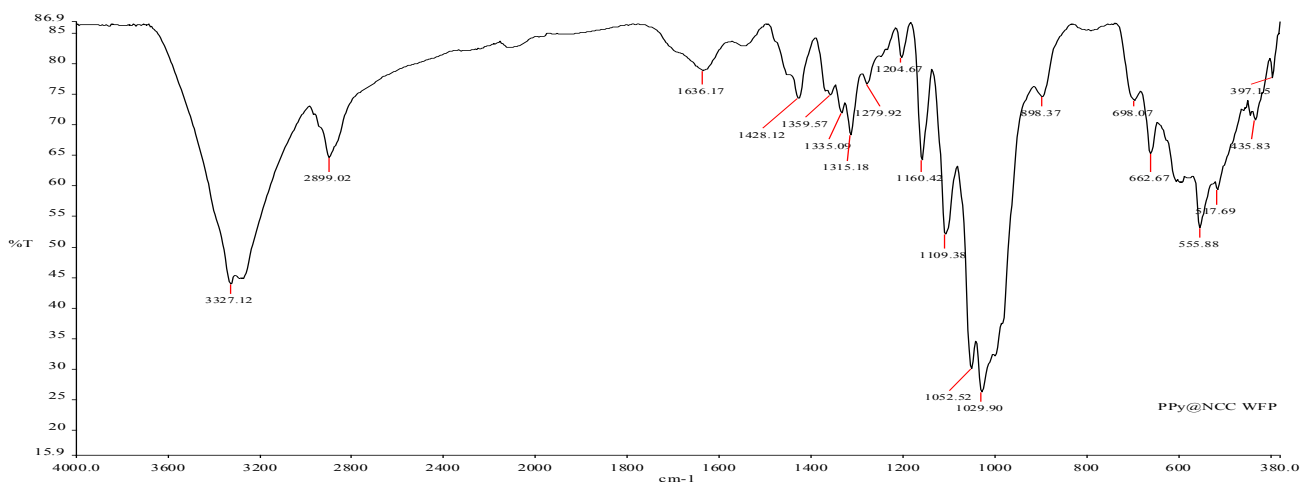


Figure 3.26. FT-IR spectra for PPy@NCC nanohybrid from Whatman filter paper (dialyzed).

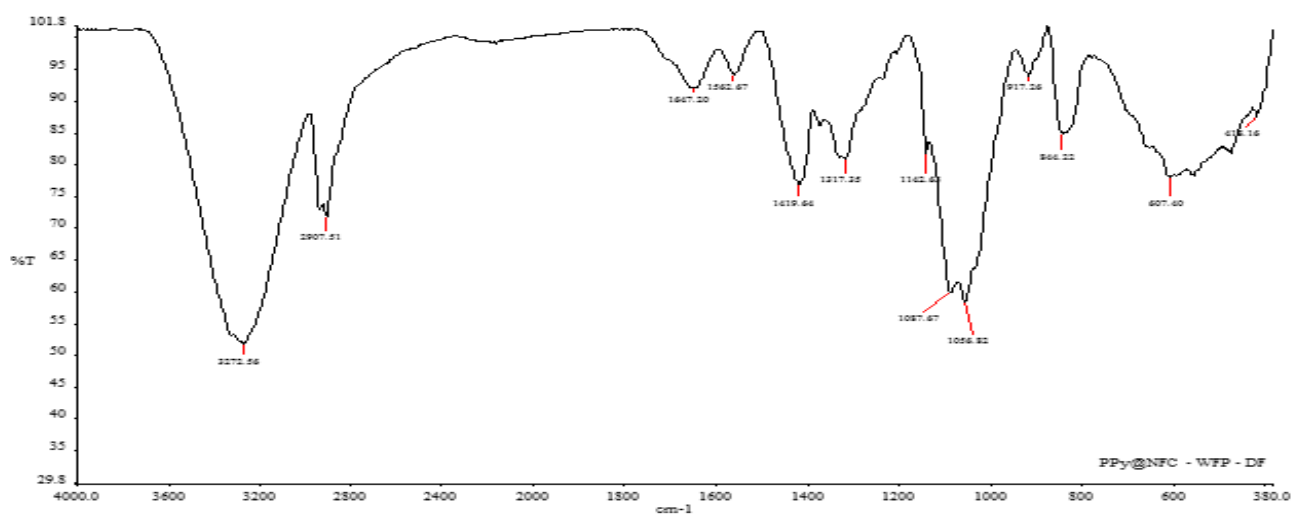


Figure 3.27. FT-IR spectra for PPy@NFC nanohybrid from Whatman filter paper (dialysis-free).

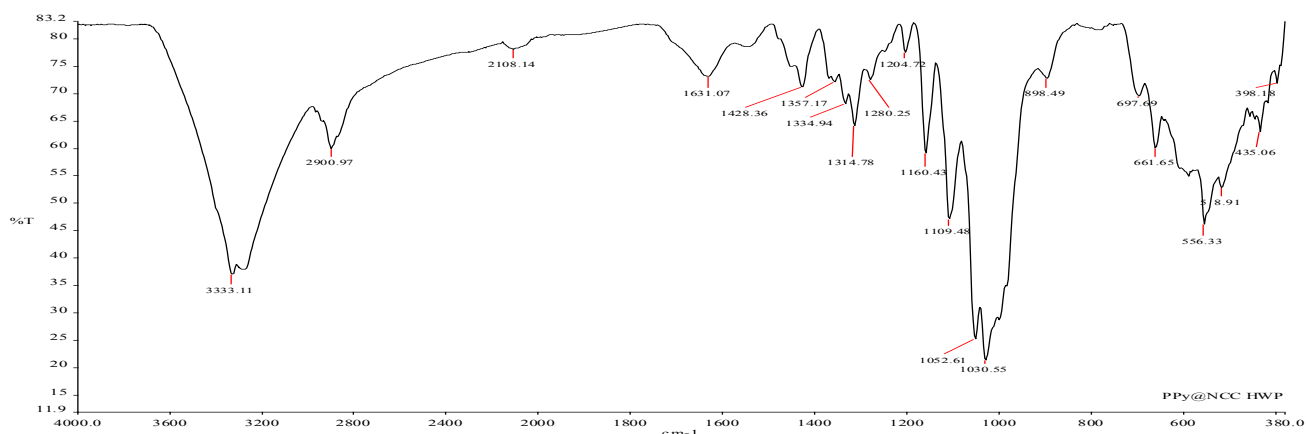


Figure 3.28. FT-IR spectra for PPy@NCC nanohybrid from hardwood pulp (dialyzed).

3.6.4. Raman spectroscopy of nanohybrid samples

From the Raman spectra for neat polypyrrole in Figure 3.29., the peak found at 932 cm^{-1} was attributed to the ring deformation associated with the di-cation (di-polaron)^[22, 23] and the peak at 981 cm^{-1} assigned to the radical cation (polaron).^[22, 23] The peak at 1042 cm^{-1} appeared due to the C-H in plane deformation. The band at 1402 cm^{-1} is due to the C-N stretch mode of polypyrrole.^[22, 24] The Raman spectra for all PPy@NCC and for all PPy@NFC composites from various cellulose sources are shown in Figure 3.30. to Figure 3.32. They show characteristic bands around 1100 cm^{-1} and 2900 cm^{-1} that are common to cellulose.^[25] Also observed are the characteristic bands ascribed to polypyrrole, where bands for the peak was found around 930 cm^{-1} which was attributed to the ring deformation associated with the di-cation (di-polaron)^[22, 23] and a peak around 980 cm^{-1} for the radical cation (polaron).^[22, 23] The peak at 1040 cm^{-1} appeared due to the C-H in-plane deformation and the band at 1400 cm^{-1} was assigned to the C-N stretch mode of polypyrrole.^[22, 24]

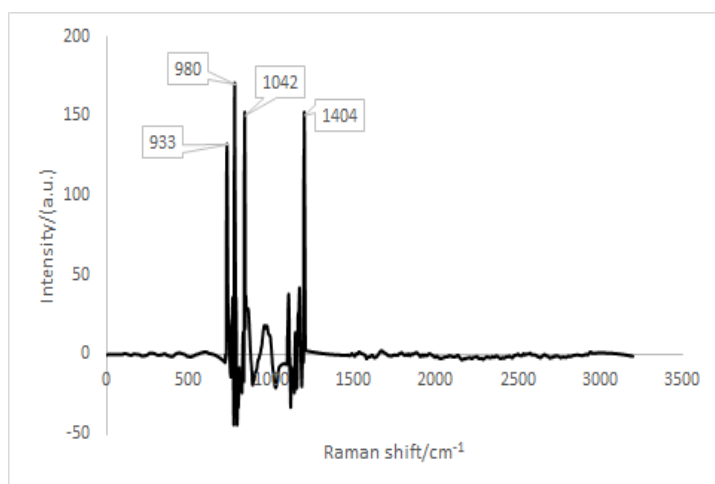


Figure 3.29. Raman spectra of neat polypyrrole.

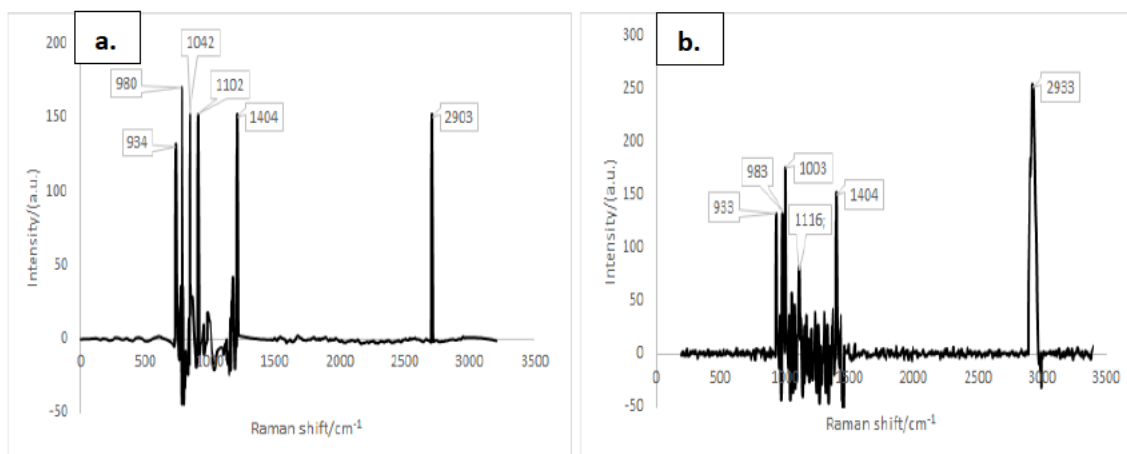


Figure 3.30. Raman spectra for (a). PPy@NCC from bacterial cellulose (dialyzed) and (b). PPy@NFC from bacterial cellulose (dialysis-free).

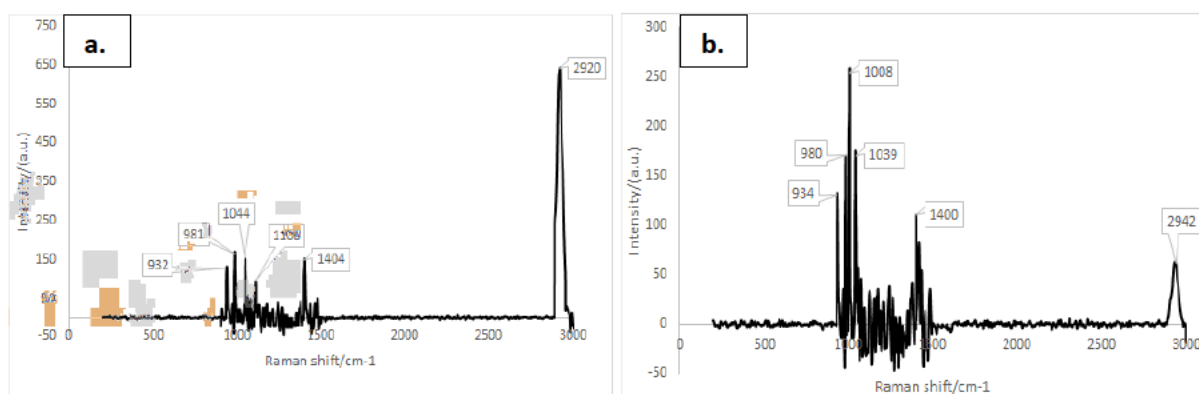


Figure 3.31. Raman spectra for (a). PPy@NCC from Whatman filter paper (dialyzed) and (b). PPy@NFC from Whatman filter paper (dialysis-free).

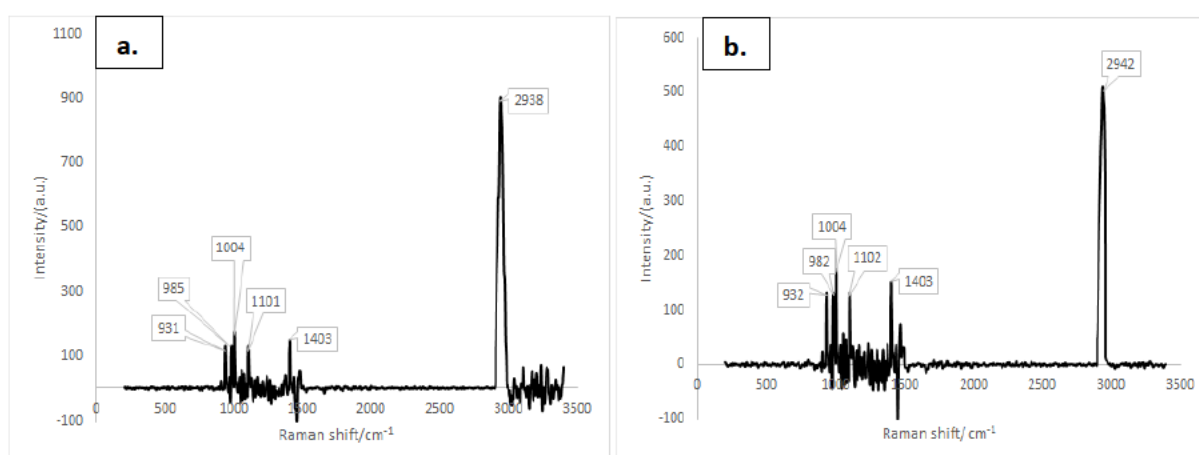


Figure 3.32. Raman spectra for (a). PPy@NCC from hardwood pulp (dialyzed) and (b). PPy@NFC from hardwood pulp (dialysis-free).

3.6.5. UV-Vis analysis

UV-Vis analysis was carried out for PPy with dialyzed nanocellulose and PPy with dialysis-free nanocellulose from bacterial grown cellulose, Whatman filter paper and hardwood pulp. The absorption peak in UV-Vis spectra of neat PPy suspension was much weaker than all PPy@NC nano hybrids. See Figure 3.33. and Figure 3.34. This was because of PPy being poorly dispersed in water and precipitating out in aggregated form. The results confirmed that the dispersibility of PPy could be significantly improved by the incorporation of renewable and biodegradable nanocellulose. In addition, when comparing the nano hybrids using the dialyzed nanocellulose data to the dialysis-free nanocellulose, the PPy@NC nano hybrid showed two absorption bands around 350 and 730 nm in the UV-Vis spectrum. The first band at 350 nm was due to the $\pi-\pi^*$ interband transition and the second broad band around 730 nm was assigned to the polaron and bipolaron band transition of PPy.^[26] This indicated the successful synthesis of PPy on nanocellulose. Thus, a PPy@NCC nano hybrid with a high aspect ratio was successfully synthesized by incorporation of nanocellulose using a dialysis-free and *in situ* doping route. Compared with neat PPy, this PPy@NC nano hybrid exhibited a good and adjustable suspension property, which makes it more suitable and effective to fabricate PPy based conductive nanocomposites.

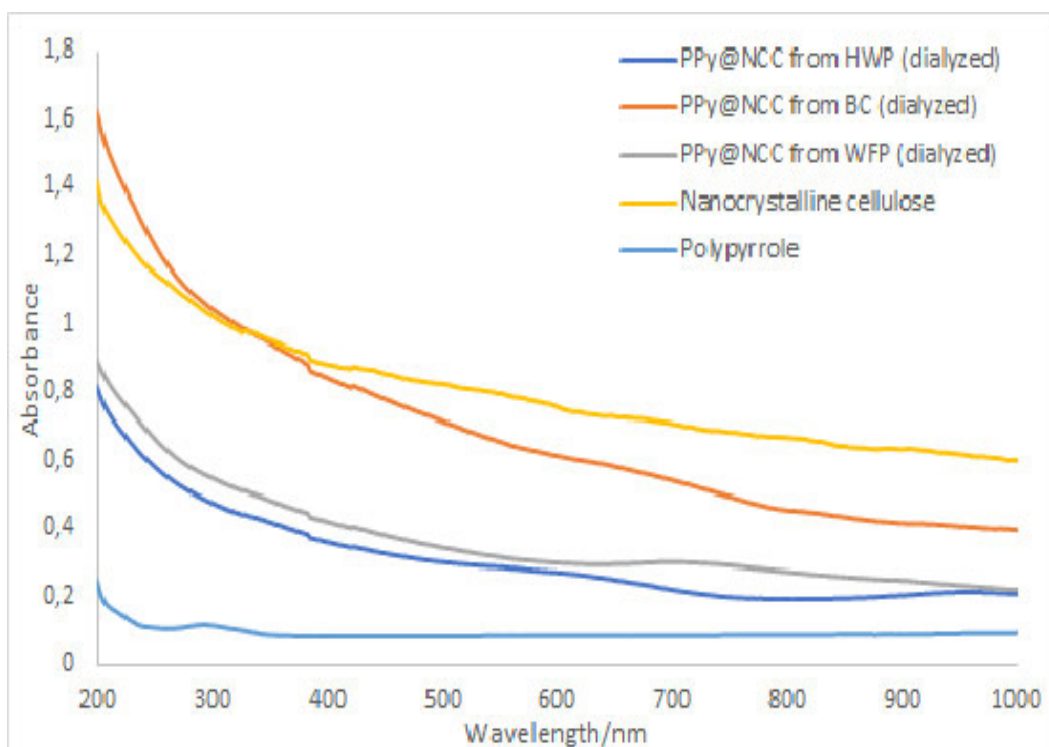


Figure 3.33. UV-Vis spectra of Polypyrrole, NCC (dialyzed) and nano hybrid from BC, WFP and HWP.

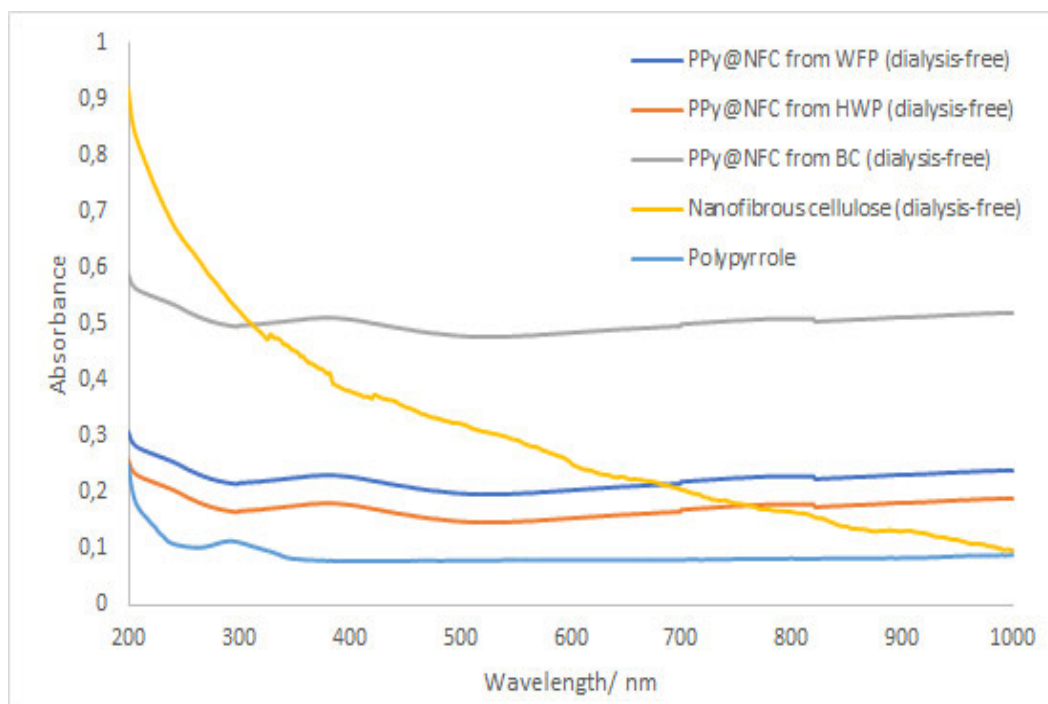


Figure 3.34. UV-Vis spectra of Polypyrrole, NFC (dialysis-free) and nanohybrid from BC, WFP and HWP.

From the results it was evident that the successful polypyrrole and nanocellulose nanohybrid was synthesized. The polypyrrole was efficaciously deposited on nanocellulose as a continuous structure, forming a PPy@NC nanohybrid. For the dispersibility tests it was evident that the ratio of 1:1 polypyrrole to nanocellulose is the optimum ratio for good distribution within solution which in turn yields a more uniform film. Between the dialysed and dialysis-free nanocellulose, there was no structural or mechanical differences found. The synthesis of polypyrrole@nanocellulose proved to be a new strategy to realize the facile and environmentally friendly production of a of the nanohybrid, which opened new opportunities for the large-scale fabrication and application of nanocellulose based nanocomposites with low cost and high performance.

3.7. References

1. Zhou, Z., *Cellulose nanocrystals as a novel support for CuO nanoparticles catalysts: Facile synthesis and their application to 4-nitrophenol reduction*. RSC Advances, 2013, **3**, 26066-26073.
2. Snook, G.A., Kao, P., Best, A.S., *Conducting-polymer-based supercapacitor devices and electrodes*. Journal of Power Sources, 2011, **196**, 1-12.

3. Shinde, S.S., *Morphological modulation of polypyrrole thin films through oxidizing agents and their concurrent effect on supercapacitor performance*. *Electrochimica Acta*, 2014, **119**, 1-10.
4. Duchet, J., Legras, R., Demoustier-Champagne, S., *Chemical synthesis of polypyrrole: Structure–properties relationship*. *Synthetic metals*, 1998, **98**, 113-122.
5. Cheng, J., Fou, A., Rubner, M., *Molecular self-assembly of conducting polymers*. *Thin Solid Films*, 1994, **244**, 985-989.
6. Shoa, T., *Electromechanical coupling in polypyrrole sensors and actuators*. *Sensors and Actuators A: Physical*, 2010, **161**, 127-133.
7. De Paoli, M.A., *Study of the electrochromism of polypyrrole/dodecylsulfate in aqueous solutions*. *Electrochimica Acta*, 1990, **35**, 1145-1148.
8. Liu, Y.-C., *Method of evaluating the ionic conductance of polypyrrole films and improvement of ionic conductance of polyethylene oxide-incorporated polypyrrole composite*. *Materials chemistry and physics*, 2003, **77**, 791-795.
9. Wang, J., *Novel electrode substrates for rechargeable lithium/polypyrrole batteries*. *Journal of power sources*, 2005, **140**, 162-167.
10. Liu, Y.-C., Hwang, B. J., *Enhancement of conductivity stability of polypyrrole films modified by valence copper and polyethylene oxide in an oxygen atmosphere*. *Thin Solid Films*, 2000, **360**, 1-9.
11. Erlandsson, R., *XPS and electrical characterization of BF₄⁻-doped polypyrrole exposed to oxygen and water*. *Synthetic metals*, 1985, **10**, 303-318.
12. Deshmukh, K., *Highly dispersible graphene oxide reinforced polypyrrole/polyvinyl alcohol blend nanocomposites with high dielectric constant and low dielectric loss*. *RSC Advances*, 2015, **5**, 61933-61945.
13. Wang, L. X., Li, X. G., Yang, Y. L., *Preparation, properties and applications of polypyrroles*. *Reactive and Functional Polymers*, 2001, **47**, 125-139.
14. Ferraz, N., *In vitro and in vivo toxicity of rinsed and aged nanocellulose–polypyrrole composites*. *Journal of Biomedical Materials Research Part A*, 2012, **100**, 2128-2138.
15. Bober, P., *Biocomposites of nanofibrillated cellulose, polypyrrole, and silver nanoparticles with electroconductive and antimicrobial properties*. *Biomacromolecules*, 2014, **15**, 3655-3663.
16. Tang, L., *Flexible conductive polypyrrole nanocomposite membranes based on bacterial cellulose with amphiphobicity*. *Carbohydrate polymers*, 2015, **117**, 230-235.

17. Zhang, X., *Dialysis-free and in situ doping synthesis of polypyrrole@ cellulose nanowhiskers nanohybrid for preparation of conductive nanocomposites with enhanced properties*. ACS Sustainable Chemistry & Engineering, 2015, **3**, 675-682.
18. Malhotra, U., Maity, S., Chatterjee, A., *Polypyrrole-silk electro-conductive composite fabric by in situ chemical polymerization*. Journal of Applied Polymer Science, 2015, **132**(4).
19. Chen, X., *The stability of polypyrrole electrical conductivity*. European polymer journal, 1994, **30**, 809-811.
20. Panero, S., *Characteristics of Electrochemically Synthesized Polymer Electrodes VI. Kinetics of the Process of Polypyrrole Oxidation*. Journal of The Electrochemical Society, 1989, **136**, 3729-3734.
21. Zhang, X., *Dialysis-Free and in Situ Doping Synthesis of Polypyrrole@Cellulose Nanowhiskers Nanohybrid for Preparation of Conductive Nanocomposites with Enhanced Properties*. ACS Sustainable Chemistry & Engineering, 2015, **3**, 675-682.
22. Zhang, B., *A facile synthesis of polypyrrole/carbon nanotube composites with ultrathin, uniform and thickness-tunable polypyrrole shells*. Nanoscale research letters, 2011, **6**, 431.
23. Chen, B., *Highly conjugated polypyrrole on multiwalled carbon nanotube templates analyzed by Raman spectroscopy*. International Conference on Smart Materials and Nanotechnology in Engineering. International Society for Optics and Photonics, 2007.
24. Mikat, J., Orgzall, I., Hochheimer, H., *Optical absorption and vibrational spectroscopy of conducting polypyrrole under pressure*. Synthetic metals, 2001, **116**, 167-170.
25. Kang, Y. R., *Fabrication of electric papers of graphene nanosheet shelled cellulose fibres by dispersion and infiltration as flexible electrodes for energy storage*. Nanoscale, 2012, **4**, 3248-3253.
26. Joulazadeh, M., Navarchian, A. H., *Polypyrrole nanotubes versus nanofibers: a proposed mechanism for predicting the final morphology*. Synthetic Metals, 2015, **199**, 37-44.

CHAPTER 4

In this study, an alternative method to the common four-point probe method, was used to measure resistivity. The current was measured using an amp meter at an applied voltage. The results were used to determine the average resistivity. When compared to the results from a four-point probe for the same sample, the results coincide, recognizing this method as a reliable alternative, but with the advantage that bulk resistivity is measured, as opposed to surface electrical behaviour only.

4.1. Experimental Procedure for Electrical Testing for Conductivity of the Polymer Samples

4.1.1. Resistivity test

For resistance testing of the polymer sample, a copper clad plate was etched with a ferric chloride solution to create a break in circuit where the sample was filled. The plate was cut into strips, Figure 4.1.

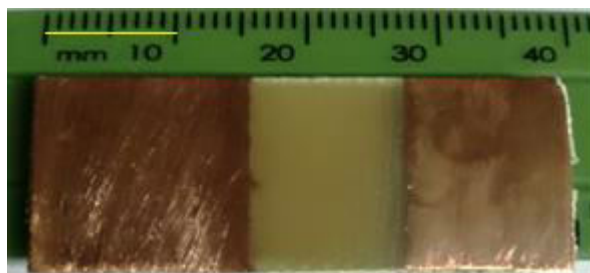


Figure 4.1. Sample of an etched copper clad board used to set sample for resistivity test.

For the resistivity test of the varying ratios of PPy:NC for bacterial nanofibrous cellulose, the corresponding plates were labelled and weighed accurately. Thereafter, an accurate volume of 0.25 mL liquid sample prepared in Section 3.2.2 for the varying ratios in PVA were then filled onto the etched space with an overlap onto the copper board to ensure contact in the circuit. This was left until dry. The sample plates were re-weighed. A digital picture was taken of each sample plate and the surface area of the etched section of the plate was measured precisely using Image-J software. For measuring the dimension on Image-J, a set scale is required. Since a digital picture is used, a ruler was utilized as the scale taken in the digital picture concurrently. The scale was measured at 10 mm as seen in an example in Figure 4.1. This was done

individually for every sample taken to ensure precision per sample board, and the dimensions were recorded.

The set up for measuring current and voltage values was set according to the image in Figure 4.2, a laboratory DC power supply Matrix model MPS-3003L-3 was used as the power source. This was directly attached to a 217.6 Ω resistor, which was connected to the sample, and a volt meter to measure the voltage applied in volts, and to an amp meter to measure the passing current in microamperes. By the division of the voltage by amperes, the average resistance is calculated. By plotting current vs. voltage, the reciprocal of the gradient is the average resistivity.

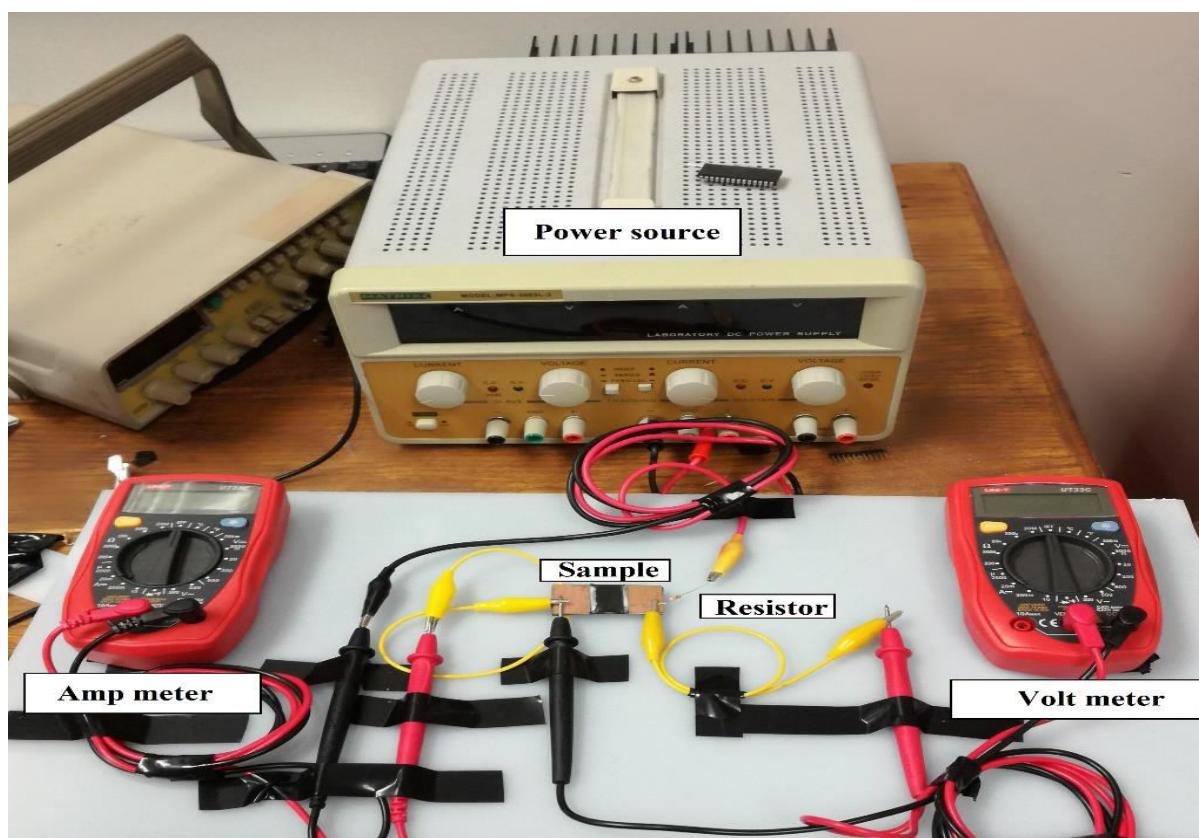


Figure 4.2. Sample set-up for resistivity test.

The same samples used in this method was then tested using a four-point probe to confirm results and approve this system methodology. This procedure of setting a film on the Cu plate and measurements was thereafter prepared in the exact method for all PPy@NC nanohybrid samples with the varying nanocellulose prepared as in Chapter 3- 3.4.2.

4.1.2. Morphological structure analysis

TEM analysis was performed using a transmission electron microscope. All liquid samples of PPy@NC/PVA, NCC/PVA and neat PVA aqueous suspensions were sonicated for 30 min to disperse the aggregation. A copper grid was dipped in the well-dispersed nanohybrid suspensions until drying and images were taken.

For the SEM study, a Zeiss Ultra Plus field emission gun scanning electron microscope (FEGSEM) equipped with energy dispersive X-ray (EDS) detector (Germany) was used. The samples were deposited separately on conductive carbon tapes stuck to aluminium stubs. Each sample was coated with gold with the aid of sputter coater to minimize charging.

The morphology of all nanohybrid samples were tested prior to subsection to the conductivity tests, as well as after the testing to note any morphological change. This was accomplished using the Zeiss LEO 1450 SEM study, samples for SEM images were taken directly from the Cu plate.

4.2. Results and Discussion

The electrical conductivity test for the varying ratios were first carried out. Figure 4.4 to Figure 4.8 shows the empty copper clad board and the board with the samples of varying ratios of bacterial nanofibrous cellulose set in. For comparison purposes, neat PVA was also analysed, Figure 4.3., which dried as a sheen plastic film that adhered to the board uniformly.

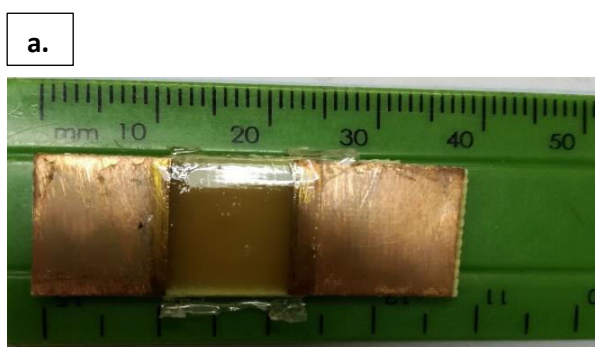


Figure 4.3. Copper plate with neat PVA (ratio PPy:NC (a). 0:0).

Figure 4.4 shows ratio 0:1 containing nanofibrous cellulose in PVA shows a cloudy film that took longer to dry than other samples. This sample contains no polypyrrole, and therefore was opaque in colour.

b.

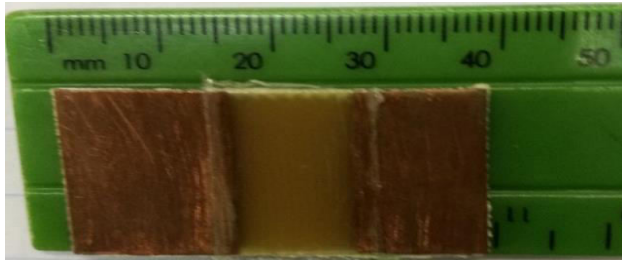


Figure 4.4. Copper plate with ratio PPy:NC (b) 0:1 using bacterial nanofibrous cellulose (dialysis-free).

Figure 4.4. showing ratio 1:2 contains more nanocellulose than polypyrrole. The film also took a significant amount of time to dry due to excess nanofibrous cellulose present.

c.

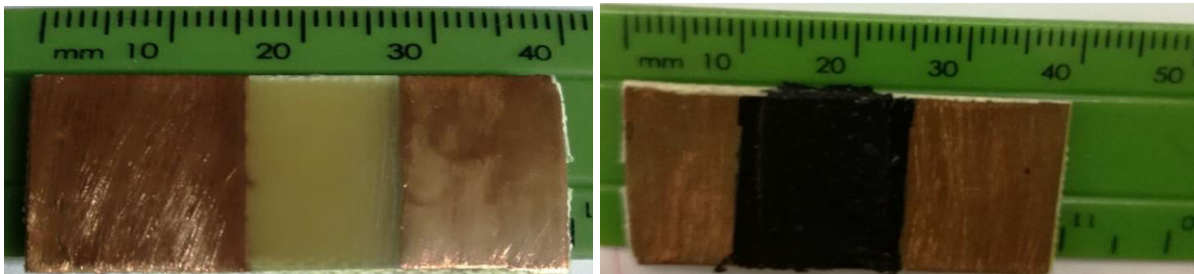


Figure 4.5. The empty copper plate and the copper plate with ratio PPy:NC (c) 1:2 using bacterial nanofibrous cellulose (dialysis-free).

The suspension of ratio 1:1, Figure 4.6., shows a neat undisturbed film with no distortions in set. The film remained smooth and interjoined after drying.

d.

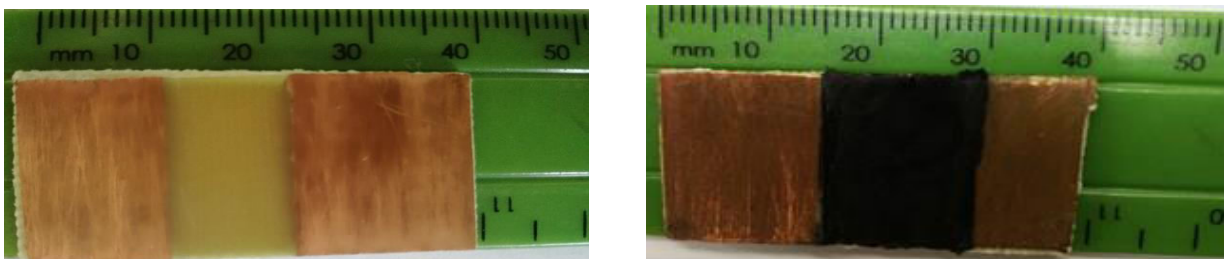


Figure 4.6. The empty copper plate and the copper plate with ratio PPy:NC (d) 1:1 using bacterial nanofibrous cellulose (dialysis-free).

Ratio 2:1, Figure 4.7., dried in a semi-uniform film on the Cu board, however, slight distortions were found in the set.

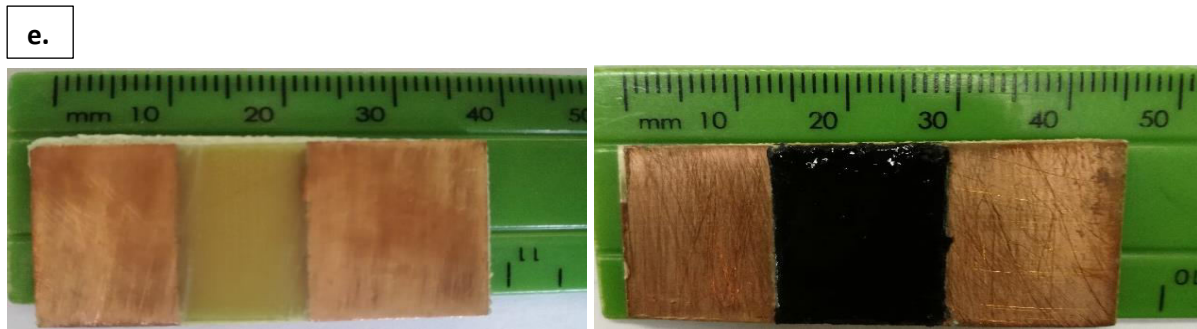


Figure 4.7. The empty copper plate and the copper plate with ratio PPy:NC (e) 2:1 using bacterial nanofibrous cellulose (dialysis-free).

Ratio 1:0 showed an irregular distribution of polypyrrole in PVA with crevices upon drying. The film has protuberances and did not show a neat network within PVA, Figure 4.8.

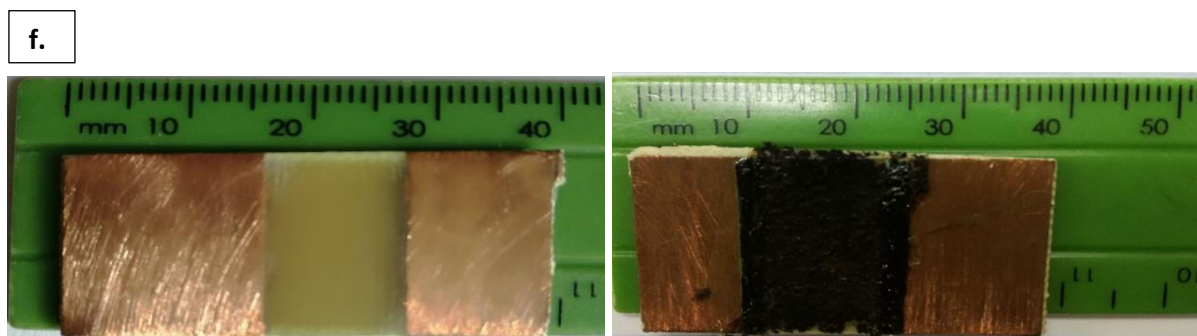


Figure 4.8. The empty copper plate and the copper plate with ratio PPy:NC (f) 1:0, Neat PPy.

TEM images were taken for all ratios i.e. ratio 0:0, 1:0 2:1, 1:1, 2:1 and 0:1 to examine the distribution within the PVA. To achieve higher conductivity at PPy content, it was expected that all the PPy can participate in the fabrication of a continuously conductive network in PVA matrix. For ratio 0:0, neat PVA, there were no particles present in the mixture. A transparent layer of PVA is seen in Figure 4.9.

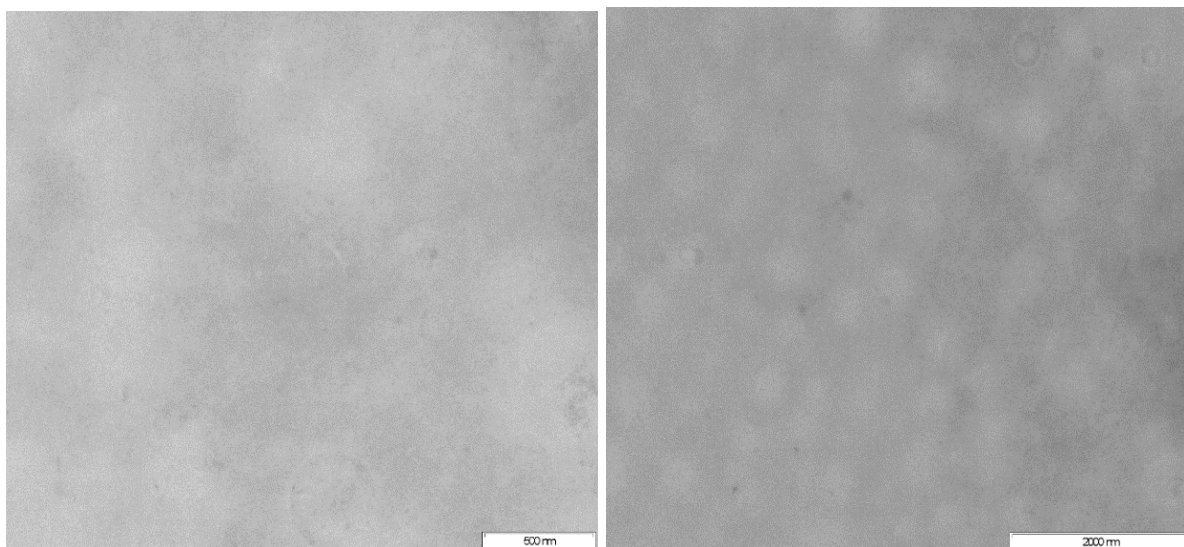


Figure 4.9. TEM image of polyvinyl alcohol (PVA).

Ratio 0:1, nanofibrous cellulose in PVA, Figure 4.10, clearly displays presence of nanofibers in a well-connected network. The nanofibers joined to each other to form a well-distributed deposit within the film.

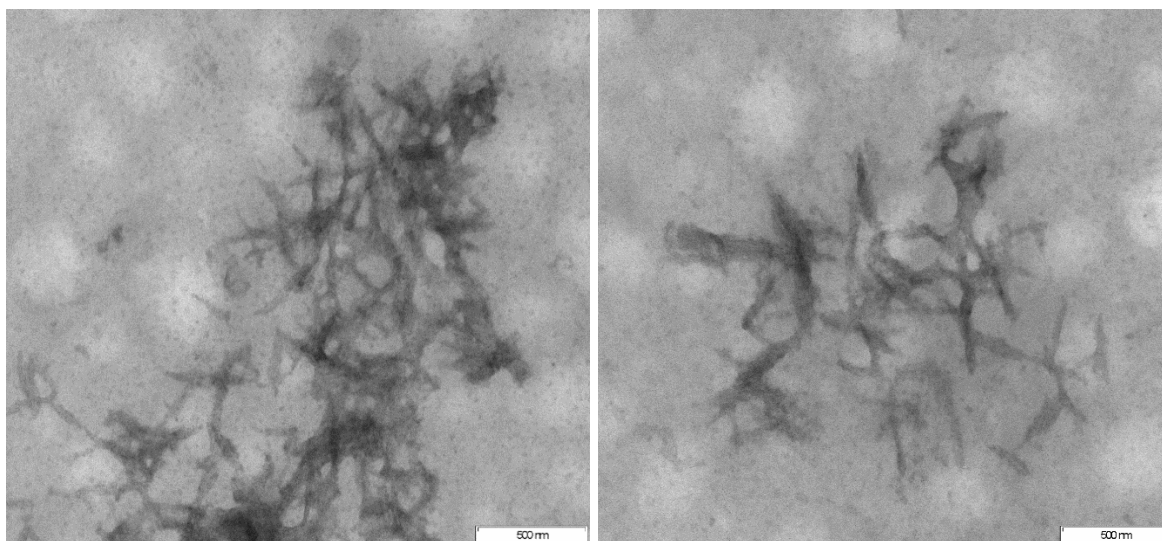


Figure 4.10. TEM image of nanofibrous cellulose from bacterial cellulose (dialysis-free) in PVA.

Ratio 1:2 showed an even distribution of nanofibers and polypyrrole. However, due to the excess ratio of nanocellulose compared to polypyrrole present, the dispersal of nanofibers formed a thin assembly of sample within the PVA, Figure 4.11.

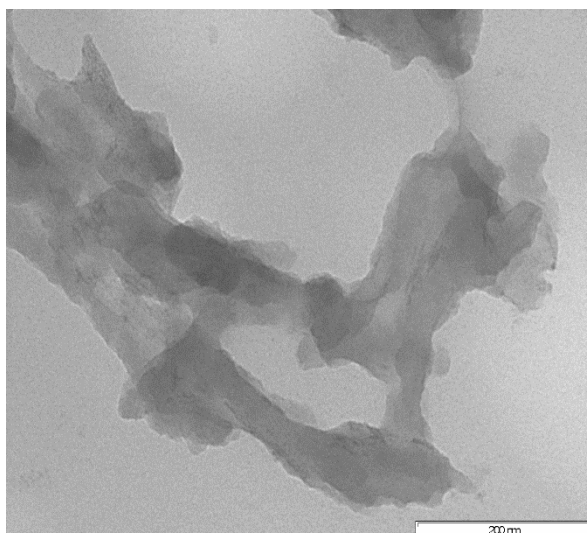


Figure 4.11. TEM image of ratio 1:2 polypyrrole to nanocellulose in PVA.

Figure 4.12 of ratio 1:1 containing polypyrrole showed an even distribution and uniform network of evenly distributed polypyrrole and nanocellulose. The nanohybrid remained adjacent to each other in the PVA suspension. The sample showed promising dissemination to ensure that a well-defined connected system existed within the sample. A continuous network structure of PPy@NC nanohybrid was formed by the incorporation of the nanocellulose due to its remarkably enhanced stability in PVA.

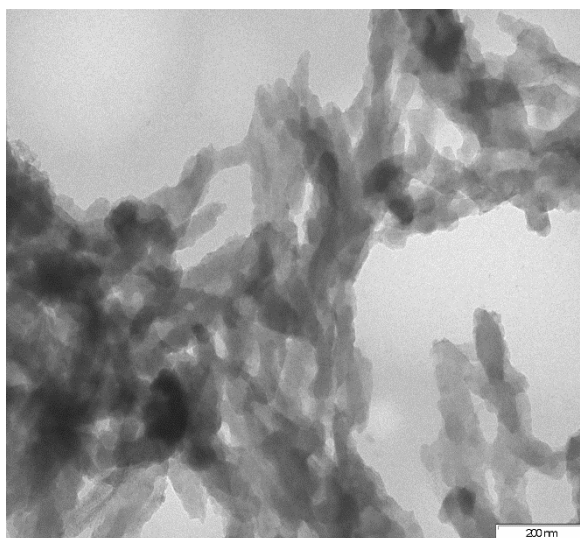


Figure 4.12. TEM image of ratio 1:1 polypyrrole to nanocellulose in PVA.

A similar network structure was found for ratio 2:1, Figure 4.13, where twice the amount of polypyrrole than nanocellulose was used. Under TEM imaging, the additional polypyrrole was found on the surface of the network, seen as the darker areas.

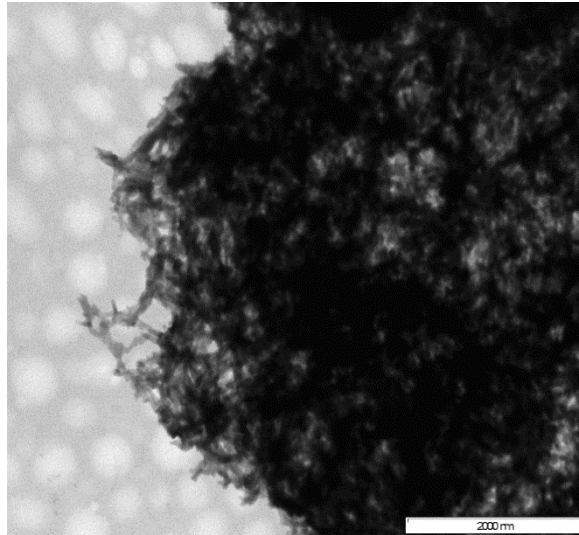


Figure 4.13. TEM image of ratio 2:1 polypyrrole to nanocellulose in PVA.

Finally, for ratio 1:0, of polypyrrole in PVA severe agglomeration was observed, see Figure 4.14. This was due to the poor suspension stability. There was minimal connectivity and thus no conductive network.

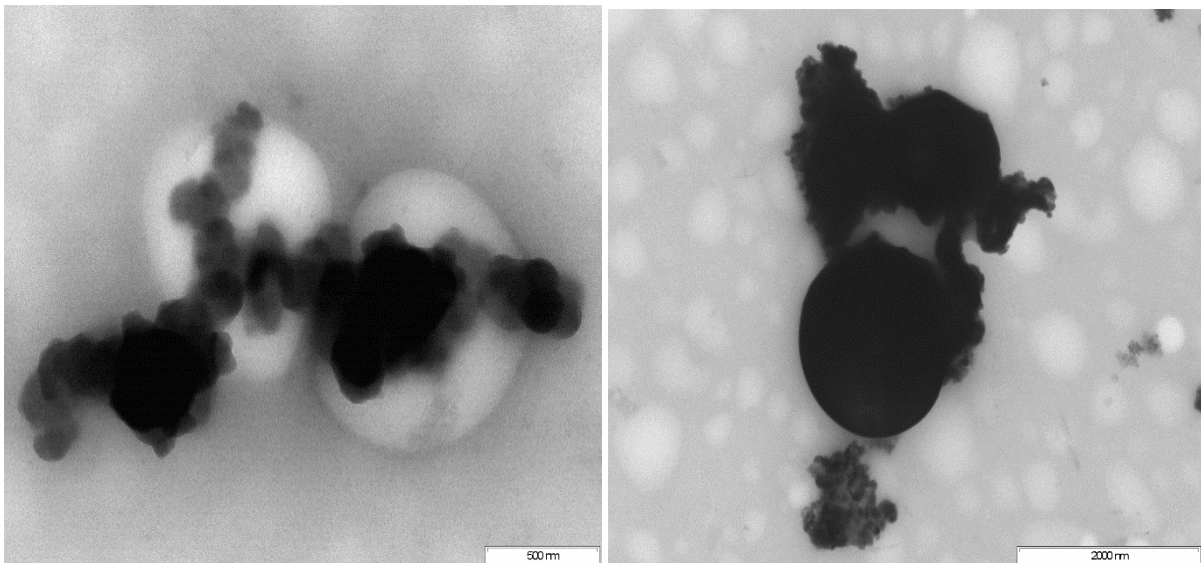


Figure 4.14. TEM image of polypyrrole in PVA.

To determine the density of each hybrid in PVA, the volume of water present had to first be determined. By weighing the wet sample on the copper board and then subtracting the weight of the sample, the mass of water could be calculated. With the known density of water at room temperature being 0.9982 g.mL^{-1} , the volume of water can be calculated from the equation:

$$\text{Density } (\rho) / \text{g.mL}^{-1} = \frac{\text{mass/g}}{\text{volume/mL}} \quad (4)$$

The total volume of sample used on the board was 0.25 mL, therefore the total volume used subtract the volume of water calculated in Equation 4, the volume of nanohybrid in PVA was obtained. The dry nanohybrid in PVA weight divided by the volume of nanohybrid yields the density of each sample, Table 4.1. The thickness of the film could then be calculated, using Equations 5 to 7:

$$\text{Volume} = (\text{length} \times \text{breadth}) \times \text{thickness} \quad (5)$$

$$\text{Volume} = (\text{surface area}) \times \text{thickness} \quad (6)$$

$$\ast \text{ thickness/mm} = \frac{\text{volume/mm}^3}{\text{surface area/mm}^2} \quad (7)$$

The volume of dried nanohybrid in PVA sample divided by the surface area of the sample on the copper clad board (that was measured with Image-J software) yielded the thickness of the film made by the nanohybrid and PVA.

Table 4.1. Quantities of mass, volume, density and thickness of varying ratios.

Sample label	a	b	c	d	e	f
	0:0	0:1	1:2	1:1	2:1	1:0
Mass of empty Cu plate/ g	2.656	3.878	3.902	3.900	3.698	3.721
Mass of wet sample + Cu plate/g	2.910	3.998	4.093	4.010	3.897	4.002
Mass of wet sample/g	0.254	0.120	0.191	0.110	0.199	0.281
Mass of dry PPy@NC in PVA + Cu plate/g	2.704	3.947	3.950	3.944	3.866	3.947
Mass of dry PPy@NC in PVA /g	0.048	0.069	0.048	0.044	0.168	0.226
Mass of water/g	0.206	0.051	0.143	0.066	0.031	0.055
Volume of water/ml	0.206	0.051	0.143	0.066	0.031	0.055
Volume of PPy@NC in PVA /ml	0.044	0.199	0.107	0.184	0.219	0.195
Density of PPy@NC in PVA /g.ml ⁻¹	1.1002	0.3469	0.4497	0.2393	0.7673	1.1596
Volume of PPy@NC in PVA / mm ³	43,629	198.908	106.742	183.881	218.944	194.901
Surface area of PPy@NC in PVA / mm ²	208.601	333.917	275.882	311.765	301.302	325.888
Thickness of PPy@NC in PVA /mm	0.2091	0.5957	0.3869	0.5898	0.7267	0.5981

According to Table 4.1, the density of ratio 0:0, neat PVA was calculated to be 1.1002 g.mL⁻¹. This value lies close to the true density of 1.19 g.mL⁻¹ known for PVA. The density of ratio 1:0 was the highest since there was only polypyrrole and PVA present in the system for the same volume. As the amount of polypyrrole increased in the ratio, the sample became denser, as expected.

The resistivity test was carried out for the ratio samples. The results for the voltage and current measured are shown in the Appendix Table 1 to Table 12 where the voltage was increased by

0.5 volts. The plot of graph current (A) vs. voltage (V) was done for all ratios. For ratio 0:0 which was neat PVA and ratio 0:1 nanocellulose in PVA showed insulating properties, as expected. Both PVA and nanocellulose in PVA are non-conducting unless modified, Figure 4.15. and Figure 4.16., showing no passing current for an applied voltage.

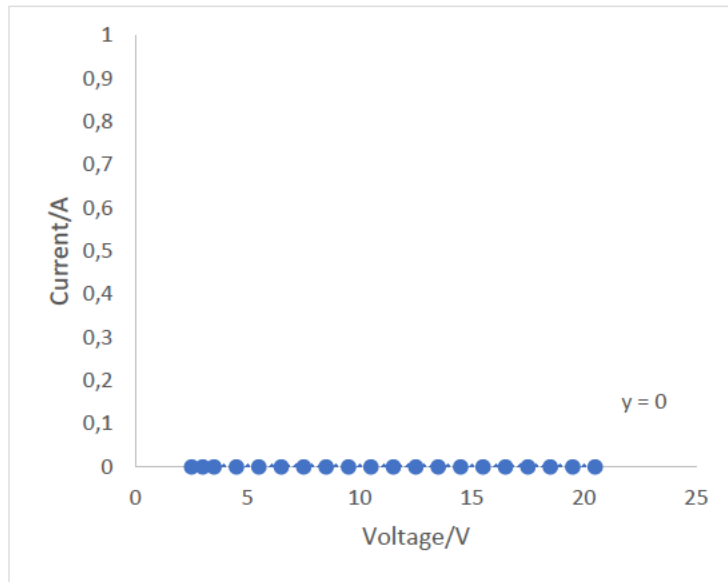


Figure 4.15. Linear relationship based on Ohm's law for sample (a) ratio 0:0 showing the change in current as voltage was applied.

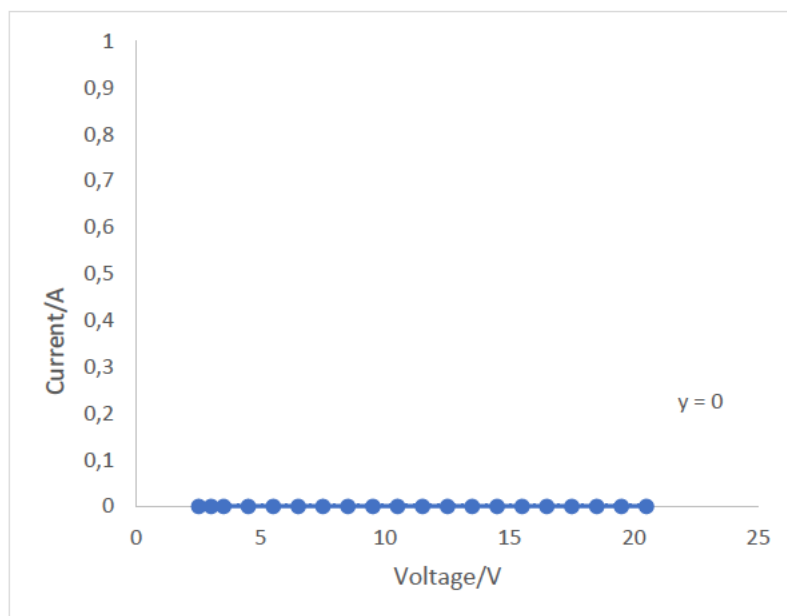


Figure 4.16. Linear relationship based on Ohm's law for sample (a) ratio 0:1 showing the change in current as voltage was applied.

Ratio 1:2 plots as a linear relationship obeying Ohm's law, Figure 4.17. The R^2 value of 0.99 shows good linearity and fit. The gradient of the graph was 3.33×10^{-6} and thus the reciprocal of 300960.06 Ω shows the resistance.

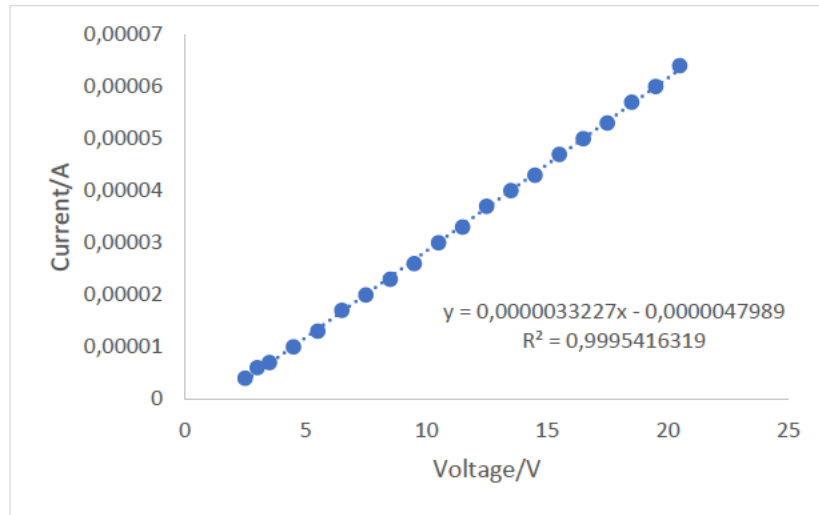


Figure 4.17. Linear relationship based on Ohm's law for sample (a) ratio 1:2 showing the change in current as voltage was applied.

Ratio 1:1 plots as a linear relationship obeying Ohm's law, Figure 4.18. The R^2 value of 0.99 indicates good linearity and fit. The gradient of the graph was 6.03×10^{-4} and thus the reciprocal of 1658.34 Ω as the resistance.

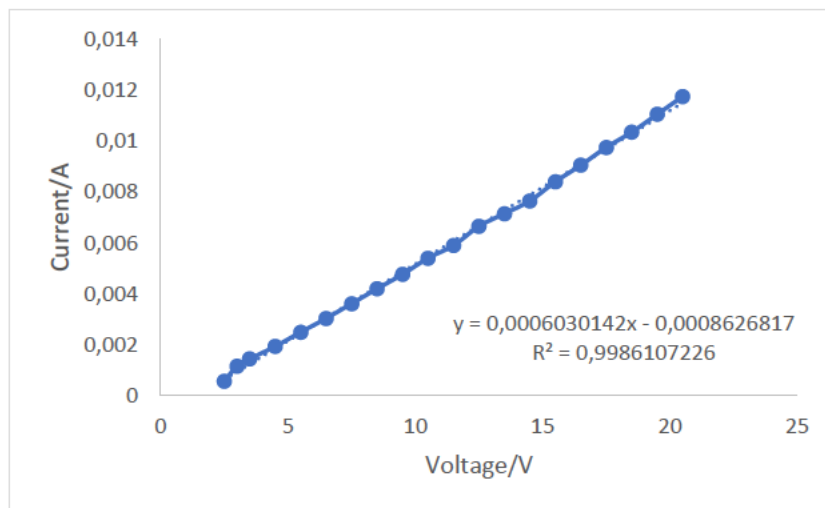


Figure 4.18. Linear relationship based on Ohm's law for sample (a) ratio 1:1 showing the change in current as voltage is applied.

Ratio 2:1 plots as a linear relationship obeying Ohm's law, Figure 4.19. The R^2 value of 0.98. The gradient of the graph was 1.68×10^{-5} and thus the reciprocal of 59384.54 Ω as the resistance.

The presence of more polypyrrole in this ratio allows for an increase in conductance. This conductance found for ratio 2:1 and is higher than ratio 1:1 due to the increased amount of conducting material present. The results show that as the amount of polypyrrole increases, so too does the conductivity. Although the desirable conductance was found for ratio 2:1, its mechanical stability fails to concur this ratio as the optimum ratio to be used.

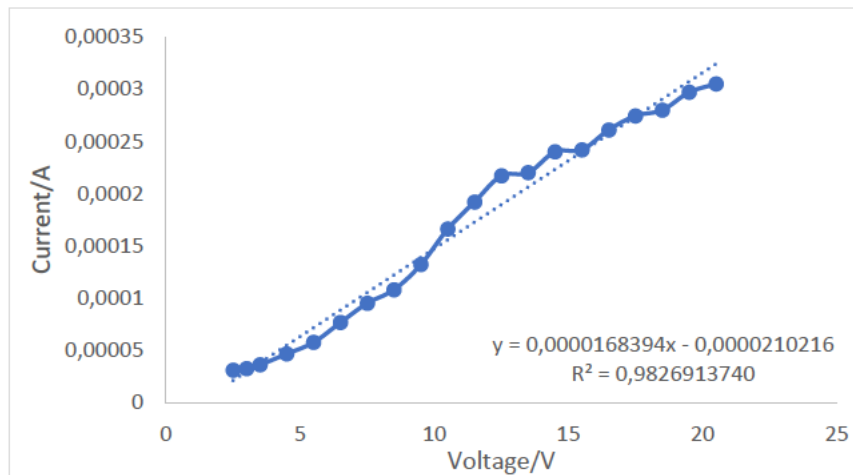


Figure 4.19. Linear relationship based on Ohm’s law for sample (a) ratio 2:1 showing the change in current as voltage is applied.

The ratio of 1:0 contains only polypyrrole in PVA yet it has a higher resistance of 333211.16 Ω calculated by the reciprocal of gradient 3.00×10^{-6} with a R^2 value of 0.95, Figure 4.20. This is due to the irregular distribution of the polypyrrole in PVA. The lack of stability within the matrix causes alteration amongst the network yielding a poorly connected system existing within the sample with minor conductivity.

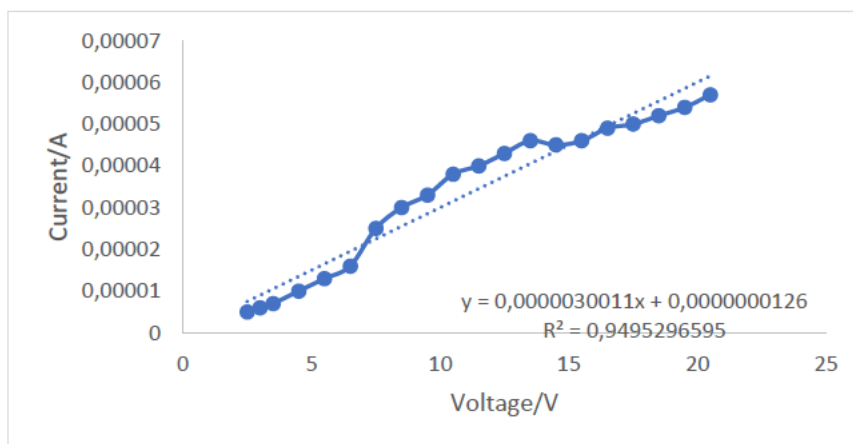


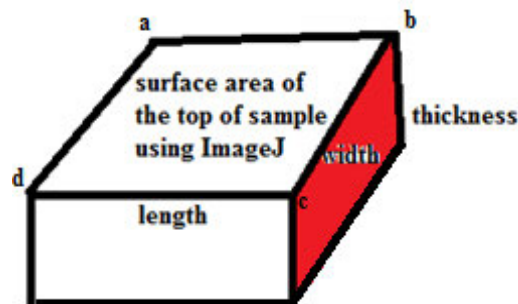
Figure 4.20. Linear relationship based on Ohm’s law for sample (a) ratio 1:0 showing the change in current as voltage is applied.

Table 4.2 shows the average resistance calculated with the standard deviation and variance for each sample's twenty individual measurements (found in Appendix Table 1 to 6).

To determine the volume resistivity where the standard equation is given by:

$$\rho = \frac{\text{Surface area}}{\text{thickness}} \times \text{resistance} \quad (8)$$

The surface area measured using Image-J software was used to determine the thickness needed in Equation (7) therefore, it cannot be used. Thus, the surface area on the side highlighted in red in Scheme 4.1. is required to be calculated.



Scheme 4.1. Schematic diagram showing the illustrated 3-dimensional sections of the film.

Using this thickness, calculated in Equation (7), multiplied by the film width bc , the surface area of the side was thus measured. Therefore, the Equation:

$$\rho = \frac{\text{Surface area}}{\text{thickness}} \times \text{resistance} \quad (9)$$

can be re-written as:

$$\rho = \frac{(\text{thickness}) \times (\text{width})}{\text{length}} \times \text{resistance} \quad (10)$$

$$\rho = \frac{\text{Surface area of the side}}{\text{length}} \times \text{resistance} \quad (11)$$

where the length (cd) labelled in Scheme 4.1 now represents the thickness of the sample if the red surface was rotated 90° anti-clockwise.

Table 4.2. The resistivity calculations for ratios 0:0, 0:1, 1:2, 1:1, 2:1 and 1:0.

Sample	a	b	c	d	e	f
	0:0	0:1	1:2	1:1	2:1	1:0
Average calculated Resistance/ Ω	-	-	383063.08	2126.09	73484.19	361048.68
Standard deviation	-	-	79543,99	589,48	13568,58	76702,08
Variance	-	-	6327246046,50	347483,57	184106407,74	5883208323,10
Thickness/mm	0.21	0.60	0.39	0.73	0.59	0.60
Width of sample (bc)/ mm	14,57	19,48	18,51	21,88	19,28	20,87
Surface Area of the side/mm ²	3,05	11,61	7,16	15,90	11,37	12,48
Length of sample (cd)/ mm	10.61	10.85	12.42	11.39	11.21	11.32
Resistivity calculated (Ω / mm)	-	-	220867.70	16401.93	74787.85	398197.90
Resistivity calculated (Ω / m)	-	-	220.87	16.40	74.79	398.20
Resistance from line of best fit ($\frac{1}{gradient}$)	undefined	undefined	300960.06	1658.34	59384.54	333211.16
Resistivity from line of best fit (Ω / mm)	-	-	173528.49	2314.67	60250.65	367496.09
Resistivity from line of best fit (Ω / m)	-	-	173.53	2.31	60.25	367.50

The results from Table 4.2 show that the average resistance for ratio 0:0 and 0:1 does not possess conducting properties and have undefined values for the resistance. Ratio 1:1 has the lowest resistance. By taking the resistance from the reciprocal of the gradient from the current vs. voltage graphs, the resistivity per mm can also be compared to the calculated resistivity per mm.

SEM images were taken for the sample before and after resistivity tests to determine if the applied voltage had any impact on the integrity of the sample. The results showed how reliable the sample was after use. If it retains structural integrity, then the sample can be re-used many times. From Figure 4.21 to Figure 4.26 it was seen there was no visible differences between before and after testing for 30 minutes and 20.5 V voltage applied. The sample remained unchanged, dependable and stable for numerous uses.

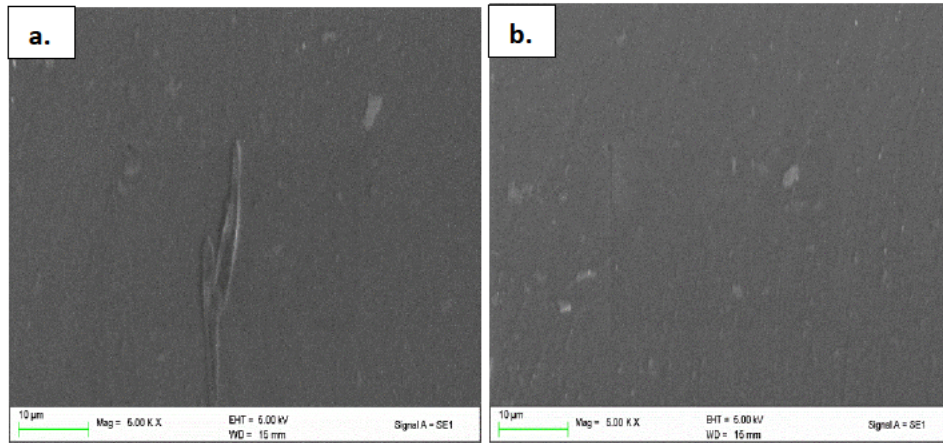


Figure 4.21. SEM image of PVA with ratio 0:0 (a) before applied voltage and (b) after applied voltage.

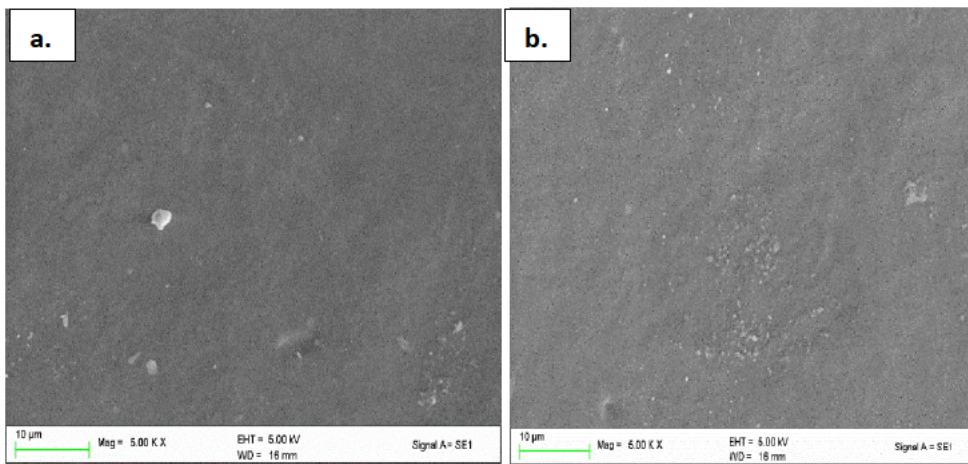


Figure 4.22. SEM image of PVA with ratio 0:1 nanofibrous cellulose from dialysis-free bacterial cellulose (a) before applied voltage and (b) after applied voltage.

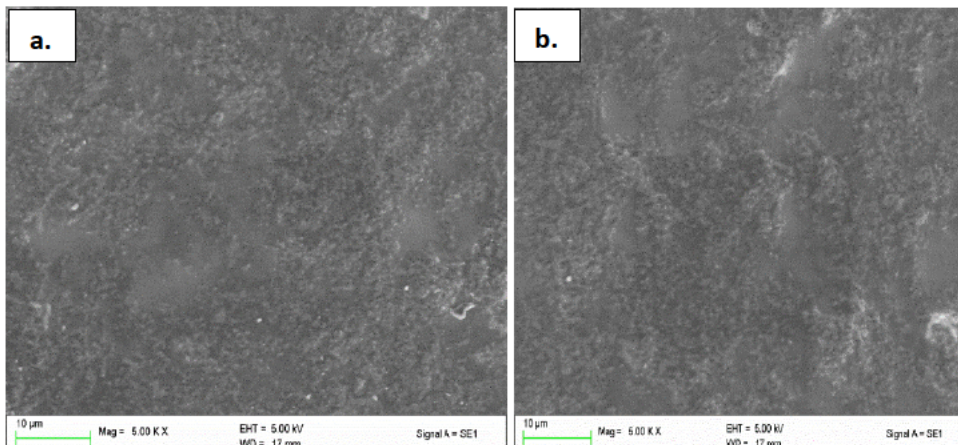


Figure 4.23. SEM image of ratio 1:2 PPy@NFC of dialysis-free bacterial cellulose in PVA (a) before applied voltage and (b) after applied voltage.

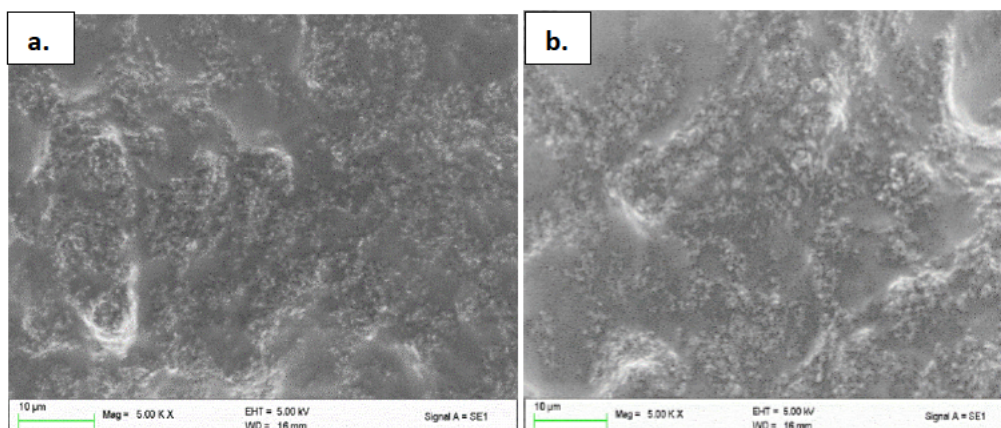


Figure 4.24. SEM image of ratio 1:1 PPy@NFC of dialysis-free bacterial cellulose in PVA (a) before applied voltage and (b) after applied voltage.

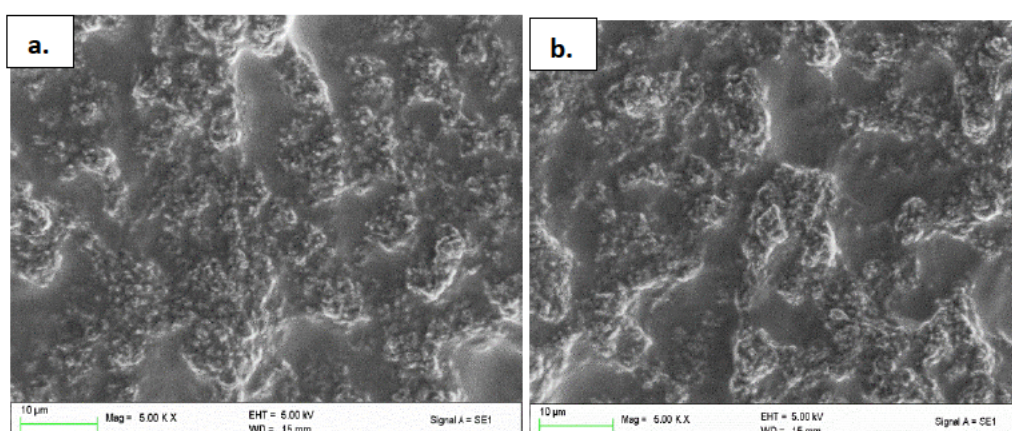


Figure 4.25. SEM image of ratio 2:1 PPy@NFC of dialysis-free bacterial cellulose in PVA (a) before applied voltage and (b) after applied voltage.

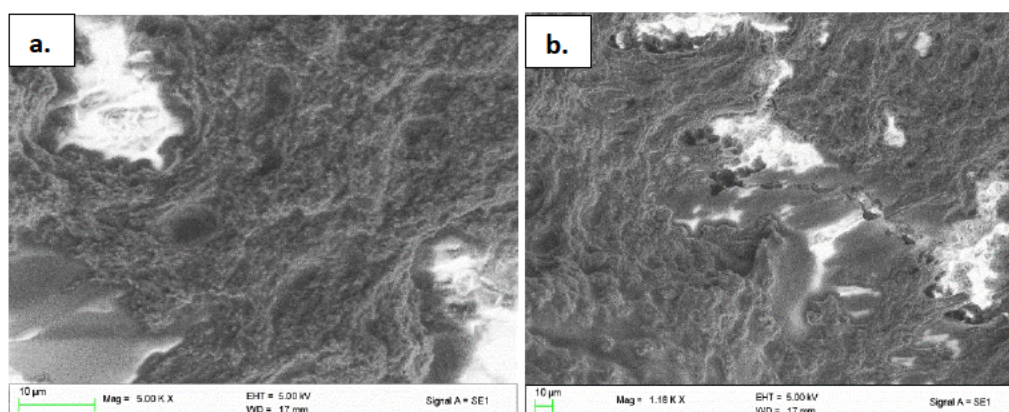


Figure 4.26. Sem image of ratio 1:0 PPy@NFC of dialysis-free bacterial cellulose in PVA (a) before applied voltage and (b) after applied voltage.

From the results, ratio 1:1 as the minimum ratio produced optimal conductivity with excellent stability and uniformity. Therefore, the exact procedure was carried out for all polypyrrole@nanocellulose samples from the variety of sources i.e. Hardwood pulp NCC, hardwood pulp NFC, Whatman filter paper NCC, Whatman filter paper NFC, Bacterial NCC and bacterial NFC at ratio 1:1.

The sample was set on the etched area of the copper clad board, shown in Figure 4.27 to Figure 4.32. All samples showed a neat undisturbed film with no distortions.

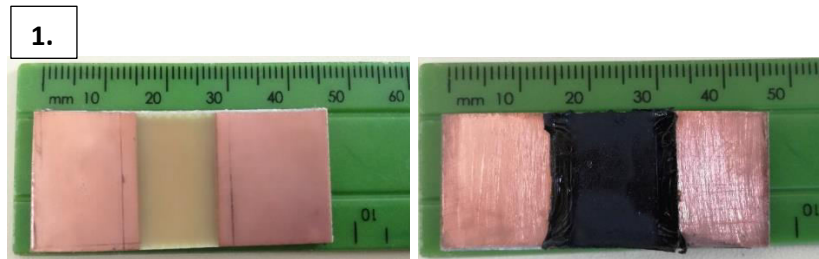


Figure 4.27. The empty copper plate and the copper plate with ratio 1:1 PPy@NCC in PVA for dialysed hardwood pulp.



Figure 4.28. The empty copper plate and the copper plate with ratio 1:1 PPy@NFC in PVA for dialysis-free hardwood pulp.

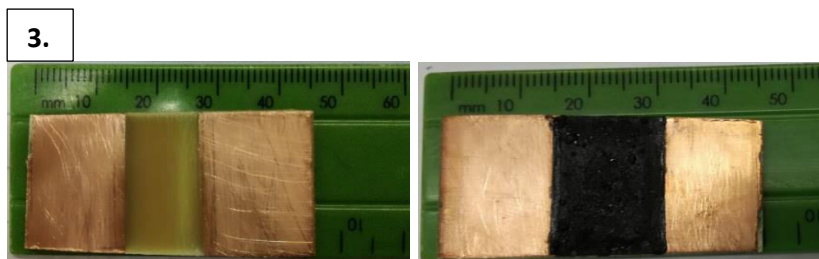


Figure 4.29. The empty copper plate and the copper plate with ratio 1:1 PPy@NCC in PVA for dialysed Whatman filter paper.

4.



Figure 4.30. The empty copper plate and the copper plate with ratio 1:1 PPy@NFC in PVA for dialysis-free Whatman filter paper.

5.

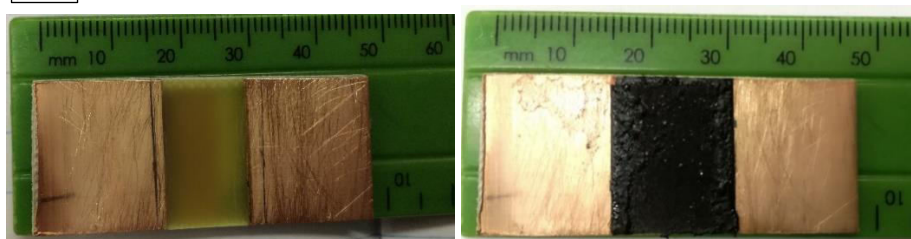


Figure 4.31. The empty copper plate and the copper plate with ratio 1:1 PPy@NCC in PVA for dialysed bacterial cellulose.

6.

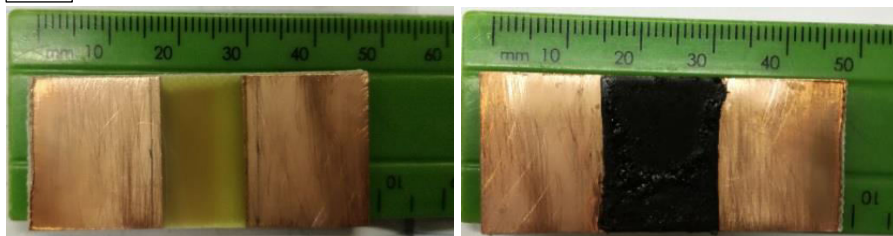


Figure 4.32. The empty copper plate and the copper plate with ratio 1:1 PPy@NFC in PVA for dialysis-free bacterial cellulose.

TEM images were recorded for all samples. The images for all samples showed polypyrrole as a dark coloured uniform network of evenly distributed polypyrrole and nanocellulose, Figure 4.33. For all samples, the nanohybrid remained adjacent to each other in the PVA suspension. The sample showed a promising distribution with a well-defined connected system within the sample which improved the conductivity through contact and interaction between each nanoparticle. A continuous network structure of PPy@NC nanohybrid was formed by incorporation of the nanocellulose due to its remarkably enhanced stability in PVA.

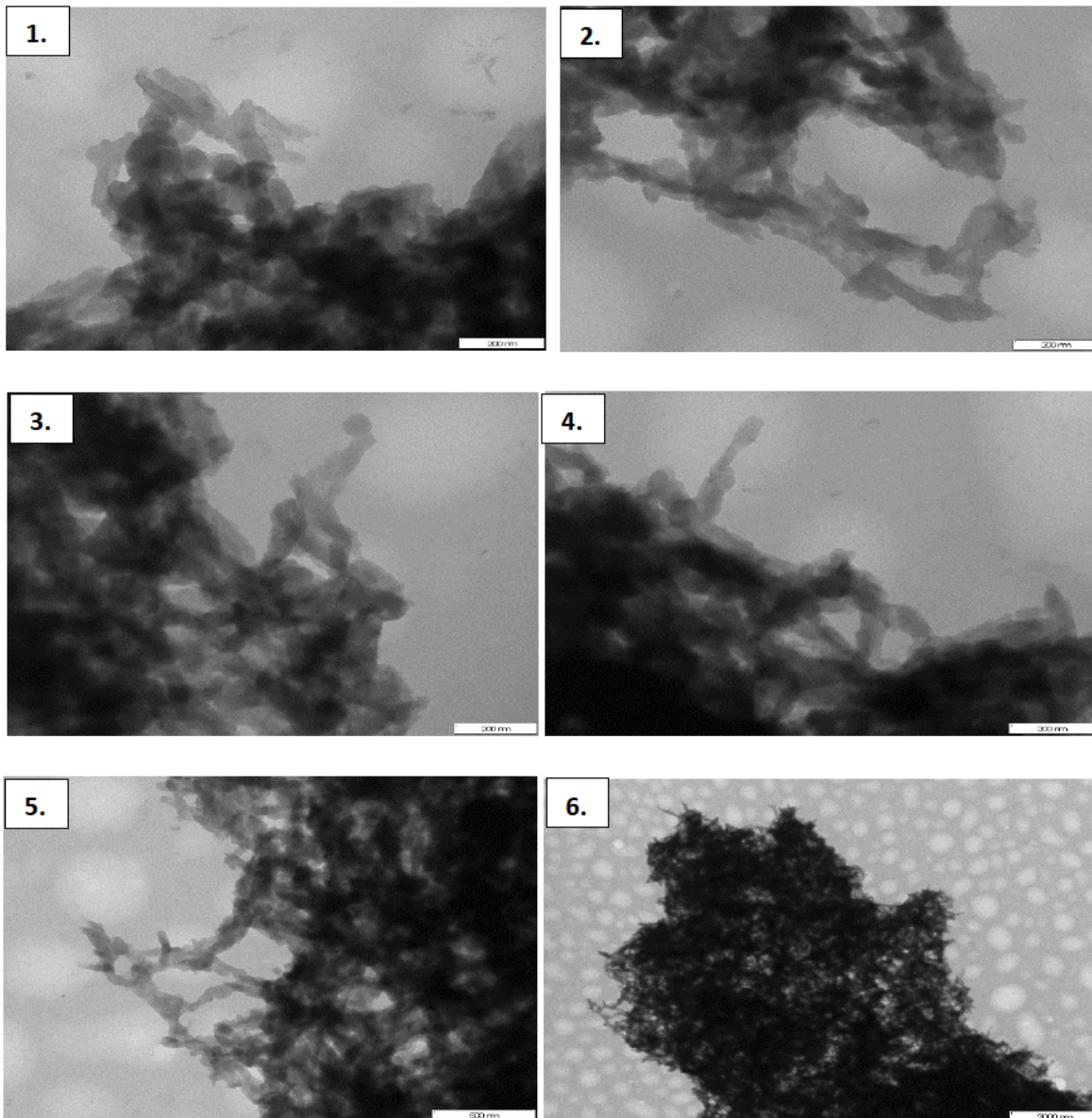


Figure 4.33. TEM images of (1) PPy@NCC from dialysed hardwood pulp, (2) PPy@NFC from dialysis-free hardwood pulp, (3) PPy@NCC from dialysed Whatman filter paper, (4) PPy@NFC from dialysis-free Whatman filter paper, (5) PPy@NCC from dialysed bacterial cellulose and (6) PPy@NFC from dialysis-free bacterial cellulose.

In the same way as previously demonstrated, the calculations in Table 4.3., showed the density calculation of all samples at ratio 1:1.

Table 4.3. Calculations of mass volume and density of all samples.

Sample label	1	2	3	4	5	6
	PPy NCC HWP	PPy NFC HWP	PPy NCC WFP	PPy NFC WFP	PPy NCC BC	PPy NFC BC
Mass of empty Cu plate/ g	3,147	3,149	3,368	3,287	3,103	3,185
Mass of wet sample + Cu plate/g	3,237	3,240	3,454	3,377	3,182	3,262
Mass of wet sample/g	0,090	0,091	0,086	0,090	0,079	0,077
Mass of dry PPy@NC in PVA + Cu plate /g	3,190	3,193	3,409	3,333	3,140	3,221
Mass of dry PPy@NC in PVA /g	0,043	0,044	0,041	0,046	0,037	0,036
Mass of water/g	0,047	0,047	0,045	0,044	0,042	0,041
Volume of water/ml	0,047	0,047	0,045	0,044	0,042	0,041
Volume of PPy@NC in PVA /ml	0,203	0,203	0,205	0,206	0,208	0,209
Density of PPy@NC in PVA /g.ml⁻¹	0,212	0,217	0,200	0,223	0,178	0,172
Volume of PPy@NC in PVA / mm³	203	203	205	206	208	209
Surface area on top/ mm²	334,490	325,124	342,000	366,714	347,314	364,660
Thickness of dry PPy@NC in PVA film/mm	0,607	0,624	0,599	0,562	0,599	0,573

The graph of current vs. voltage for all samples is shown in Figure 4.34. From these results, PPy@NFC from bacterial cellulose showed the greatest conductivity followed by PPy@NFC from Whatman filter paper. The conductance from the hybrid synthesized from dialysis-free nanocellulose was larger than samples subjected to dialysis.

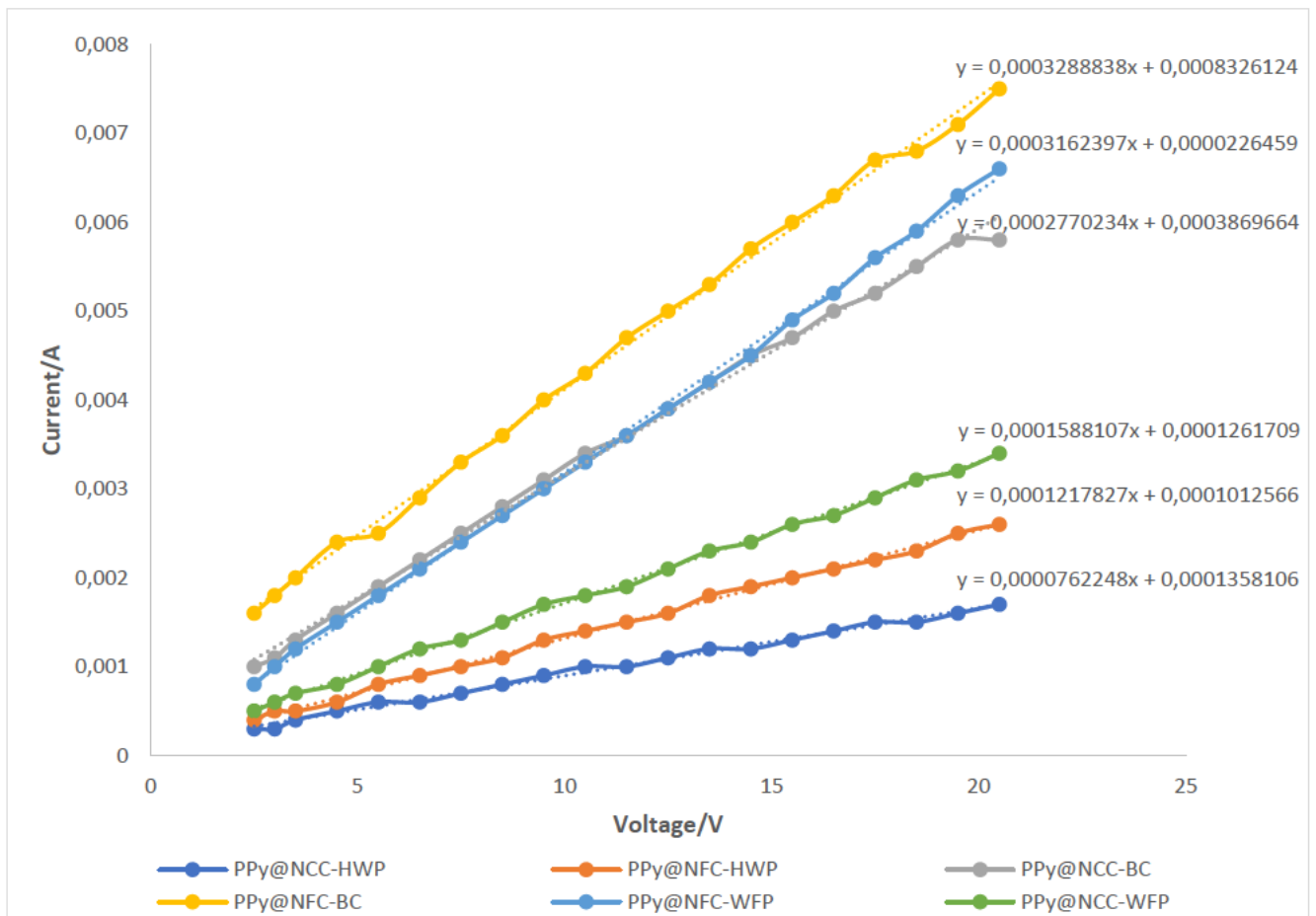


Figure 4.34. Linear relationship based on Ohm's law for all samples showing the change in current as voltage was applied.

Table 4.4. The resistivity calculations for all variations of samples.

Sample	1	2	3	4	5	6
	PPy@NCC/PVA-HWP	PPy@NFC/PVA-HWP	PPy@NCC/PVA-WFP	PPy@NFC/PVA-WFP	PPy@NCC/PVA-BC	PPy@NFC/PVA-BC
Average calculated Resistance/Ω	10831,51	7439,14	5725,67	3122,42	3091,47	2339,94
Standard deviation	1224.87	543.75	372.54	79.315	266.52	360.22
Variance	1500304.05	295659.93	138787.38	6290.93	71035.38	129758.25
Thickness/mm	0,57	0,60	0,62	0,56	0,61	0,60
Width of sample (ad)/mm	19.73	20.92	20.11	20.82	21.62	21.17
Surface Area of the side/mm²	11,31	12,53	12,55	11,70	13,12	12,69
Length of sample (cd)/mm	17.66	15.80	15.96	16.18	16.18	16.48
Resistivity calculated (Ω / mm)	9515.15	7225.48	6112.42	2257.78	3470.81	2495.48
Resistivity calculated (Ω / m)	9.52	7.23	6.11	2.26	3.47	2.50
Resistance from line of best fit ($\frac{1}{gradient}$)	13119.92	8211.33	6296.79	3162.16	3609.81	3040.59
Resistivity from line of best fit (Ω / mm)	8402.42	6514.94	4953.76	2286.52	2928.07	2341.21
Resistivity from line of best fit (Ω / m)	8.40	6.52	4.95	2.29	2.93	2.34

Table 4.4 shows the average resistance calculated with the standard deviation and variance for each sample's twenty individual measurements found in the thesis Appendix from Table 7 to Table 12. The results show that the average resistance for PPy@NFC in PVA made from dialysis-free bacterial nanocellulose has the lowest average resistance closely followed by PPy@NCC in PVA made from dialysed bacterial nanocellulose. This was followed by PPy@NFC in PVA made from dialysis-free Whatman filter paper and PPy@NCC in PVA made from dialysed Whatman filter paper nanocellulose. PPy@NFC in PVA made from dialysis-free hardwood pulp and PPy@NCC in PVA made from dialysed hardwood pulp nanocellulose

showed the lowest conductance. The calculated volume resistivity per mm calculated by using the average calculated by the multiplication of the resistance by the surface area over the length illustrated in Scheme 4.1 and Equation 8 yielded the volume resistivity, and in the same order as expected: samples 6 and 5 had the largest conductance followed by sample 4 and 3 and then followed by sample 2 and 1. By taking the resistance from the reciprocal of the gradient from the current vs. voltage graphs, the resistivity per mm can also be compared to the calculated resistivity per mm. These values lie in proximity to those calculated from the average resistance. Sample 1 average volume resistivity per mm was calculated at 9515.15 Ω/mm with the corresponding volume resistivity from the line of best fit of 8402.42 Ω/mm . Sample 2 had an average volume resistivity per mm that was calculated 7225.48 Ω/mm with the corresponding volume resistivity from the line of best fit of 6514.94 Ω/mm . The average volume resistivity per mm for sample 3 was calculated at 6112.42 Ω/mm with the corresponding volume resistivity from the line of best fit of 4953.76 Ω/mm . Sample 4 average volume resistivity per mm was calculated at 2257.78 Ω/mm with the corresponding volume resistivity from the line of best fit of 2286.52 Ω/mm . Sample 5 average volume resistivity per mm was calculated at 3470.81 Ω/mm with the corresponding volume resistivity from the line of best fit of 2928.07 Ω/mm . Finally, the calculated average volume resistivity per mm for sample 6 was measured to be 2495.48 Ω/mm and the corresponding volume resistivity from the line of best fit was calculated to be 2341.21 Ω/mm . The closeness of the results showed accuracy and precision in measurement between each sample's calculated volume resistivity from the average resistances to its individual volume resistivity from the line of best fit. It was found that dialysis-free sourced nanocellulose possessed a higher conductivity than dialysed nanocellulose per source.

The morphology of PPy@NC/PVA nanocomposite was characterized by SEM observation before resistivity tests were carried out on the samples, and after the samples were subjected to a voltage to determine the integrity of the sample. As shown in Figure 4.37 to Figure 4.42, the PPy@NC nanohybrid was well dispersed in the PVA forming a continuous network. The results showed that the samples were consistently reliable after being used, and the sample can be re-used many times. There were no visible differences found from before and after testing over 30 minutes at 20.5 V voltage applied. The sample remained the consistent, dependable and stable for numerous uses. The results showed there was good dispersion of nanoparticles and high aspect ratio of the PPy@NC nanohybrid. The continuous network structure enhances the electrical conductivity as well as mechanical properties of the PPy@NC/PVA nanocomposites.

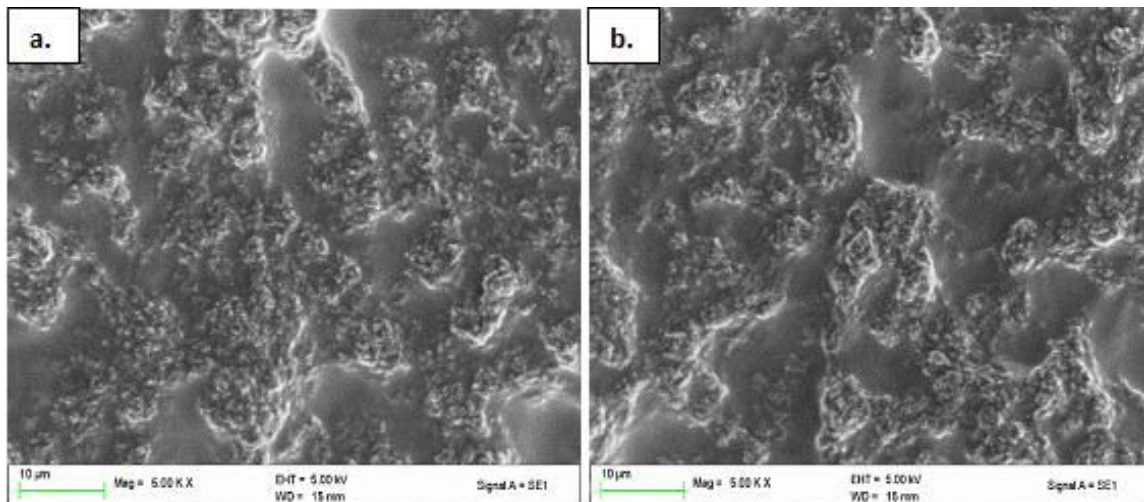


Figure 4.35. SEM image of PPy@NCC of dialysed hardwood pulp in PVA with ratio 1:1 (a) before applied voltage and (b) after applied voltage for resistivity testings.

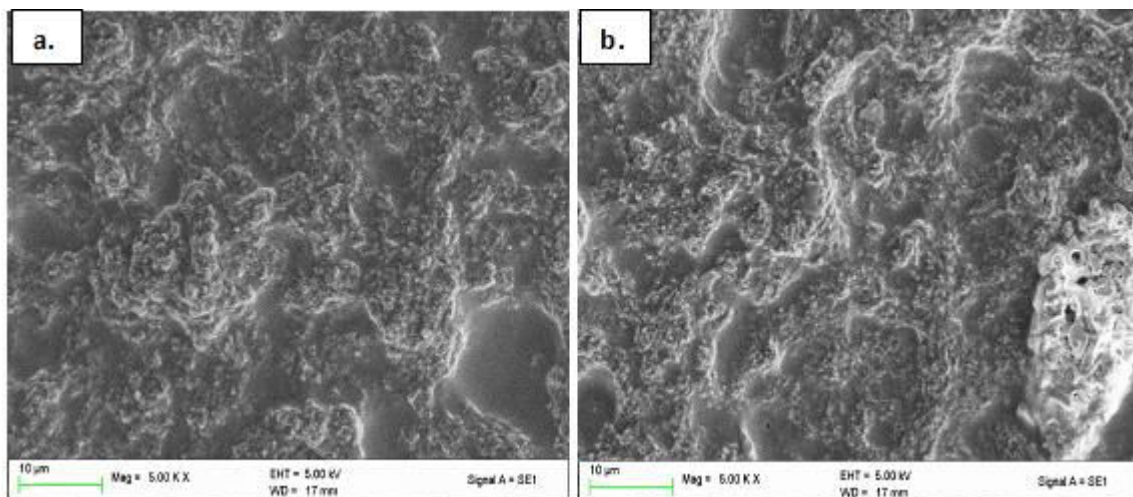


Figure 4.36. SEM image of PPy@NFC of dialysis-free hardwood pulp in PVA with ratio 1:1 (a) before applied voltage and (b) after applied voltage for resistivity testings.

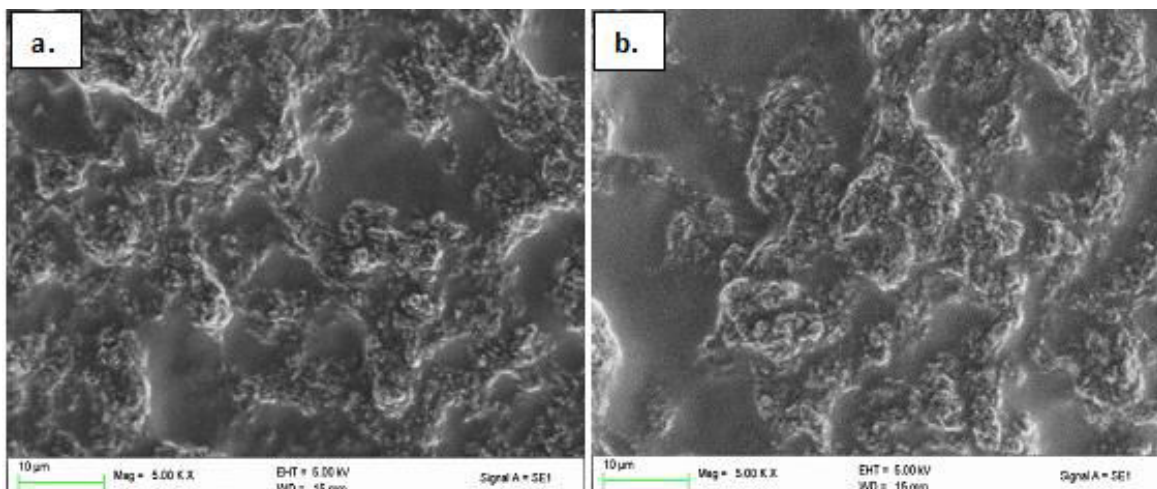


Figure 4.37. SEM image of PPy@NCC of dialysed Whatman filter paper in PVA with ratio 1:1 (a) before applied voltage and (b) after applied voltage for resistivity testings.

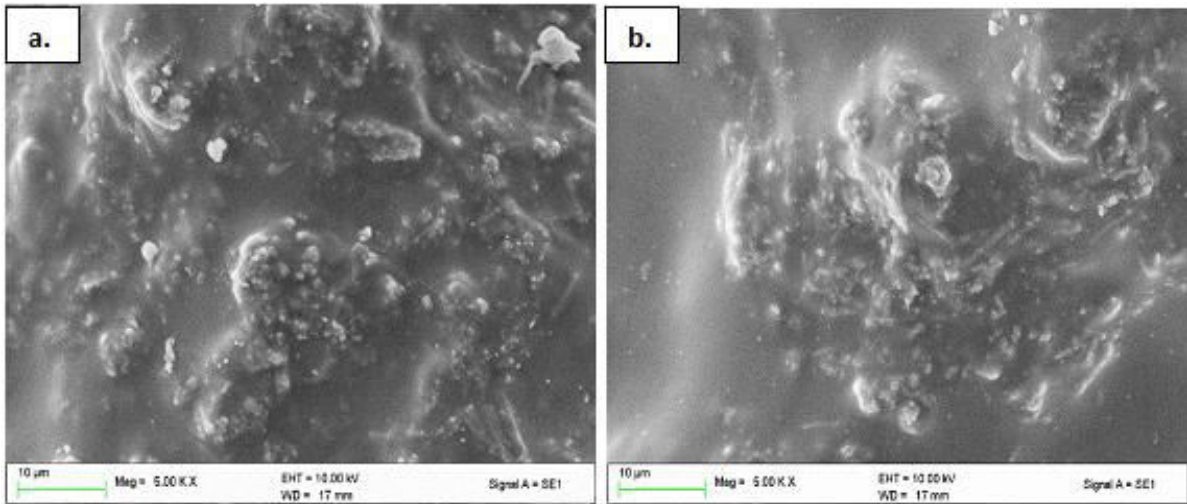


Figure 4.38. SEM image of PPy@NFC of dialysis-free Whatman filter paper in PVA with ratio 1:1 (a) before applied voltage and (b) after applied voltage for resistivity testings.

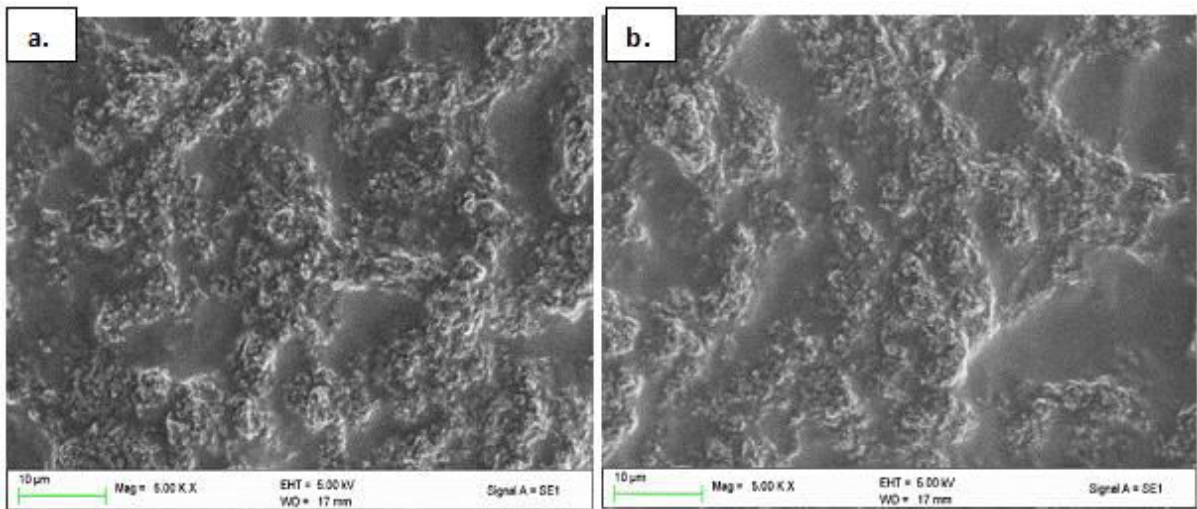


Figure 4.39. SEM image PPy@NCC of dialysed bacterial cellulose in PVA with ratio 1:1 (a) before applied voltage and (b) after applied voltage for resistivity testings.

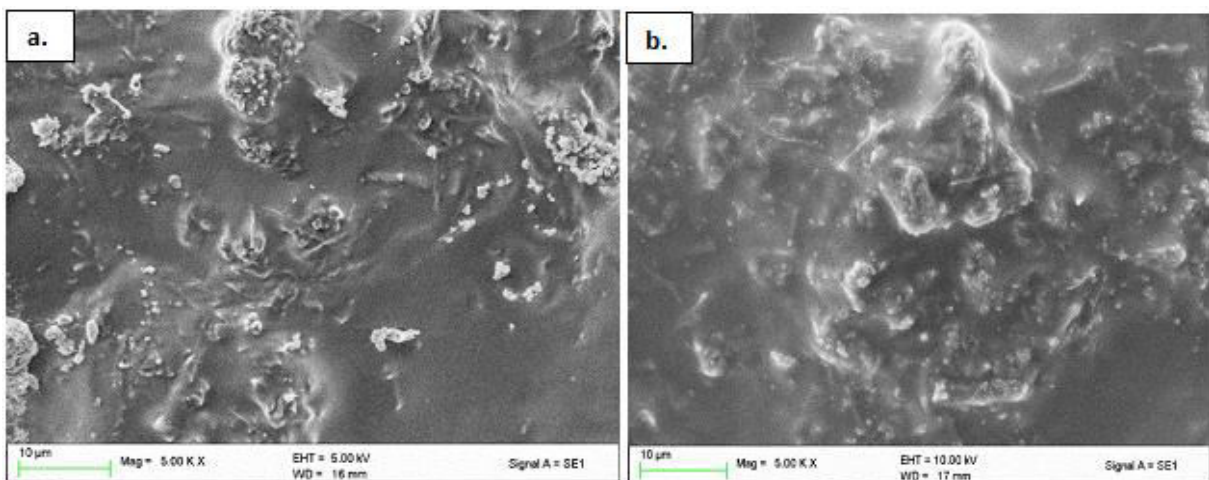


Figure 4.40. SEM image of PPy@NFC of dialysis-free bacterial cellulose in PVA with ratio 1:1 (a) before applied voltage and (b) after applied voltage for resistivity testings.

The results obtained by using a simple amp meter and volt meter gave outstanding results. When repeat experiments were performed and compared using a four-point probe measurement, the results matched. This method proved to provide an excellent alternate route when a four-point probe is not available. It is evident that for all samples that the dialysis-free nanocellulose used to synthesize each polypyrrole hybrid yielded larger conductivities than the dialysed hybrid. This is presumably due to the PPy on nanocellulose being doped again by the residual H_2SO_4 which promotes electrical conductivity. PPy@NFC/PVA from bacterial nanocellulose had the highest conductance due to the purity of bacterial cellulose ensuring a direct flow of current which indicates the effectiveness of nanohybrid in fabrication of conductive composites from the source it is produced from. This work proves that by capitalizing on the physiognomies of nanocellulose not subjected to dialysis, its unique traits can be exploited as an advantage for useful applications. By avoiding the costly and laborious dialysis step, one could easily utilize the residual acid as a doping agent that contribute to the desired conductance required. This enhancement benefitted from the good dispersion property and high aspect ratio of the nanohybrid to produce a more cost effective, environmentally friendly process to obtain a conductive polymer.

CHAPTER 5 - CONCLUSIONS

The extraction of nanocellulose from i) bacterial cellulose (grown using "Symbiotic 'Colony' of Bacteria and Yeast" or SCOBY), ii) Whatman filter paper, and iii) hardwood pulp was successfully investigated in this study. All sources proved to be successful in producing nanocellulose through acid hydrolysis where one dimension was under 100 nm. The nanocellulose prepared by the conventional dialysis route to produce nanocrystalline cellulose, NCC, was compared to a dialysis-free method to produce nanofibrous cellulose, NFC. Both synthetic methodologies gave nano-whisker cellulose and no difference in morphology was found. The concentration of nanocellulose for bacterial cellulose was higher than Whatman filter paper and hardwood pulp due to its high purity cellulose content. The nanocellulose from bacterial cellulose has acceptable aspect ratio for ideal stress transfer within the interaction between fibres and matrix.

The nanocellulose was used as a stabilizer for polypyrrole, PPy, to produce an electrical conducting polymer. The hydrolysis products of NFC were used without further separation as the starting materials for preparation of the PPy@NFC nanohybrid. The PPy@NFC was *in situ* doped by the residual hydrolysis acid, enhancing the PPy@NFC nanohybrid's improved electrical conductivity when compared to PPy@NCC. It was found that PPy deposits on NC as a continuous network structure, forming a nanohybrid with the desired electric conductivity and adjustable dispersibility. In addition, the prepared PPy@NC/PVA nanocomposites, as well as neat PPy/PVA nanocomposites were prepared for comparison. The PVA served as an excellent medium to facilitate the nanohybrid in a well dispersed form. The results showed that the minimum ratio for improved structure stability and optimum conductivity was 1:1 polypyrrole: nanocellulose. A simple method was used to measure the current and voltage and thus the resistance was calculated. These results were confirmed with a traditional four-point probe and the method was validated. PPy@NC/PVA nanocomposites exhibited significant improvement in both electrical conductivity and mechanical properties when compared with neat PPy/PVA composites, and the PPy@NFC/PVA exhibited enhanced performance compared to PPy@NCC/PVA nanocomposites. Therefore, a facile, reproducible, sustainable, cost-effective, and scalable approach to prepare a nanocellulose *via* a dialysis-free and *in situ* doping strategy was achieved. This work provides a new strategy for an environmentally friendly production of PPy@NC nanohybrid, which open new opportunities for the large-scale fabrication and application of nanocellulose based conductive nanocomposites at low cost and high performance.

APPENDIX

Table 1. Voltage, Current and Resistance measurements for Ratio 0:0.

Sample A ratio 0:0		
Voltage/V	Current/A	Resistance/Ω
2,5	0	-
3	0	-
3,5	0	-
4,5	0	-
5,5	0	-
6,5	0	-
7,5	0	-
8,5	0	-
9,5	0	-
10,5	0	-
11,5	0	-
12,5	0	-
13,5	0	-
14,5	0	-
15,5	0	-
16,5	0	-
17,5	0	-
18,5	0	-
19,5	0	-
20,5	0	-
	Average resistance/Ω	0

Table 2. Voltage, Current and Resistance measurements for Ratio 0:1.

Sample B ratio 0:1		
Voltage/V	Current/A	Resistance/Ω
2,5	0	-
3	0	-
3,5	0	-
4,5	0	-
5,5	0	-
6,5	0	-
7,5	0	-
8,5	0	-
9,5	0	-
10,5	0	-
11,5	0	-
12,5	0	-
13,5	0	-
14,5	0	-
15,5	0	-
16,5	0	-
17,5	0	-
18,5	0	-
19,5	0	-
20,5	0	-
	Average resistance/Ω	0

Table 3. Voltage, Current and Resistance measurements for Ratio 1:2.

Sample C ratio 1:2		
Voltage V	Current/A	Resistance/Ω
2,5	0,000004	625000,00
3	0,000006	500000,00
3,5	0,000007	500000,00
4,5	0,00001	450000,00
5,5	0,000013	423076,92
6,5	0,000017	382352,94
7,5	0,00002	375000,00
8,5	0,000023	369565,22
9,5	0,000026	365384,62
10,5	0,00003	350000,00
11,5	0,000033	348484,85
12,5	0,000037	337837,84
13,5	0,00004	337500,00
14,5	0,000043	337209,30
15,5	0,000047	329787,23
16,5	0,00005	330000,00
17,5	0,000053	330188,68
18,5	0,000057	324561,40
19,5	0,00006	325000,00
20,5	0,000064	320312,50
	Average resistance/Ω	383063,0751

Table 4. Voltage, Current and Resistance measurements for Ratio 1:1.

Sample D ratio 1:1		
Voltage/V	Current/A	Resistance/Ω
2,5	0,000031	80645,16
3	0,0000325	92307,69
3,5	0,000036	97222,22
4,5	0,0000465	96774,19
5,5	0,0000575	95652,17
6,5	0,0000765	84967,32
7,5	0,000095	78947,37
8,5	0,000108	78703,70
9,5	0,000132	71969,70
10,5	0,000166	63253,01
11,5	0,000192	59895,83
12,5	0,000217	57603,69
13,5	0,00022	61363,64
14,5	0,00024	60416,67
15,5	0,000242	64049,59
16,5	0,000261	63218,39
17,5	0,0002745	63752,28
18,5	0,00028	66071,43
19,5	0,000297	65656,57
20,5	0,000305	67213,11
	Average resistance/Ω	73484,19

Table 5. Voltage, Current and Resistance measurements for Ratio 2:1.

Sample E ratio 2:1		
Voltage/V	Current/A	Resistance/Ω
2,5	0,000564	4432,62
3	0,00116	2586,21
3,5	0,001445	2422,15
4,5	0,001935	2325,58
5,5	0,002495	2204,41
6,5	0,003035	2141,68
7,5	0,003615	2074,69
8,5	0,0042	2023,81
9,5	0,004765	1993,70
10,5	0,0054	1944,44
11,5	0,0059	1949,15
12,5	0,00665	1879,70
13,5	0,00715	1888,11
14,5	0,00765	1895,42
15,5	0,0084	1845,24
16,5	0,00905	1823,20
17,5	0,00975	1794,87
18,5	0,01035	1787,44
19,5	0,01105	1764,71
20,5	0,01175	1744,68
	Average resistance/Ω	2126,09

Table 6. Voltage, Current and Resistance measurements for Ratio 1:0.

Sample F ratio 1:0		
Voltage/V	Current/A	Resistance/Ω
2,5	0,000005	500000,00
3	0,000006	500000,00
3,5	0,000007	500000,00
4,5	0,00001	450000,00
5,5	0,000013	423076,92
6,5	0,000016	406250,00
7,5	0,000025	300000,00
8,5	0,00003	283333,33
9,5	0,000033	287878,79
10,5	0,000038	276315,79
11,5	0,00004	287500,00
12,5	0,000043	290697,67
13,5	0,000046	293478,26
14,5	0,000045	322222,22
15,5	0,000046	336956,52
16,5	0,000049	336734,69
17,5	0,00005	350000,00
18,5	0,000052	355769,23
19,5	0,000054	361111,11
20,5	0,000057	359649,12
	Average resistance/Ω	361048,68

Table 7. Measured current/A for Sample 1, at applied voltage/V with calculated resistance.

Sample 1		
Voltage/V	Current/A	Resistance/Ω
2,5	0,0003	8333,33
3	0,0003	10000,00
3,5	0,0004	8750,00
4,5	0,0005	9000,00
5,5	0,0006	9166,67
6,5	0,0006	10833,33
7,5	0,0007	10714,29
8,5	0,0008	10625,00
9,5	0,0009	10555,56
10,5	0,001	10500,00
11,5	0,001	11500,00
12,5	0,0011	11363,64
13,5	0,0012	11250,00
14,5	0,0012	12083,33
15,5	0,0013	11923,08
16,5	0,0014	11785,71
17,5	0,0015	11666,67
18,5	0,0015	12333,33
19,5	0,0016	12187,50
20,5	0,0017	12058,82
	Average resistance/Ω	10831,51

Table 8. Measured current/A for Sample 2, at applied voltage/V with calculated resistance.

Sample 2		
Voltage/V	Current/A	Resistance/Ω
2,5	0,0004	6250,00
3	0,0005	6000,00
3,5	0,0005	7000,00
4,5	0,0006	7500,00
5,5	0,0008	6875,00
6,5	0,0009	7222,22
7,5	0,001	7500,00
8,5	0,0011	7727,27
9,5	0,0013	7307,69
10,5	0,0014	7500,00
11,5	0,0015	7666,67
12,5	0,0016	7812,50
13,5	0,0018	7500,00
14,5	0,0019	7631,58
15,5	0,002	7750,00
16,5	0,0021	7857,14
17,5	0,0022	7954,55
18,5	0,0023	8043,48
19,5	0,0025	7800,00
20,5	0,0026	7884,62
	Average resistance/Ω	7439,14

Table 9. Measured current/A for Sample 3, at applied voltage/V with calculated resistance.

Sample 3		
Voltage/V	Current/A	Resistance/Ω
2,5	16	156250,00
3	18	166666,67
3,5	20	175000,00
4,5	24	187500,00
5,5	25	220000,00
6,5	29	224137,93
7,5	33	227272,73
8,5	36	236111,11
9,5	40	237500,00
10,5	43	244186,05
11,5	47	244680,85
12,5	50	250000,00
13,5	53	254716,98
14,5	57	254385,96
15,5	60	258333,33
16,5	63	261904,76
17,5	67	261194,03
18,5	68	272058,82
19,5	71	274647,89
20,5	75	273333,33
	Average resistance/Ω	233994,02

Table 10. Measured current/A for Sample 4, at applied voltage/V with calculated resistance.

Sample 4		
Voltage/V	Current/A	Resistance/Ω
2,5	0,0008	3125,00
3	0,001	3000,00
3,5	0,0012	2916,67
4,5	0,0015	3000,00
5,5	0,0018	3055,56
6,5	0,0021	3095,24
7,5	0,0024	3125,00
8,5	0,0027	3148,15
9,5	0,003	3166,67
10,5	0,0033	3181,82
11,5	0,0036	3194,44
12,5	0,0039	3205,13
13,5	0,0042	3214,29
14,5	0,0045	3222,22
15,5	0,0049	3163,27
16,5	0,0052	3173,08
17,5	0,0056	3125,00
18,5	0,0059	3135,59
19,5	0,0063	3095,24
20,5	0,0066	3106,06
	Average resistance/Ω	3122,42

Table 11. Measured current/A for Sample 5, at applied voltage/V with calculated resistance.

Sample 5		
Voltage/V	Current/A	Resistance/Ω
2,5	0,0005	5000,00
3	0,0006	5000,00
3,5	0,0007	5000,00
4,5	0,0008	5625,00
5,5	0,001	5500,00
6,5	0,0012	5416,67
7,5	0,0013	5769,23
8,5	0,0015	5666,67
9,5	0,0017	5588,24
10,5	0,0018	5833,33
11,5	0,0019	6052,63
12,5	0,0021	5952,38
13,5	0,0023	5869,57
14,5	0,0024	6041,67
15,5	0,0026	5961,54
16,5	0,0027	6111,11
17,5	0,0029	6034,48
18,5	0,0031	5967,74
19,5	0,0032	6093,75
20,5	0,0034	6029,41
	Average resistance/Ω	5725,67

Table 12. Measured current/A for Sample 6, at applied voltage/V with calculated resistance.

Sample 6		
Voltage/V	Current/A	Resistance/Ω
2,5	0,001	2500,00
3	0,0011	2727,27
3,5	0,0013	2692,31
4,5	0,0016	2812,50
5,5	0,0019	2894,74
6,5	0,0022	2954,55
7,5	0,0025	3000,00
8,5	0,0028	3035,71
9,5	0,0031	3064,52
10,5	0,0034	3088,24
11,5	0,0036	3194,44
12,5	0,0039	3205,13
13,5	0,0042	3214,29
14,5	0,0045	3222,22
15,5	0,0047	3297,87
16,5	0,005	3300,00
17,5	0,0052	3365,38
18,5	0,0055	3363,64
19,5	0,0058	3362,07
20,5	0,0058	3534,48
	Average resistance/Ω	3091,47